Doctoral Dissertation
Doctoral Program in Chemical Engineering (XXXII cycle)

Stable production of commodity chemicals in cyanobacterial cell factories

Beatrice Battaglino

* * * * * *

Supervisors
Dr. C. Pagliano, Politecnico di Torino
Prof. G. Saracco, Politecnico di Torino

Doctoral examination committee
Prof. A. Bertucco, Università degli Studi di Padova (IT)
Dr. A. P. Casazza, Consiglio Nazionale delle Ricerche (CNR)—Milano (IT)
Prof. D. Fino, Politecnico di Torino (IT)
Dr. B. Menin, Istituto Italiano di Tecnologia (IT)
Prof. P. Nixon, Imperial College of London (UK)

Politecnico di Torino
2020

I hereby declare that, the contents and organisation of this dissertation constitute my own original work and does not compromise in any way the rights of third parties, including those relating to the security of personal data.

....

Beatrice Battaglino

Turin, 2020

Summary

The sustainable production of commodity chemicals is becoming urgent, given the depletion of petrochemical resources and the climate change effects that we are witnessing. Production based on cyanobacterial cell factories can represent a feasible alternative, since these photosynthetic microorganisms are able to directly convert atmospheric CO_2 into valuable chemical compounds. Upon proper genetic modifications, the range of metabolites produced by cyanobacteria has been broaden, however classic metabolic engineering approaches often introduce a trade-off between biomass growth and product formation. This divergence can lead to genetic instability of such engineered strains, because a positive selection pressure is active towards the cells that accumulate mutations causing the loss of the production trait and a gain in the microbial fitness (retro-mutants). These advantaged mutant cells would easily outcompete the producer cells determining a drastic drop in productivity, which compromises scale-up in real industrial settings.

In this work, a metabolic engineering strategy that aims at aligning microbial fitness and product synthesis has been applied to the production of fumarate and malate in the cyanobacterium *Synechocystis* sp. PCC 6803. Fumarate and malate are two dicarboxylic acids interesting from the biotechnological point of view, since they are widely used in the food and feed industry, as well as in the bio-plastic and polymers sector.

By means of an algorithm analysing the genome scale metabolic model of *Synechocystis* sp. PCC 6803, it was possible to identify the compounds that can be produced in a growth-coupled fashion as sub-products of anabolic reactions, and the genetic modifications necessary to obtain their accumulation. Among these compounds there was present fumarate, which has been chosen as target metabolite in this study. Moreover, the strategy has been extended to malate, a compound that, although not recognized as a strict growth-coupled metabolite, uses as precursor fumarate which is a stoichiometrically growth-coupled compound. Different deletion mutants, able to accumulate fumarate and malate, have been engineered and tested in a laboratory scale photo-bioreactor in different cultivation modes, including day-night regime. The fumarate and malate producing strains were able to reach a cumulative titer of ~1.2 m M and 1.0 m M after about 10 and 14 days of cultivation in batch under continuous illumination, respectively. The genetic stability of the most promising strains has been tested through an evolution experiment, which revealed that the mutants were stable for over

one month of continuous cultivation, thus demonstrating the effective success of the metabolic engineering strategy adopted.

Finally, a mathematical model that describes the dynamics of retro-mutants into a population of photosynthetic microorganism has been developed. The model has been used to simulate the dynamics of formation of retro mutants in a semi-continuous cultivation setting, where dilutions are performed at certain time-intervals. A sensitivity analysis of different parameters allowed to identify the optimal set of conditions to carry out an evolution experiment. Indeed, the cultivation mode adopted directly influences the time instant at which the retro-mutants can be observed. However, in a generation time-scale the simulations highlighted that only two parameters (i.e., the production burden and the mutation rate), which are intrinsic genetic features of the strain, determine the appearance of retro-mutants.

Acknowledgements

"Every two hundred years, every atom of carbon that is not congealed in materials by now stable (such as, precisely, limestone, or coal, or diamond, or certain plastics) enters and reenters the cycle of life, through the narrow door of photosynthesis. Do other doors exist? Yes, some syntheses created by man; they are a title of nobility for man-the-maker, but until now their quantitative importance is negligible. They are doors still much narrower than that of the vegetal greenery; knowingly or not, man has not tried until now to compete with nature on this terrain, that is, he has not striven to draw from the carbon dioxide in the air the carbon that is necessary to nourish him, clothe him, warm him, and for the hundred other more sophisticated needs of modern life. He has not done it because he has not needed to: he has found, and is still finding (but for how many more decades?) gigantic reserves of carbon already organicized, or at least reduced. Besides the vegetable and animal worlds, these reserves are constituted by deposits of coal and petroleum: but these too are the inheritance of photosynthetic activity carried out in distant epochs, so that one can well affirm that photosynthesis is not only the sole path by which carbon becomes living matter, but also the sole path by which the sun's energy becomes chemically usable".

The Periodic Table, 1975. Primo Levi

List of Abbreviations

2PG   2-phosphoglycerate

3PG   3-phosphoglycerate

CA   carbonic anhydrase

CBB   Calvin Benson Bassham

CCM   carbon concentrating mechanism

CEF   cyclic electron flow

COI   compound of interest

CRISPR   clustered regularly interspaced short palindromic repeats

$D-GTP$ D-glutamate-pyruvate transaminase

DHA   docosahexaenoic acid

DHAP   dihydroxyacetone phosphate

ECR   enoyl-CoA carboxylase/reductase

ETC   electron transfer chain

F6P   fructose 6-phosphate

FBA   flux balance analysis

FumC   fumarase C

FVA   flux variability analysis

GABA γ-aminobutyric acid

GOT   glutamate-oxaloacetate transaminase

GSMM   genome scale metabolic model

IPCC   Intergovernmental Panel on Climate Change

LAC   lactate

LDH   lactate dehydrogenase

MCF   microbial cell factory

Mdh   malate dehydrogenase

Me   malic enzyme

MEP   methylerythritol phosphate

MoClo modular cloning

NPQ   non-photochemical quenching

NSI   neutral site insertion

OCPs orange carotenoid proteins

OD   optical density

OPPP oxidative pentose phosphates pathway

PAM   protospacer adjacent motif

PAR   photosynthetically active radiation

PBR   phycobilisomes

PEP   phosphoenolpyruvate

PEPc   phosphoenolpyruvate carboxylase

PHA   polyhydroxyalkanoate

PHB   polyhydroxybutyrate

PSI   photosystem I

PSII   photosystem II

PYR   pyruvate

RBS   ribosome binding sites

RuBP ribulose 1,5-bisphosphate

TCA	tricarboxylic acid
TIC	total ion current
TRAP	tripartite ATP-independent periplasmic transporter
WT	wild type
zwf	glucose-6-phosphate 1-dehydrogenase

Contents

Chapter 1

Introduction

1.1 General context

As reported by the Intergovernmental Panel on Climate Change (IPCC) in 2018, in less than two centuries (between 1880 and 2012) the global average surface temperature warmed by 0.85 °C. Since the global warming is increasing at 0.2 °C per decade, the world would reach an induced temperature increment of 1.5 °C compared to the pre-industrial scenario by 2040. This alarming increase was largely due to the anthropic activities related to our current economic and production life-style, which still relies on the oxidation of carbon-containing fossilized deposits. Since 2000, the global concentration of the main greenhouse gas, CO_2, has increased of about 20 ppm per decade, a rate that is 10 times faster than any experienced rise during the past 800,000 years (IPCC 2018).

Consequences of the climate change, including ocean rising levels, alteration and/or disruption of ecological-niches, air/water/soil pollution, are threatening our planet and our society. Both the governance institutes and the scientific community share the duty of dealing with this pressing issue, whereas the societal perception of the climate change is becoming sharper, as witnessed by the current protests of schoolchildren.

In 2015, by signing the Paris Agreement, several countries committed themselves to reduce the greenhouse gas emissions with the aim of maintaining the global average temperature below 2 °C above pre-industrial levels. Alongside with this agreement, the paradigm of the *circular economy* has imposed in the agenda of the policy makers. For instance, in the European Circular Economy package (European Commission, 2015) a transition towards a production model based "on the maintenance of the value of products, materials and resources in the economy for as long as possible and on the minimization of waste generation", is encouraged. From this new viewpoint, particular attention is given to the so-called *secondary raw materials*, i.e. those wastes that result from the primary production processes and that can be re-feed in the flow of an idealistically closed loop (European Circular Economy package, 2015). Secondary raw materials include crop waste, lignocellulosic residues, but also municipal solid waste, sewage,

syngas (mixture of H_2, CO and CO_2 derived from thermal gasification of biomass or other materials) and CO_2 waste streams [1, 2, 3].

Thanks to the cross-talk between engineering and biotechnological disciplines it is possible to exploit these renewable, low cost resources and to convert them into value-added products, like fine and bulk chemicals, biofuels, pharmaceutical compounds, nutraceuticals and bio-based materials with enhanced properties and new functionalities, such as biodegradability, compostability or biocompatibility [4].

1.2 Technological contribute towards a bio-based economy: microbial cell factories

1.2.1 Heterotrophic microbial cell factories

Currently, the bio-based production is mainly focused on the use of plant-derived sugars (sugarcane, molasses, whey, cellulosic material, etc.) as substrate to sustain microbe growth. These established processes rely on fermentation or on aerobic respiration of heterotrophic microorganisms, as extensively shown by literature. Acetone, buthanol, ethanol (ABE) fermentation by *Clostridium* genus [5], polyhydroxyalkanoates (PHAs) production by *Raelstonia eutropha* [6, 7], lactic acid production by lactic acid bacteria (LAB) [8, 9], ethanol production by *Saccharomyces cerevisiae* [10] are only representative examples.

The main disadvantage of heterotrophic microbial cell factories (MCF) depends on the cost of the carbon feedstock, which can represent a considerable percentage of the total cost of the process. Moreover, seasonality of plant-derived sugars does not guarantee constant amount, properties and quality of the input material [11, 12, 13].

1.2.2 Autotrophic microbial cell factories

On the other hand, autotrophic microorganisms do not need an organic carbon source to grow, because they evolved specialized systems to perform carbon fixation through the chemosynthesis (archea, acetogens) or the photosynthesis (microalgae, cyanobacteria, purple sulfur bacteria). This metabolic capability makes autotrophic MCF able to covey the production of added-value products while sequestering CO_2 from streams derived from industrial processes.

Chemosynthetic microbial cell factories

Chemoautotrophs exploit the oxidation of inorganic compounds (e.g. hydrogen gas and reduced sulfur, nitrogen and iron) or C_1 compounds (e.g. methane, methanol, formic acid, etc.) as source of energy for ATP synthesis and production of reducing equivalents which are subsequently used to convert CO_2 or (CH_4) into organic matter.

Several examples of bio-refineries based on chemosynthetic microorganisms already exist and some of them have been scaled-up in industrial settings. For instance, by combining biotechnological and chemical engineering expertise, LanzaTech has pioneered a gas fermentation process using anaerobic acetogenic microbes capable of fixing carbon oxides to produce Carbon Smart^{TM} products. Recently the company has set-up a commercial scale gas fermentation plant that uses emissions coming from the steel production as feedstock (https://www.lanzatech.com/section-carbonsmart accessed on 29 July 2019). Electrochaea with the BioCat project aims at producing renewable bio-methane from CO_2 and H_2. The biomethanation is carried out by a highly productive methanogenic Archea strain, and the process is operated at a lower temperature compared to the thermo-chemical methanation, resulting tolerant to contaminants and flexible. A pilot system has been built near Copenhagen, Denmark, and it includes the electrolyzer for H_2 production (1 MWe), the anaerobic digester for biogas production (with a composition of 60% methane and 40% carbon dioxide) and the methanation reactor (3800 L). The renewable gas obtained owns the necessary features (molecular composition, heating value, Wobbe number) for direct injection into the local 3-bar gas distribution grid (http://www.electrochaea.com/technology/ accessed on 29 July 2019).

Photosynthetic microbial cell factories

Photosynthetic organisms use water as electron donor and sunlight as source of energy for the synthesis of ATP and reducing equivalents (NADPH) which are used during the Calvin–Benson–Bassham (CBB) cycle to fix atmospheric CO_2.

Both photoautotrophic prokaryotic (cyanobacteria) and eukaryotic (microalgae) microorganisms have been exploited as hosts for the commercial production of chemicals and biofuels. MCF based on cyanobacteria will be discussed in detail in Chapter 2.

Microalgae are eukaryotic photosynthetic organisms simpler than plants showing faster growth, higher biomass yield and lower cultivation costs [14]. Nevertheless, being eukaryotic cells, they have specialized intracellular compartments (nucleus, vacuole, chloroplast, mitochondria, etc). The major complexity of microalgae, compared to the prokaryotic blue-green algae (cyanobacteria), makes them attractive hosts for the possibility of directly synthesize or temporarily store compounds in specific subcellular organelles (vacuoles), making even feasible the accumulation of toxic products [15]. Microalgae have been extensively investigated for their accumulation potentiality of natural (pigments, lipids, antioxidants, starch, proteins) and exogenous (plant terpenoids, bio-ethanol) compounds [16, 17, 18].

Lipid synthesis by *Chlorella vulgaris* for bio-fuel production constitutes a well- established platform and industrial settings for its massive cultivation and harvesting have been developed [19]. The freshwater microalga *Hematococcus pluvialis* is the major natural accumulator of astaxanthin, a carotenoid widely used as pigmentation source or as antioxidant in several industrial fields, including aquaculture, food industry, cosmetics and nutraceuticals. A two steps process, combined with nutrient limitation, is

generally advised for higher yield of astaxanthin from *H. pluvialis* [20]. During the first "green" stage microalgae are grown in closed photobioreactors under saturating, but not photoinhibitory, light condition to achieve maximum biomass growth rate. In the following "red" phase, performed in open ponds, cell proliferation is inhibited by high light intensities to induce astaxanthin accumulation [21].

The green microalgae *Chlamydomonas reinhardtii* and *Nannochloropsis gaditana* and the diatom *Phaeodactylum tricornutum* represent model organisms and they have been investigated as host for MCFs, since genetic tools to access both their chloroplast and nuclear genome are available. Proof of concept for squalene production [22], protein targeting in the thylakoid lumen [23] and diterpenoid synthesis [24] have been recently demonstrated in *C. reinhardtii. P. tricornutum* has been engineered to accumulate the high value omega-3 long chain polyunsaturated fatty acid docosahexaenoic acid (DHA) by expressing a Δ5-elongase from the picoalga *Ostreococcus tauri* [25]. By means of TALEN genome editing, triacylglycerol accumulation of *P. tricornutum* was enhanced 45-fold compared to the WT [26].

1.3   Metabolic engineering and synthetic biology for cell factories improvement

Even though many bio-based products have been showcased in the literature, only few of them reached the commercial scale because of some disadvantages mainly related to high costs of raw materials, recovery or purification. It is of paramount importance to ameliorate strain performance and to make the whole process competitive with the respective petrochemical counterpart [13]. Recombinant molecular biology techniques have hugely broadened the possibilities to improve and tune the metabolism of microbial host towards the formation of the desired product(s), leading to higher performances in terms of titers, rate (i.e., productivity) and yields (TRY metric) [27]. Moreover, genetic engineering interventions could address some of the major challenges associated with the MCF, such as the extraction of intracellular synthesized products (pigments, bio-lipids, PHA) and an increased tolerance to high concentration of product.

Metabolic engineering and synthetic biology provide a new approach to this purpose. Through metabolic engineering studies, it is possible to enhance or redirect the flux of specific metabolic pathways by genetically altering the enzymatic activities involved. Metabolic engineering makes use of genome scale metabolic models (GSMM), flux balance analysis (FBA) [28], flux variability analysis (FVA) [29] and elementary flux analysis [30, 31] to predict the phenotypic behavior of the cell. Synthetic biology refers to the development of the tools necessary to implement the genetic modifications in the biological system [32, 33]. A peculiarity of the synthetic biology is a bottom-up approach and the adoption of an electronic engineering perspective to design the synthetic parts that can be assembled and freely combined to build new modular pathways [27].

The construction of a catalog of well-characterized biological parts (e.g. the iGEM Registry of Standard Biological Parts) and standardized methods to assemble the "modules" is the end-goal of this discipline.

However, full characterization of biological modules, which would allow an effective transferability among different species, remains a challenge. This is mainly due to the fact that many parts are non-orthogonal with consequent interactions with other genes in the native and/or in the host strain metabolism [34]. Cell engineering approaches can be clustered in few categories including: pathway over-expression, transporter engineering, de-branching (i.e., elimination of competing pathways), removal of product consuming reactions, co-factor engineering, regulation of feedback mechanisms, precursor enrichment, and signal transduction engineering [35]. In some cases, it may be wise to introduce a non-native biosynthetic pathway into the metabolic network of a host microorganism. This choice could be driven, for example, by the availability of the entire genomic sequence of the host candidate, the presence of specific set of genetic tools, as well as the better characteristics of the phenotype (fast growth, absence of metabolic inhibition, etc.) or peculiar metabolic capabilities.

Chapter 2

Cyanobacterial cell factories: state of the art

Cyanobacteria are gram-negative prokaryotes recognized as the most ancient organisms capable of performing oxygenic photosynthesis [36]. A variety of morphology has been described inside the cyanobacteria phylum, including unicellular (*Synechocystis, Synechococcus, Prochlorococcus*) and filamentous strains (*Anabaena, Arthrospira, Nostoc*), some of them also presenting differentiated cell types. They can tolerate different environmental growth conditions, such as wide range of temperature, pH and water availability (both saline and freshwater) [37]. Metabolic capabilities are also diverse: they mainly grow photoautotrophically, but mixotrophic or chemoheterotrophic growths have been reported in some strains [38]. Certain filamentous genera (i.e. *Anabaena* and *Nostoc*) are known for nitrogen-fixing abilities thanks to the presence of specialized cells, called heterocysts, which encapsulate the O_2-sensitive nitrogenase enzyme performing an ATP-driven conversion of molecular nitrogen into ammonium [39]. Some unicellular cyanobacteria avoid oxygen mediated inactivation of the nitrogenase by temporarily separating the oxygenic photosynthesis (light period) from the nitrogen fixation (dark period) [40].

Cyanobacteria are natural producers of manifold interesting products, including polyhydroxyalkanoates (PHAs), pigments, vitamins, cyanophycin, fatty acids and amides [41, 42]. In addition, genetic engineering efforts have been made to re-direct their metabolism toward the accumulation of non-native products, such as alcohols [43, 44], hydrocarbons [45, 46], organic acids [47], fatty acids [48, 49], polyols [50]. Cyanobacterial biomass could be finally valorized as animal feed supplement or as fertilizer [51].

The biological features of cyanobacteria make them an attractive host for cell factories. The main advantages are summarized below:

- cyanobacteria need CO_2, light and water to grow. These limited nutrient requirements result into the double benefit of eliminating the cost of the carbohydrate feedstock and of avoiding the "food for feed" ethical issue. Indeed, since they can

be cultivated in non-arable locations they would not compete for water and land with agricultural crops;

- photoautotrophy can be exploited to directly convert CO_2 into valuable products [52];

- cyanobacteria can be cultivated in non-potable water. Some species, as *Spirulina platensis*, grow at alkaline pH and high salinity conditions, making them suitable for cultivation in wastewater [53]. The use of halotolerant species would also minimize the risk of culture contamination in photobioreactor systems. Moreover, cyanobacteria can contribute to the remediation of water by degrading pollutants or xenobiotics [54];

- cyanobacteria have a higher photosynthetic efficiency and a shorter life-cycle compared to higher plants [55];

- several species are genetically accessible and their genome has been fully sequenced and freely available on public database (Cyanobase) [56];

- easy to genetically manipulate. Most cyanobacterial strains are prone to natural transformation and homologous recombination. Moreover, toolbox for genetic engineering have been developed for model organisms [37, 57, 34].

Nevertheless, there are limitations and concerns about the implementation of cyanobacteria in large-scale industrial processes because of:

- slower division rate and lower productivity compared to heterotrophic host strains as *E. coli* and *S. cerevisiae* [34]. The model organism *Synechocystis* sp. PCC 6803, for instance, has a doubling time around 7-12 h [37]. Compared to heterologous biorefineries, the productivity of phototropic cell factories is, on average, about 100 times lower [58];

- fewer genetic tools specific for cyanobacteria in comparison to the heterotrophic counterpart. Moreover, the available molecular tools have been designed for model strains, as *Synechocystis* sp. PCC 6803, *Synechococcus elongatus* PCC 7942, *Nostoc* PCC 7120 and few others. A genetic toolbox for promising strains with shorter doubling time, like *Synechococcus elongatus* UTEX 2973 [59, 60] and *Synechococcus* sp. PCC 11901 [61], needs to be adapted;

- increased challenges in the bioreactor and outdoor cultivation system design. To mention few examples, light penetration into large photobioreactor is limited and circadian rhythm imposed by natural light availability requires flexible growth strategies [62].

2.1 Cyanobacterial photosynthetic and carbon-fixation systems

The photosynthetic machinery of cyanobacteria is located in the thylakoid membrane system, which is dispersed in the cytoplasm. The primary photosynthetic pigments of cyanobacteria responsible for harvesting solar radiation are the chlorophyll *a* (chl *a*) and the phycobilins (phycoerythrin, phycocyanins and allophycocyanins). The membrane-bound molecules of chl *a* are bound to the photosystem I (PSI) and II (PSII), whereas the phycobilins pigments are bound to the phycobilisomes (PBS), the mobile peripheral light-harvesting antenna that transfers the excitation energy to the photosystems. Besides the main photosynthetic pigments, cyanobacteria have also carotenoids (β-carotene and xanthophylls), which show both harvesting and photoprotective functions [63]. The water splitting takes place in the PSII reaction center, where molecular oxygen, protons and electrons are generated. The electron transfer chain (ETC) proceeds following a Z-scheme from PSII to PSI (linear electron flow) aided by several integral and soluble carriers, including plastoquinones, cytochrome b_6f, and plastocyanin. Electrons from the PSI reaction center are then transferred through the ferrodoxin to the ferredoxin-NADP$^+$ reductase that finally reduces NADP$^+$ to NADPH, concomitantly a proton gradient is generated across the thylakoid membrane that is utilized as proton motive force for the following ATP synthesis.

High light intensity causes photoinhibition, leading to a reduction in the photosynthetic capacity of the cell. PSII is the photosynthetic component most sensitive to high-light intensities, getting rapidly damaged and thus being continuously recycled. When exposed to high-light an imbalance in the rate of damage and repair processes occurs and photoinhibition leads to the production of reactive oxygen species (ROS) that inactivate PSII [64]. To preserve the activity of the photosynthetic machinery from the highly oxidizing chemistry of water splitting, efficient photoprotection mechanisms are of paramount importance. Among these, there are: fast recycling of the damaged PSII reaction center D1 subunit [65, 66]; expression of the flavodiiron proteins Flv1/Flv3 [67] and Flv2/Flv4 [68]; activation of non-photochemical quenching (NPQ) mechanism mediated by orange carotenoid proteins (OCPs) [69, 63]; and cyclic electron flow (CEF) activation [70].

Cyanobacteria evolved a carbon concentrating mechanism (CCM) to regulate the uptake and fixation of carbon dioxide. The accumulation of inorganic carbon in the cytoplasm is mediated by different CO_2 and HCO_3^- transporters [71]. Specific intracellular protein microcompartments, called carboxysomes, sequester the first enzyme of the Calvin Benson Bassham (CBB) cycle, Rubisco, which catalyzes the CO_2 fixation into a ribulose-1,5-bisphosphate molecule, and the carbonic anhydrase (CA) responsible for the HCO_3^-/CO_2 conversion [72]. Structural studies of the carboxysome at atomic resolution revealed that more than a thousand subunits form an icosahedral protein shell composed by smaller hexameric units in the faces and pentameric units at the vertices

[73]. The sophisticated and tightly controlled structure of the carboxysome is of fundamental importance to create a high CO_2 and low O_2 environment that enhances the carboxylase activity of Rubisco. Indeed, Rubisco is a bifunctional enzyme, showing both carboxylase and oxygenase activity, and it is a slow catalyst, with a turnover frequency between 1 and 10 s^{-1} [74, 75]. Therefore the carboxysome allows cyanobacteria to lower the oxygen concentration close to the catalytic site, thus reducing the oxygenase activity of the Rubisco that produces the metabolite 2-phosphoglycolate, instead of the 3-phosphoglycerate, which has to be converted by the cell through the photorespiration pathway with considerable CO_2 and energy losses [76].

2.2   Tools for synthetic biology in cyanobacteria

New molecular tools are increasing the potentiality of genetically manipulating several microbial hosts. However, compared to *E. coli*, the characterization of biological parts for bioengineering work in cyanobacteria is quite limited [77, 78]. Only recently, attempts to systematically organize and characterize genetic tools for these microbial hosts are spreading. For instance, a system called Cyanogate, a collection of a standardized modular cloning (MoClo) parts, has been developed and tested for the model organisms *Synechocystis* sp. PCC 6803 and *Synechococcus* UTEX 2973, with the aim of expanding the synthetic biology tools for cyanobacteria [79]. In particular, the system describes the generation of vectors and modules for marked/unmarked gene deletions using integrative vectors and transient multigene expression/repression systems using replicative vectors.

Characterized biological parts

Concerning transcriptional control, many native and heterologous promoters have been characterized in the model cyanobacterial organisms, including strong promoters, metal and metabolites inducible promoters and light-controlled promoters [57, 77]. The most common utilized strong promoters are accounted for the light-induced PsbA2 [80], the promoter controlling the transcription of Rubisco large chain, PrbcL, [81] and the PcpcB controlling the gene of the c-phycocyanin β-subunit [82]. Among the metal-inducible promoters, the Ni^{2+}-inducible PnrsB [83] and the Zn^{2+}-inducible Pzia [84] are some of the most representative. Finally, different promoters from *E. coli* have been characterized also in cyanobacteria, including the IPTG-inducible PtetR, Ptrc and PlacO [37, 57].

Translational control is crucial to achieve high enzymatic levels, and thus maximizing the conversion of substrate into products in industrial relevant strains. For this reason efforts to characterize the ribosome binding sites (RBSs), i.e. the sequences that recruit ribosomes to start the translation, are currently increasing also in cyanobacteria [85, 77, 86]. Riboswitches are also a precious tool to control gene expression. Precisely,

a riboswitch is a metabolite-inducible element composed of an aptamer sequence capable of inducing a change in secondary structure of mRNA, consequently modulating the translation efficiency, either repressing or activating it [87]. Even though their identification in cyanobacteria is not complete yet, some riboswitches have already been described in *Synechococcus elongatus* PCC 7942 [88], *Synechocystis* sp. PCC 6803 [89], *Synechococcus* PCC 7002 [90].

Genome editing in cyanobacteria

Since most cyanobacterial strains – *Synechocystis* sp. PCC 6803, *Synechococcus elongatus* PCC 7942, *Synechococcus* sp. PCC 7002 – are capable of natural transformation and homologous recombination [57], integrative plasmids are common vectors to stably insert a construct in the host genome [37]. However, specific features of cyanobacteria have to be taken into account for genetic manipulation. Polyploidy, that is the presence of multiple copies of their genome inside the cell, imposes the necessity of several round of segregation to completely knock-out or insert a gene, making the whole process time-consuming. The availability of neutral sites, that are loci from which no transcripts are expressed, is also a crucial issue for multiple gene insertions. Several neutral sites, both chromosomal and in plasmids, have been identified and protein expression induced by different combination of neutral sites and promoters have been characterized [91].

Trans- genetic modification with replicative vectors in cyanobacteria have been investigated even though the availability of plasmid is quite limited. Commonly used shuttle vectors are pSCR119, specific for shuttling DNA between *E. coli* and *Nostoc*, and plasmids based on the replicon RF1010, which are broad-host-range vectors suitable to different final destination cyanobacteria [37]. Native cyanobacterial plasmids represent a suitable tool to be exploited. For instance, the plasmid CA2.4 from *Synechocystis* can be used as an expression vector since it is stably maintained during cell divisions in abundant copy number [92].

To introduce multiple modifications, for instance, to delete multiple genes, different selection markers are necessary, because each gene is usually replaced by an antibiotic marker, which is used to select the recombinant mutant. However, the number of available markers is restricted, thus limiting the number of genetic modifications applicable. Alternatives to this method are the markerless selections, which have been widely used in model cyanobacterial hosts [34]. A common counter-selection method relying on the Ni^{2+} inducible toxic gene *mazF* from *E. coli* was developed for *Synechocystis*, and requires two plasmids for two consecutive selection rounds (see Material and Methods Chapter) [93]. Another markerless method developed for *Synechocystis* makes use of the *nptI-sacB* double selection cassette contained in a single vector, thus requiring only one transformation step [94].

Clustered regularly interspaced short palindromic repeats (CRISPR) techniques are currently becoming a valid alternative to classic cloning methods also for cyanobacteria [95, 96, 97]. This genome-editing technology allows single step modification of DNA

sequences to generate markerless knock-in, knock-out or point mutations in several species, thus accelerating the chromosome modification process. A variant of CRISPR, the CRISPR-interference (CRISPRi) method, has been successfully proved in *Synechocystis* to simultaneously repress the expression of 4 [42] and 6 genes [98] respectively, thus lowering the accumulation of carbon storage compounds (PHB and glycogen) in the first case, and preventing the consumption of long-chain acyl-ACP pool in the second. The efficiency of CRISPRi system has also been showcased in *Synechococcus elongatus* sp. PCC 7942, in which the genes involved in glycogen accumulation (*glgC*) and succinate conversion to fumarate (*sdhA* and *sdhB*) were suppressed [99], and in *Synechococcus* sp. PCC 7002, where the metabolic flux was redirected by down-regulating different genes towards the accumulation of lactate [100]. In the mentioned works, the authors used the nuclease-deficient Cas9 (dCas9) from the type-II CRISPR/Cas of *Streptrococcus pyogenes*, which can bind the target DNA without cleaving it. The RNA-dCas9 complex prevents the binding of the RNA polymerase or the elongation activity, leading to gene knock-down [101]. Another unconventional CRISPR systems, CRISPR/Cpf1, has been investigated in *Synechococcus*, *Synechocystis* and *Anabaena* [102]. Cpf1 from *Francisella novicida* is a RNA directed dsDNA nuclease that resulted to be nontoxic to cyanobacteria. It cuts 17 bp downstream of the recognized protospacer adjacent motif (PAM) with 5 staggered 5bp, thus preserving the PAM site that can be cut a second time. This system has been proved to be efficient for complex genetic modification in cyanobacteria which were not possible with previous existing Cas9-based technologies [102].

2.3   Improving cyanobacterial cell factories

Engineering of cyanobacteria can be carried out by acting at many levels, including the light and dark phases of the photosynthesis, and the metabolic pathways downstream of the CBB cycle.

Increasing the solar energy utilization efficiency

Cyanobacteria have an efficiency of light utilization, i.e., the efficiency in the conversion of light energy into chemical energy (glucose), of about 12% [103] and they are able to capture only part of the solar spectrum by the light-harvesting antenna system. Several approaches to remodel the cyanobacterial physiology have been explored so far to improve their capacity of solar energy capture and utilization [58].

Cyanobacteria mainly absorb light radiation in the range of 400-700 nm wavelength (i.e., photosynthetically active radiation (PAR)), with peaks falling in the 430-660 nm region, thus excluding all the infra-red radiations (> 700 nm) [104]. Moreover, the absorption capacity in the region between 450 and 550 nm, the so called green gap, is low for some cyanobacterial species [105]. For this reason, research investigation has been directed toward the expansion of the PAR spectrum also to the infra-red region and to cover the green gap.

Chlorophyll *d* and *f*, present in some cyanobacteria living in stomatolites or in tidal regions, show absorption peaks at 720 and 740 nm, respectively [106, 107]. The introduction of these red-shifted pigments in the photosynthetic reaction centers (PSI and PSII) could increase the exploitation of the solar spectrum, but their functionalization in heterologous hosts is currently challenging [108]. To complement the PAR spectrum in the green band, the introduction of green absorbing pigments, such as bacteriorhodopsins (for instance, the proteorhodopsin (PR) or the *Gleobacter rhodopsin* (GR)) could represent a feasible strategy [109]. Bacteriorhodopsins are light-driven ion pumps that transport protons from the cytoplasm to the extracellular space to generate an electrochemical gradient driving ATP synthesis. Recently, the characterization of a PSI deletion mutant of *Synechocystis* expressing a PR showed an enhanced growth rate compared to the control ΔPSI strain under photoheterotrophic, but not under photoautotrophic conditions. Probably the extra proton gradient generated by PR might influence the NADPH synthesis, thus hampering the photoautotrophic growth of the ΔPSI strain [110]. The GR from *Gloeobacter violaceus* PCC 7421 has also been considered as a complementary proton-pump in *Synechocystis*. GR did not appear to increase the growth rate of the derivative ΔPSI strain under photoheterotrophic condition, but it increased the proton motive force [111].

Another strategy to ameliorate the photosynthetic efficiency consists in the modulation of the response of cyanobacteria to high-light intensities so to increase the illumination tolerance. Indeed, in high-light conditions the rate of photon absorption mediated by the PBS is higher than the rate of photon utilization of the reaction centers of the photosystems. The excess of light-energy is therefore dissipated through NPQ in order to prevent photoinhibition and photodamages [112]. To circumvent this wasteful dissipation, that reduces the photosynthetic efficiency, the modulation of the size and composition of PBS has been proposed as a strategy to prevent the over-absorption of photons by single cells [113, 112, 114]. In this way, every single cells would absorb less light and the availability of light for the inner regions of the culture vessel would increase, thus the light penetration in the culture volume would result improved. The potentiality of this approach has been proved in cyanobacteria by means of a phycocyanin-deficient mutant of *Synechocystis* sp. PCC 6803 which exhibited higher biomass accumulation with respect to the wild type (WT) under high light condition (> 800 µmol photons/m^2/s) [112].

Enhancing the carbon fixation capabilities

Improving the carbon fixation could represent a valid strategy to increase the flux through the metabolic network of cyanobacteria, leading to higher availability of intermediate metabolites that can be rerouted to target pathways and/or to enhance the biomass growth. For this reason, Rubisco, the major carbon-fixing enzyme, is a key target of several studies [115, 116]. For instance, the overexpression of Rubisco in cyanobacteria has been investigated by Liang and co-workers [116] who engineered mutated

strains of *Synechocystis* sp. PCC 6803 expressing 2.1 and 1.4 times the amount of Rubisco of the WT allowing faster growth and increased photosynthetic activity. As mentioned above, Rubisco is a bifunctional enzyme, showing both carboxylase and oxygenase activity [74, 75]. Protein engineering of Rubisco to improve either its selectivity for CO_2, thus decreasing the susceptibility to O_2, or its catalytic activity, results challenging because of the complex structure of this protein complex [117, 75]. An alternative solution to face the energy and CO_2 losses associated to the photorespiration cycle, consists in defining synthetic by-passes to re-assimilate 2-phosphoglycolate into the CBB without carbon loss [118].

Recently, *in silico* and *in vitro* studies have been targeted to discover other enzymes with carboxylase activities, potentially more efficient than the Rubisco [119]. Using rational design approach, a propionyl-CoA synthase from *Erythrobacter* sp. NAP1 and an acrylyl-CoA reductase from *Nitrosopumilus maritimus* have been engineered with improved CO_2 binding and kinetic parameters [120]. The structure of the most efficient natural CO_2 fixing enzyme, the enoyl-CoA carboxylase/reductase (20 fold higher catalytic rates compared to Rubisco), has recently been characterized, widening the knowledge about the C-fixation mechanism [121].

Another target for increasing carbon fixation is the phosphoenolpyruvate carboxylase (PEPc) enzyme, which utilizes HCO_3^- and phosphoenolpyruvate to form oxaloacetate and inorganic phosphate. In so doing, this enzyme provides carbon skeletons to the nitrogen metabolism in cyanobacteria and in C3 plants and results more efficient than the Rubisco in CO_2 fixation. Durall and co-workers [122] tested the effect of the overexpression of PEPc in *Synechocystis* sp. PCC 6803. Under low light intensities, when the reducing equivalents and the energy production are limited and the Rubisco's carboxylase activity is reduced, the presence of extra amounts of PEPc produced an enhancement of the growth rate of the cyanobacterium [122].

Expanding or improving the CBB-downstream metabolic pathways

The introduction of new synthetic pathways and/or the improvement of the native metabolic network of model cyanobacteria is a well-established and expanding research field as witnessed by the wide literature available [123, 124, 15, 125, 126]. For instance, proof of principle and/or optimization of the production of ethanol [127], lactate [128], polyhydroxybutyrate (PHB) [129, 130], 2,3-butanediol [131, 43], 1-butanol [132], ethylene [133, 45], 1,3-propanediol [134], non-native pigments [135], polyunsaturated fatty acids (PUFAs) [136], amino acids [137], hyaluronic acid [107] etc. in cyanobacteria have been showcased to date.

Metabolic engineering schemes often involve some central intracellular intermediates, also referred to as "branching points"[41], which are then converted by the inserted heterologous enzymes into the compound of interest (COI). Common features of these

intermediates are i) a relatively short distance, in terms of number of enzymatic reaction steps, from the central metabolisms (i.e., the CBB, the glycolysis, the pentose phosphate pathway) and ii) a high abundance. Widely exploited metabolites for rerouting metabolic flows are pyruvate, dihydroxyacetone phosphate (DHAP), acetyl-coenzyme A (CoA), fructose 6-phosphate (F6P) [124, 15, 41, 138]. Also metabolisms with low flux, such as the methylerythritol phosphate (MEP) pathway, through which cyanobacteria synthesize carotenoid precursors, have been genetically engineered. Precisely, strategies to enhance the MEP pathway have been advised for the production of long chain isoprenoids and isoprene for fuel jet [139, 140, 85, 141].

With the exception of the upstream acetyl-CoA, that can be tapped to produce acetate [142], 3-HB [143], acetone, 1-butanol and isopropanol [138], and the intermediate 2-oxoglutarate, for the production of ethylene [45, 133], the tricarboxylic acid (TCA) cycle is an underutilized target in cyanobacterial metabolic engineering works. The flux into the TCA cycle is low, as suggested by the small pool size of its intermediates compared to *E. coli* pool sizes [144], and its function in cyanobacteria remained obscure for long time. Indeed, since cyanobacteria obtain ATP and NADPH necessary to sustain the growth through photosynthesis, the TCA cycle in these microorganisms mainly plays an anaplerotic rather than an energetic function. Even under photomixotrophic growth conditions the oxidative pentose phosphates pathway (OPPP) is preferred to the TCA cycle to generate reducing equivalents [145, 144]. Moreover, the TCA cycle in cyanobacteria, including *Synechocystis* sp. PCC 6803 [145] and *Synechococcus* sp. PCC 7002 [146], is different from the traditional cycle since it lacks two enzymes which act consecutively to convert 2-oxoglutarate to succinyl-coA and then to succinate [147, 148]. The cycle is completed through two routes: i) the γ-aminobutyric acid (GABA) shunt [148] or ii) the Oxo/Sucsem/Suc route [82]. These properties of TCA cycle of cyanobacteria suggest that, in order to enhance the flux toward this pathway, the reduction or truncation of competing pathways, such as the OPPP, is needed especially in dark condition [144, 149]. Similarly, the elimination of competing pathways deriving from PHB [42] and glycogen [150] accumulation, has been utilized so that more carbon could be diverted towards the formation of the COI.

Strategies that aim at increasing the level of precursors or intermediates necessary for the production of the COIs have also been proposed. For instance, the overexpression of phosphoketolase combined to the modulation of the nitrogen levels, led to an increased production of acetyl-CoA, which can be exploited to synthesize *n*-butanol [151].

When an oxidoreductase mediated step is required to complete a synthetic pathway, the design process should comply with the cofactors balance of the host cell. In cyanobacteria the most abundant redox cofactor is NADPH, which is produced during the light reactions of photosynthesis [152]. For this reason, a NADPH-dependent enzyme should be preferred to a NADH-dependent one when possible, otherwise, the expression of a trans-hydrogenase for the conversion of NADPH to NADH could be considered to optimize cofactor availability. For instance, the latter approach has been

applied to a lactate-producer strain of *Synechocystis* whose productivity was enhanced by expressing an energy indipendent soluble trans-hydrogenase concurrently with a lactate dehydrogenase (LDH) converting pyruvate into lactate [128].

The export is an important aspect of the engineering process, especially for toxic COIs, since specific transporters for compounds produced heterologously might not be available or might not be expressed at the level requested for efficient transport [153]. As reported for other strains, as *E. coli*, the absence of an effective efflux system for the product could lead to growth deficiencies and cell size increase, due to accumulation of compounds which alter the intracellular balance of metabolites and redox cofactors [154]. Korosh *et al.* [137] investigated lysine production in *Synechococcus* sp. PCC 7002. In order to achieve extracellular efflux of this molecule, they introduced a heterologous lysine transporter, thus avoiding fitness hamper of the producing-strain.

2.4 Challenges to the industrial application and possible solutions

The effective application of MCFs in industrial settings is threatened by the genetic instability of the engineered strains that causes decreases in productivity [155]. This phenomenon is related to the evolvability of microbes which, undergoing several cell divisions, can acquire genetic mutations. Quite often the production of the COI results expensive for the economy of the cell in terms of carbon commitment and resource allocation. Cells that accumulate mutations in the synthetic pathway, and thus loose the production trait, will therefore experiment a fitness gain reverting to the WT phenotype. These retro-mutant cells will be selected and fixed inside the population and will eventually outcompete the slowest cells, i.e., the producers.

Genetic instability is an issue common to all MCFs, but it is especially experienced in those that require long period of cultivation to reach high product titers, because more generations occur and, consequently, the probability to accumulate mutations increases. This is the case of cyanobacteria-based processes, where the achievement of high product titers generally needs sustained productivity for prolonged cultivation [156]. However, so far knowledge about the genetic instability in engineered cyanobacteria is limited, because in many studies present in literature the productivity is usually monitored for relatively short cultivation periods (< 30 days since the generation of the mutant strain) [157].

Genetic instability in cyanobacteria

Different cases of productivity decrease related to the inactivation of the synthetic pathways have been reported in engineered cyanobacteria [45, 128, 158, 159, 160]. Indeed, random mutations affecting the transcription or translation of the involved enzymes are likely fixed because they restore the original fitness [157].

Sequencing analysis of the inserted expression cassette revealed that gene inactivation often occurs in mutational hot spots which usually consist of repetitive motifs [161, 45, 128]. To circumvent gene inactivation, a strategy could be the design of a new version of the expression cassette carrying silent mutations in the identified mutational hot spots and preserving the correct amino acid sequence. This strategy has been successfully applied to an ethylene producing strain of *Synechocystis* sp. PCC 6803 in which the inserted *efe* gene was opportunely modified allowing the mutant to maintain ethylene production over several serial sub-cultures [45].

As mentioned before, the production of a COI might lower the cell fitness because of possible interference with many cellular processes, including: i) depletion of metabolic intermediates, ii) accumulation of toxic intermediates and/or of the COI itself inside the cell (if it has toxic or osmotic effects, for instance) iii) competition for the RNA polymerases or ribosomes, causing transcriptional and translational imbalance, respectively.

Since different constraints can be responsible for the loss of productivity, it is important, though challenging, to discern which is the major contribution in order to devise a shrewd metabolic engineering strategy [156]. In some producing strains it has been possible to identify the burden associated to the observed instability. This is the case of a lactate producing strain of *Synechocystis* sp. PCC 6803 carrying an LDH enzyme for the conversion of pyruvate into L-lactate [162]. In this work, the authors enhanced the activity of LDH by using increasing concentrations of an allosteric regulator, which resulted into a higher initial production rate of lactate. However, in the latest growth phase, there was a drop in lactate production, due to the accumulation of mutations inside the inserted *ldh* gene. Since the conversion of lactate was achieved by modulating the enzymatic activity rather than by increasing the level of expression of the enzyme, the phenotypic instability unlikely derived from a burden at the protein level. On the contrary, the authors hypothesized that the burden was mainly related to the diversion of carbon from the biomass to the product synthesis. Such results indicate that, besides the optimization of the genome stability (e.g. through optimized gene design, removal of mobile genetic elements, elimination of gene inactivation systems), also a compromise between microbe's fitness and biotechnological interest in high production must be found.

Testing the genetic stability of engineered strains

A common method to study the genetic stability of an engineered strain consists in the adoption of evolution experiments in which the microorganisms are kept under a defined selection pressure for a long period of cultivation. Evolution experiments can be carried out by means of serial batch cultures or through continuous culturing (chemostat or turbidostat). The first method is the simplest, since it is generally conducted in flasks and it is implemented by iteratively transferring a certain amount of the culture into fresh medium and thus initiating every time new rounds of growth. On the other hand, continuous culturing modes represent sophisticated methods with the advantage

of allowing a more fine control of the selection pressure, making easier to understand the connection between the adaptive phenotype and the phenotypic consequences.

Independently of the chosen method, evolution experiments aim at monitoring the selection of mutations arising into an initial monoclonal population [163, 164]. In the specific case of the evaluation of genetic stability, the interest is directed towards the detection of the retro-mutants, i.e. cells that, by losing production capacity, restore the WT fitness, which can be observed as an increased growth rate. Despite their unquestionable utility, these experiments require notable efforts in terms of time and resources, thus *in silico* models to predict the dynamics of retro-mutants population would be a useful tool. Simulations of large-scale fermentations to predict arising retro-mutants have been performed for heterotrophic microorganisms, such as *E. coli* [165, 166], however to the best of author's knowledge, mathematical models describing retro-mutants appearance in photo-autotrophic microorganisms are missing. A discussion about the dynamics of retro-mutants in a population of phototrophic microorganisms is presented in Chapter 5.

Growth-uncoupled production strategies

A feasible strategy to avoid the competition for carbon resource needed for the growth of the biomass and for product formation consists in delaying the activation of the synthetic pathways until the culture is no more growing, i.e. during the stationary phase of a batch cultivation. To realize this decoupling, it is possible to act at the expression level, for instance by using inducible promoters to trigger the synthetic pathway at specific growth phases. In this way the possible differences in growth rate between the producers and the retro-mutants would be minimized, because during the exponential phase they would have in principle the same phenotype. On the other hand, when they enter the stationary phase even if the burden becomes maximum—because the producing pathway has been activated—the growth advantage of the retro-mutants would not be sufficient to outcompete the producing cells. In general, inducible promoters must guarantee no leaking activity in absence of the inducer, which is essential especially when the products of the inserted genes are toxic. In cyanobacteria, few inducible systems in which transcription is induced by temperature [167], light [168], IPTG [169], metal-ions [170], anhydrotetracycline [171] and rhamnose [172], have been characterized.

The uncoupling strategy has been extensively studied in WT chemoheterotrophic organisms, in which is well known that when cells start to experience nutrient limitation in presence of a surplus of carbon and energy, the accumulation of some storage compounds (PHB, etc) is triggered. This overflow mechanism has also been investigated in cyanobacteria, even though the strict linkage between energy management and growth and carbon partition in photoautotrophs makes more difficult to set the experimental conditions that allow overflow. Recently glycogen metabolism has been found to play an important role in energy balance, besides its storage function. Indeed,

glycogen is usually produced as a carbon storage compound under nitrogen depletion conditions. In a *Synechocystis* sp. PCC 6803 mutant with impaired glycogen synthesis an overflow metabolism to deal with the excess of energy input is triggered. Precisely, organic acids (pyruvate and 2-oxoglutarate) are released in the extracellular medium when this mutant is grown under high light intensities, reaching the highest titers during the stationary phase [173]. The excess of photosynthate in glycogen-deficient mutants could be therefore exploited to drive the overflow of the desired metabolite, even in absence of nutrient starvation conditions.

Growth-coupled production strategies

The alternative strategy that aims at minimizing the burden on the microbial growth is the growth-coupled approach. In this case, the rational consists in aligning the synthesis of the COI with the cell growth of the host strain and can be achieved by coupling the product formation to the energetic, the catabolic and the anabolic metabolisms. Attempts to link the production of the COI to the regeneration of energy or redox cofactors have been undertaken in chemoheterotrophic organisms, however in photoautotrophic organisms, due to the complex regulation of the energetic metabolism, the implementation of this strategy results challenging. Theoretical approaches have been proposed for growth-coupled production associated to energy and redox cofactors based on *in silico* simulation of genome scale model of cyanobacteria [174, 152, 175, 176], however few experimental validations are available. From modeling analysis emerged that this goal can be achieved, for instance, by reducing the ATP/NADPH ratio produced by the photosynthetic electron transport chain to a value which is below that required for biomass formation. The idea is that by removing the cyclic and the various alternative electron flows present in cyanobacteria, the ATP and the NADPH will exclusively derive from the linear electron flow, generating a sub-optimal ratio of these energetic molecules. Consequently, the synthesis of the COI would be used as a sink to lower the excess of redox cofactors (NADPH) and it would become mandatory in order to adjust the ATP/NADPH ratio balance necessary for the growth [177].

On the other hand, there are strategies that seek for coupling product formation with the catabolic or anabolic metabolism of the cell [178, 142, 179]. In the case of the coupling to the anabolic metabolism, the goal is to create a stoichiometric dependency between the product formation and biomass synthesis, so that the production of the COI becomes strictly necessary for growth. Thanks to the analysis of GSMM and computational framework, as OptKnock [180], it is possible to identify, respectively, the key reactions (by someone referred to as "anchor reactions" [178]) and the metabolic changes that enable the establishment of a growth-coupled accumulation. Suitable targets are the anabolic reactions that produce side-products together with biomass precursors. The side-products can indeed be considered as growth-coupled compounds, because their formation is essential for the cell growth, whereas their re-utilizaion is not. By deleting the re-utilization pathways of the side-products, it is possible their
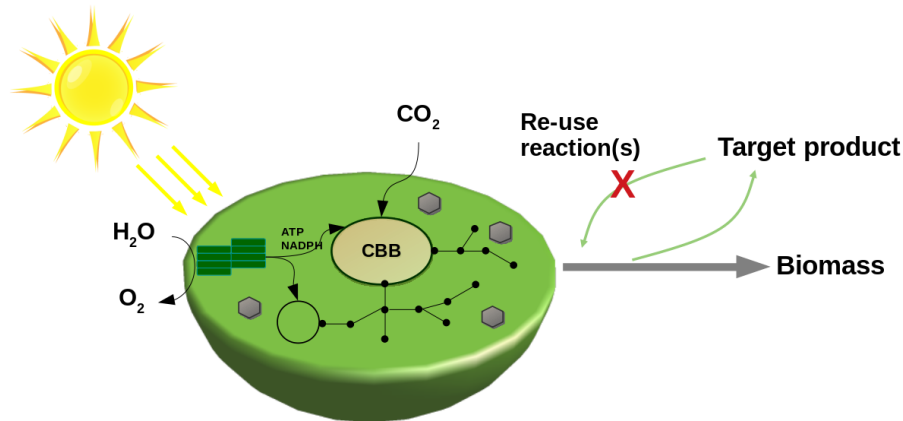
Figure 2.1: Schematic representation of a general growth-coupled production strategy in a cyanobacterium. In growing cells, a by-product (target product) deriving from an anabolic process can be accumulated if its consumption pathways are removed. CBB indicates the Calvin–Benson–Bassham Cycle.

stable accumulation (Figure 2.1).

Recently, an algorithm called "Find Reactions Usable In Tapping Side-Products" (FRUITS) to search these key reactions has been developed [142]. By analyzing the GSMM of *Synechocystis* sp. PCC 6803 and by allowing a maximum of 4 gene deletions, FRUITS identifies 9 candidate metabolites. Furthermore, the algorithm provides the computed maximum biomass formation rate and the minimum flux towards the candidate compounds. The target metabolites are generated as side-products of reactions involved in biomass precursor synthesis, therefore they are not directly used in anabolic pathways. If the native re-cycling routes of these compounds are truncated by gene removal, it is possible to achieve their accumulation without altering the microbial fitness. Since the acquisition of removed genes is unlikely, a production process based on a mutant engineered with this approach is expected to be stable for a considerable long period.

This strategy has been experimentally validated in *Synechocystis* sp. PCC 6803 for the production of acetate [142] and fumarate (Chapter 4.2), but it is potentially applicable to every organism with a GSMM available. Nevertheless, it is worth noting that by using the FRUITS approach only a limited number of compounds can be produced, because the key reactions identified by the algorithm must satisfy strict requirements such as i) being anabolic reactions that produce a side-product and ii) not being involved in the intracellular redox-balance [156]. Therefore, strategies to enlarge the pool of target compounds should be devised. One solution, applied to malate synthesis, is proposed in Chapter 4.3.

2.5 Towards the scale-up of photosynthetic cell factories

Despite the potential economical and biotechnological relevance of processes based on photosynthetic organisms, large-scale applications of cyanobacteria and microalgae are relatively limited [18]. Considerable efforts are directed towards strain improvement to obtain high yields, rates, productivity and genetic robustness, and to make the process competitive with the current – often petrochemical – production counterpart. In particular, the carbon partitioning, i.e. the fraction of fixed carbon that is utilized by the cell for product formation, has become a common parameter to evaluate the success of a metabolic strategy [41]. However, metabolic optimization of the microorganism is only one of the action necessary to boost the up-scaling of photosynthetic cell factories. Indeed, process design is of paramount importance to tackle different operative issues emerging at the level of biomass cultivation, product recovery and purification.

The major issue in the cultivation of photosynthetic microorganisms is the light supply. The solar radiation would be the cheapest and the most sustainable solution, even though its utilization for photoautotrophic microorganisms' cultivation poses some constraints. Firstly, it implies day-night cycles that usually cause minor productivity because cells do not grow in the dark [181]. Secondly, the latitude at which the cultivation systems operate influences the availability of light on a seasonal time-scale. For these reasons, artificial illumination or mixed systems are generally preferred [182].

Both closed photobioreactors and outdoor open reactors suffer from poor light penetration which is due to the decrease of light along the light-path. The latter is the sum of two contributions, namely photon absorption by the organisms and cell scattering. Several configurations of photobioreactor and outdoor open reactor have been proposed to face this problem. The most promising aims at minimizing the light path, such as the case of flat panel reactors characterized by very short light path (< 2 cm) which showed higher performances in term of biomass concentration and volumetric productivity [62]. Another possibility to reduce the light decrease is to irradiate the culture directly from the inside of the cultivation vessel, by means of optical fibers or LEDs.

The photosynthetic efficiency (i.e. the percentage of solar energy converted into biomass) is another factor that can be affected by the photobioreactor design. Recently, a close photobioreactor in which an ethylene producing strain of *Synechocystis* is energized by red monochromatic LED has been proved to be more efficient than reactor illuminated with white light [183]. A wavelength of about 650 nm is, indeed, optimal for *Synechocystis* growth and yields increased biomass.

As mentioned in previous sections, high light intensities are dangerous for photosynthetic cells, causing photoinhibition. However, by optimizing photobioreactor geometry it is possible to circumvent photodamages of cultures exposed to photoinhibitory light intensity. Precisely, by enhancing the ratio between the volume per ground area of

the photobioreactor it is possible to dilute the solar radiation and, thus, improving photosynthetic efficiency. Configurations that optimize this ratio are the top illuminated vertical ones, such as flat panels and vertical tubular photobioreactors [62, 184, 18].

High concentrations of O_2 can inhibit photosynthetic activity, whereas low concentration of CO_2 can limit the C-fixation rate[185, 186]. For this reason, another essential factor to take into account for the up-scaling is the gas exchange of O_2 and CO_2 inside the culture volume which can be addressed thanks to specific devices. The apparatus for controlling the gas-liquid transfer can be either placed inside (i.e. in bubble column, flat-panel and airlift) or outside (i.e. tubular photobioreactor) the cultivation vessel [62].

The risk of biological contamination threatens both open pond cultivation and, to a lesser extent, closed photobioreactors. In the case of open ponds, the contamination can be controlled by working at extreme environmental conditions, such as extreme pH, high nutrient concentrations or high salinity. However, this strategy results only applicable to tolerant species such as *Spirulina*, *Chlorella* and *Dunaliella*. For less tolerant species, the use of closed systems can be useful to prevent contamination. On the other hand, sterilization of the media, use of antibiotic and utilization of chemicals to clean the containers and all the materials represent an economical and environmental cost. Opportune genetic modifications can help to preserve axenic conditions without need of antibiotics or sterile conditions. For instance, Loera-Quezada and co-workers [187] engineered *C. reinhardtii* to make it able to grow on phosphite as a sole phosphorous source. Microalgae can use only phosphate as source of phosphorus, whereas other reduced forms of phosphorous are non-metabolizable. Therefore, the mutant generated is capable to become the dominant species in a mixed culture uniquely fertilized with phosphite.

Downstream operations account for a large percentage of the cost of the process and need to be improved. The cost for the biomass harvesting depends on the cultivation system, ranging from 5-7% for closed system to 23% for raceways, of the total [18]. After the separation of the biomass from spent medium, it is necessary to dry and/or to extract the biomass, or to recover the compound from the supernatant. Environmentally sustainable solvents have been considered for the extraction process. For instance, instead of the classic chloroform/sodium-hypochlorite methods for PHB extraction, methods based on ionic liquid and other non-halogenated solvents are under investigation [188, 189].

In the case of secreted compounds, continuous recovery has been proposed as an economically viable alternative [164]. Instead of separating the biological conversion from down-stream processes in an integrated product recovery these steps occur simultaneously. This system would prolong production times and increase the volumetric productivity of photobioreactor, mainly because through continuous removal of the desired molecule possible product toxicity is minimized. However, it is fundamental that the separation technologies employed guarantee the availability of light, CO_2 and the other nutrients necessary for growth and that cell lysis due to stress factors (shear, nutrient, temperature or chemical stress) is minimized. Depending on the nature of the

product and photobioreactor characteristics, different typologies of product recovery can be used, including *in situ* (i.e., recovery phase inside the cultivation volume) and in stream (i.e., separation technology outside the bioreactor) [164].

Chapter 3

Material and Methods

3.1 *In silico* simulation and tools

The genome-scale metabolic model (GSMM) iJN678 [174] was used to simulate light-limited photoautotrophic growth of *Synechocystis*. All the details concerning the constraints imposed to perform metabolic flux analysis through Flux Variability Analysis (FVA) [29] and Flux Balance Analysis (FBA) [28] are reported in [142]. FBA and FVA were performed using PySCeS-CBMPy [190] (http://cbmpy.sourceforge.net) in combination with ILOG CPLEX Optimization Studio (IBM) under an academic license. Additional visualization of modeling simulations were carried out using a resource specifically developed for *Synechocystis* [191] available at the FAME online modeling environment [192].

3.2 Strains and general growth conditions

Molecular cloning was carried out in *E. coli* DH5α grown at 37 °C in LB medium, either liquid in flask with a shaking speed of 200 rpm, or solidified in plates (by adding agar 1.5% w/v). In order to propagate a specific plasmid, the appropriate antibiotics were added to the culture medium, with a final concentration of 100 μg mL^{-1} for ampicillin and 50 μg mL^{-1} for kanamycin. A glucose-tolerant strain of *Synechocystis* sp. PCC 6803 (hereafter *Synechocystis*), obtained from D. Bhaya, University of Stanford, Stanford, CA, [193] was used in this study. All the strains of *Synechocystis* (i.e., WT and constructed mutants) have been grown in BG-11 medium [194] supplemented with 10 mM TES-NaOH (pH 8.0) as a buffer, at 30 °C in a shaking incubator (Innova 43, New Brunswick Scientific) at 100 rpm, under constant moderate white-light illumination ($\sim$ 20 μmol photons/m^2/s, measured with a LI-250A light meter, LI-COR). For *Synechocystis* mutants' selection, the medium was supplemented with kanamycin (final concentration of 50 μg mL^{-1}) or nickel sulfate (final concentration of 5.3 mg L^{-1}). Cell growth was monitored by measuring the optical density at 730 nm wavelength (OD$_{730}$) in the

spectrophotometer (Biochrom WPA, Lightwave II).

3.3 Plasmids and generation of *Synechocystis* mutants

3.3.1 Markerless deletion method

The strains and plasmids used in this work are listed in Table 3.1 shown at the end of this Chapter. In order to knock-out the genes involved in this study, namely *fumC* (fumarase C), *zwf* (glucose-6-phosphate-1-dehydrogenase), *me* (malic enzyme), *mdh* (malate dehydrogenase) and *sll1314* locus (putative C_4-dicarboxylate transporter), from *Synechocystis* a markerless deletion method has been used, as described in [142]. Briefly, two plasmids are needed for two consecutive transformation rounds. The first plasmid contains the up- and downstream homologous regions ($\sim$ 1 kb each) of the target gene. The second plasmid, in between the two homologous regions, carries a selection cassette composed of a kanamycin resistance and a nickel-induced mazF expression fragment [93]. MazF is an endoribonuclease that cleaves the mRNA at the ACA triplet sequence, acting as inhibitor for protein synthesis [195]. In the first round of transformation, the native locus in the chromosome of *Synechocystis* is replaced by the selection cassette through homologous recombination, and addition of kanamycin to the culturing medium allows selecting the positive colonies (Figure 3.1a). During the second round of transformation, the fully segregated selection cassette is removed from the chromosome by using the plasmid containing just the homologous regions. In this case, the recombinant colonies are those able to grow in a nickel supplemented medium (Figure 3.1b).

3.3.2 Construction of plasmid for markerless deletions

To build the plasmids, the corresponding homologous regions flanking the target genes were amplified from the genomic DNA of *Synechocystis*, and subsequently fused together using Herculase II Fusion DNA Polymerase (Agilent Technologies). In this step a restriction site in between the two fragments has been inserted. The fused fragments were gel extracted and purified (Stratec Molecular) and then adenylated to their 3' end using Taq DNA polymerase (Thermo Scientific). The extra adenosine ("A") allows the TA cloning of the fragments in the BioBrick "T" vector pFL-AN [82], resulting in the plasmids containing the up and down regions for homologous recombination (pWD060, pWD084, pWD71, pWD73, pWD05) (Table 3.1). The selection cassette from pWD42 [196] contains either an XbaI or SpeI restriction site on both sides and can therefore be inserted into the previously built plasmids, obtaining pWD061, pWD085, pWD72, pWD74, pWD06 (Table 3.1). All the fragments amplified were confirmed by Sanger sequencing at Macrogen Europe (The Netherlands), and the primers used are listed in Table 3.2, shown at the end of this Chapter.
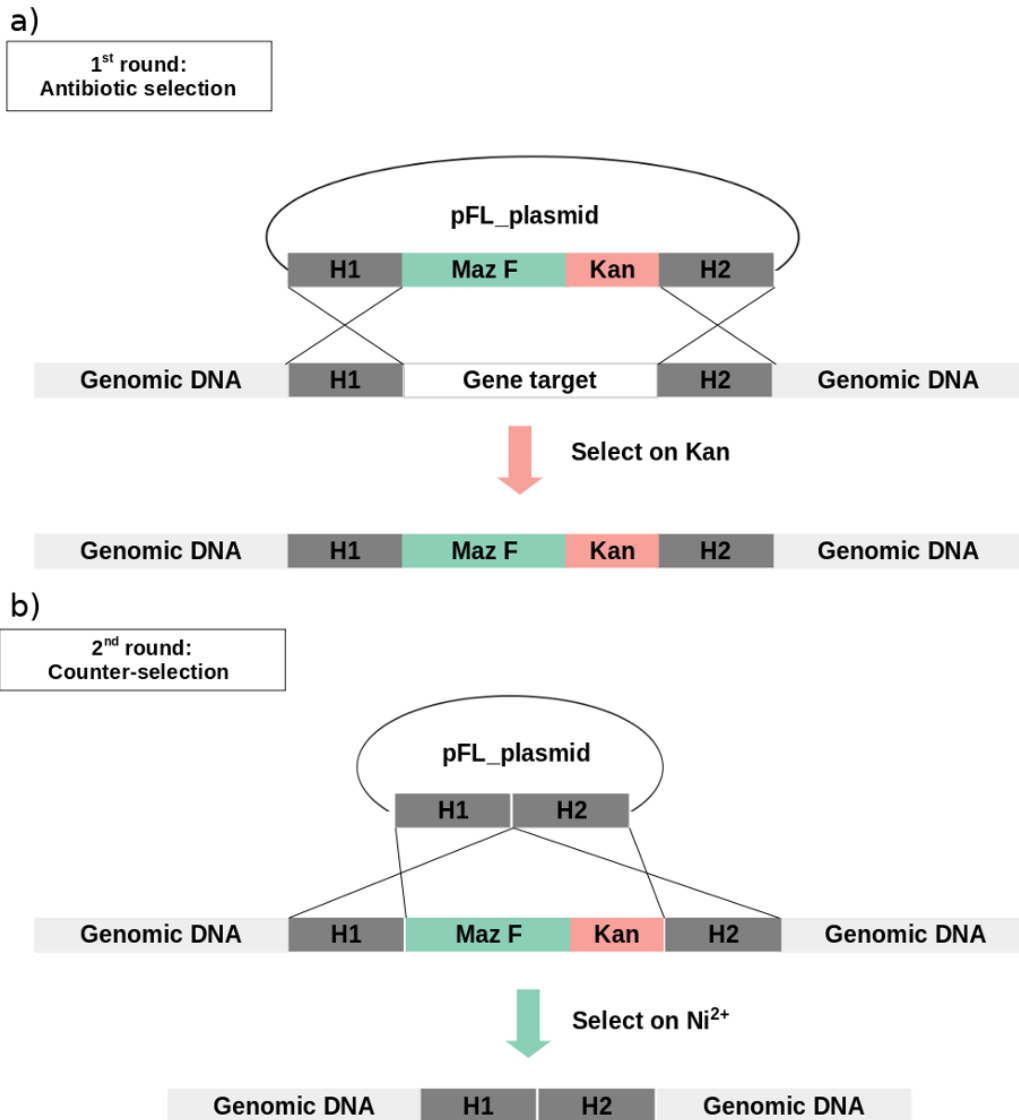
Figure 3.1: Schematic representation of the markerless deletion method described in [93]. a) In the first round of transformation the target gene is removed from the genomic DNA by replacement by the H1-MazF-Kan-H2 cassette. Recombinant colonies are selected on kanamycin supplemented medium. b) In the second round of transformation fully segregated selection cassette is removed from the chromosome by homologous recombination with H1-H2 regions. Recombinant colonies are selected on nickel supplemented medium.

3.3.3   Integrative vector for FumC overexpression

To overexpress the fumarase C enzyme (FumC) in *Synechocystis*, *fumC* gene from *E. coli* was amplified by Herculase II Fusion DNA Polymerase (Agilent Technologies) introducing two restriction sites, i.e. NdeI to the 5' end and BamH1 to the 3' end. The fragment was purified (Stratec molecular) and cloned in between the two homologous regions to the neutral site *slr0168* of the integration vector pHKH001 [128] under the control of the cpcBA promoter and the native RBS sequence of the *cpcB* gene, resulting in pBB1. All the fragments amplified were confirmed by Sanger sequencing at Macrogen Europe (The Netherlands), and the primers used are listed in Table 3.2, shown at the end of this Chapter.

3.3.4   Tranformation procedure

To transform *Synechocystis* with the plasmids, fresh cells were collected either from the plate or from liquid culture ($OD_{730} \sim 1$), and washed twice with fresh sterile BG-11 medium through centrifugation (5000 rpm, 5 min, Himac CT 15RE Centrifuge). Cells were then concentrated to a total volume of 200 μL ($OD_{730} \sim 2$), mixed with the specific plasmid to a final concentration of $10\,\mu g\,mL^{-1}$ and illuminated for 5-6 h with white light of moderate intensity ($\sim 50\,\mu mol$ photons/m^2/s). At the end of the incubation the mixture was spread on a commercial membrane (Pall Corporation) lying on a BG-11 agar plate and illuminated for further 16-24 h. The membrane was then transferred to a new BG-11 plate containing the appropriate selection marker (kanamycin in the first round, nickel sulfate in the second round). Positive colonies, which grew in the presence of the selective pressure, were submitted to PCR confirmation. Segregation was monitored by using the primers pairing with the homologous regions of the target genes listed in Table 3.2 (shown at the end of this Chapter) and several cycles of growth in liquid culture were performed when necessary.

3.4   Cultivation modes

3.4.1   Batch cultivation

Batch cultivation experiments were carried out in a Multi-Cultivator (MC1000-OD, PSI, Czech Republic), with emitted light intensity controlled through a LED panel, equipped with "cool-white" LEDs (PSI, CZ). BG-11 supplemented with 10 mM TES-NaOH (pH 8.0) was used as medium to grow *Synechocystis* in the reactor. The cultures grew at 30 °C bubbled with a mixture (v/v) of 99% air and 1% CO_2 supplied at a flow rate of $150\,mL\,min^{-1}$. Precultures from shake flasks ($OD_{730} \sim 1$-1.5) were used for inoculation in the Multi-Cultivator, working with a volume of $\sim 60\,mL$ (area exposed to the light = $0.0028\,m^2$, height of the water column = 10.32 cm) and initial OD_{730} of 0.05. After inoculation, a continuous irradiation of 30 μmol photons/m^2/s was applied until the cultures

reached an OD_{730} of 0.6, then increased to 120 μmol photons/m^2/s and kept constant up to the end of the experiment. Samples were collected daily and used for OD_{730} determination, product quantification in the extracellular broth and for cell count and cell diameter measurement where indicated.

3.4.2   Photonfluxostat

Photonfluxostat mode is a cultivation approach to control cell growth at different yet constant growth rates [197]. In photonfluxostat experiments, all the cultivation conditions were the same as batch cultivation except for the light intensity settings. At the inoculation time the light intensity was 30 μmol photons/m^2/s. Once the OD_{720} (measured through the build-in OD sensor of the Multi-Cultivator at 720 nm) reached 0.6, light intensity was automatically adjusted every 5 min to ensure light intensity per OD_{720} was constant. This light regime was maintained until maximum capacity of the LED panel was reached. In particular, the light regimes applied were 32.5, 35, 37.5, 42.5, 45, 52.5, 55, 57.5, 70, 80, 90, 100 μmol photons/m^2/s/OD. In the photonfluxostat mode, a "steady-state" is achieved and a constant growth rate can be reliably obtained. Samples were collected every few hours during this phase, for OD_{730} measurements and product quantification.

3.4.3   Day-night batch cultivation

To simulate a day-night regime a dependency between light intensity and time was created by using a custom-made software package as previously reported [197]. The light intensity time dependency can be described using the function

$$I = A \sin\left(\frac{2\pi\tau}{P} + X_{\text{offset}}\right) + Y_{\text{offset}} , \tag{3.1}$$

Where I is the desired intensity, A the amplitude of the regime, τ the time since the start of the regime (in seconds) and P the period of the regime (in seconds). Using the X_{offset} the start position in the regime can be adjusted, while the Y_{offset} changes the ratio between day and night. The dependency was parameterized such that the intensity oscillates between -1 and 1 (A = 1) in combination with a cut-off – setting negative values to zero. This effectively creates a sinusoidal regime oscillating between 0 and 1. P was set to 86 400 s to create a 24h period and in order to smoothly transit from continuous light to day-night, the regime was started at midday by setting the X_{offset} to $\pi/2$. The Y_{offset} was left to 0, giving us a 12h – 12h period with a peak at 1. Since the regime oscillates between 0 and 1 the output can be interpreted as percentage intensity and combined with the photonfluxostat regime a rhythm, where at midday there is 100% of the intensity given by the photonfluxostat regime, was obtained. The usage of the photonfluxostat allows to create a condition in which growth rate achieved at each stage of a day period is relatively stable over multiple days. After the inoculation, the

light intensity was set to $30\,\mu$mol photons/m^2/s. When the OD$_{720}$ (measured through the build-in OD sensor of the Multi-Cultivator at 720 nm) was above 0.3 the photonfluxostat regime was started, in order to automatically adjust the light intensity to keep the ratio of light intensity over biomass constant at $100\,\mu$mol photons/m^2/s/OD. One day after inoculation the day-night regime was configured to start at midday 16:00, therefore every day thereafter dawn occurred at 10:00 and dusk at 22:00. Samples were taken daily immediately before dawn and immediately after dusk for OD measurement and fumarate quantification.

3.4.4 Turbidostat

In the turbidostat mode [198] microbial populations are kept at a fixed biomass density by diluting the culture with fresh medium at the same rate as the populations grows. This feedback loop applies a strong selection pressure on cells to grow at the maximal specific growth rate achievable. The turbidostat setup used in this work is based on a modified Multi-Cultivator, equipped with additional pumps (Reglo ICC, IS-MATEC, Germany) for the transfer of fresh medium to the cultures, and subsequently, to a waste container (i.e. as in a classical chemostat). The "pycultivator" software package that controls the Multi-Cultivator and adjunct hardware, activates the pumps to dilute the cultures if the selected OD$_{720}$ threshold is reached. Cells from pre-cultures in shake flasks were inoculated at OD$_{720} \sim 0.05$ in 4 independent cylindrical vessels of the Multi-Cultivator, using the same conditions as specified before, except for the incident light intensity, which was fixed at $100\,\mu$mol photons/m^2/s. The OD$_{720}$ was recorded every 5 min. When the threshold of OD$_{720} > 0.6$ was reached, cultures were diluted by 8% (v/v) with fresh BG-11. Strain stability was assessed by monitoring growth rate and fumarate- and lactate-production at regular time points. Samples for exometabolite production were collected periodically throughout the cultivation period. The variation in production rate, expressed in percentage, was calculated relative to the one observed at the beginning of the cultivation experiment.

3.4.5 Serial batch cultivation

Serial propagation experiments were performed in $100\,$mL Erlenmeyer flasks at $30\,°$C in a shaking incubator (Innova 43, New Brunswick Scientific) at $100\,$rpm, under constant moderate white-light illumination ($\sim 20\,\mu$mol photons/m^2/s, measured with a LI-250A light meter, LI-COR). Cultures have been grown in BG-11 medium [194] supplemented with 10 mM TES-NaOH (pH 8.0) as a buffer and with kanamycin ($50\,\mu$g mL^{-1}) when necessary. Precultures deriving from the original stock of each strain (OD$_{730} \sim 1$-1.5) were used for inoculation of the experimental batches. Every strain has been tested in triplicate. Every day, each culture at OD$_{730} \sim 1$ has been diluted to OD$_{730} \sim 0.6$ by keeping a constant volume of 20 mL. Samples were collected at periodic intervals before the dilution procedure and used for product quantification in the extracellular broth.

3.5 Strain characterization

3.5.1 Cell count and size measurements

The average cell diameter and cell number were determined with the CASY counter instrument (Roche Applied Science) equipped with a capillary of 60 μm diameter. A volume of 10 μL of harvested culture was opportunely diluted in 10 mL of CASY ton solution. The average cell size was measured working in a range of calibration between 0-10 μm.

3.5.2 Extracellular fumarate, malate and lactate quantification

Extracellular concentrations of fumarate, malate and lactate were determined in samples collected from different strains. Briefly, 1 mL of culture sample was harvested and after centrifugation for 5 min at 14 500 rpm (Himac CT 15RE Centrifuge) at 4 °C, the supernatant was filtered (Sartorius Stedin Biotech, minisart SRP 4, PES, 0.22 μm) for product measurements.

Fumarate concentration was measured on a HPLC system (LC-20AT, Prominence, Shimadzu) equipped with a Photo Diode Array UV/VIS detector (SPD-M30A, NexeraX2, Shimadzu) and a Refractive Index Detector (RID 20A, Shimadzu). A volume of 10 μL of sample was injected through an autosampler (SIL-20AC, Prominence, Shimadzu) onto a Rezex ROA-Organic Acid H+ (8%) column (250 x 4.6 mm; Phenomenex). The compounds were eluted at 45 °C with an isocratic flow rate of $0.15 \, \text{mL} \, \text{min}^{-1}$ of 5 mM H_2SO_4. The detection UV wavelength was set at 210 nm. Peaks identity and quantification were assigned using external standards. In this system, the retention time of fumarate was about 17 min and detection limit was 20 μM.

Malate and lactate were quantified by using commercial enzymatic kits (Megazyme) according to the manufacturer's instructions. The assays, consisting of two consecutive enzymatic reactions, were performed in 96-well plate (SpectraPlate 96 MB, PerkinElmer) at 30 °C. In the case of the L-malic acid kit, the first reaction is catalyzed by the glutamate-oxaloacetate transaminase (GOT) which in the presence of L-glutamate consumes the oxaloacetate in the sample by converting it into 2-oxoglutarate and L-aspartate. During the second reaction, the L-malate dehydrogenase oxidizes the L-malic acid to oxaloacetate by using the reduction of nicotinamide-adenine dinucleotide (NAD^+) to NADH. The formation of NADH is stoichiometrically coupled to the conversion of L-malic acid into oxaloacetate. In the case of the L-lactic acid kit, the first reaction consists in the conversion of pyruvate to D-alanine and 2-oxoglutarate, with the enzyme D-glutamate-pyruvate transaminase (D-GPT) in the presence of a large excess of D-glutamate. The second reaction is catalyzed by L-lactate dehydrogenase (L-LDH) which oxidizes L-lactic acid (L-lactate) to pyruvate by using the reduction of NAD^+ to NADH. The formation of NADH is stoichiometrically coupled to the conversion of L-lactic acid in pyruvate. The amount of NADH produced during the reactions is quantifiable as an increase

in absorbance at 340 nm, which was measured using a plate reader (SPECTROstar Nano, BMG LABTECH). According to the kit, the detection limit was 1.9 μM for malate and 2.3 μM for lactate. For quantification, a standard curve was performed for calibration of the enzymatic assay.

3.5.3   Intracellular malate and fumarate quantification

Three independent cultures for each strain were inoculated from an exponential growth phase pre-culture in 50 mL of BG-11 medium supplemented with 10 mM TES-NaOH (pH 8.0). Axenic conditions were assessed by monitoring LB agar plate incubated at 37 °C previously streaked with samples from the experimental cultures. Samples for intracellular measurements were collected from exponential growth phase cultures ($OD_{730} \sim$ 0.8-1) according to [199]. Briefly, 10 mL of culture was concentrated by centrifugation at 4 °C for 5 min at 3900 rpm (Eppendorf 5810 R Centrifuge). The pellet was then re-suspended in fresh BG-11 and further centrifuged at 4 °C for 2 min at 14 000 rpm (Himac CT 15RE Centrifuge). The supernatant was removed and the pellet frozen in liquid nitrogen. Samples were stored at -80 °C until further analysis. Metabolites extraction was performed following a procedure adapted from [200]. 300 μL of 80% methanol was added to the frozen pellet and mixed until complete suspension for 30 min at room temperature under shaking conditions. At the same time, 2.5 μL of Malic acid-2,3,3-d3 at $100 \, \mu g \, L^{-1}$ (98 atom % D, Sigma-Aldrich) and 2.5 μL of Fumaric acid-d4 at $100 \, \mu g \, L^{-1}$ (98 atom % D, Sigma-Aldrich) were added as internal standards for absolute quantification. Samples were mixed with 200 μL chloroform and agitated for 5 min. Phase separation was induced by adding 400 μL of mQ water and the upper polar phase was recovered by 5 min centrifugation at 14 000 rpm at 4 °C (Fresco 21, Thermo Scientific). A volume of 500 μL was concentrated and dried overnight by vacuum centrifugation at 2000 rpm at 25 °C. For chemical derivatization samples were first mixed with 10 μL of methoxyamin dissolved in pyridine ($20 \, g \, L^{-1}$ concentration) for 90 min at 30 °C. 45 μL of BSTFA was then added and agitated for 30 min at 37 °C. Bi-dimensional gas chromatography–time of flight mass spectrometry (GCxGC-TOF/MS) was performed using an Agilent 7890B GC (Agilent Technologies, USA) and Pegasus (BT 4D) TOF-MS system (Leco Corporation, USA) equipped with an Rxi–5ms column (30 m × 0.25 mm × 0.25 μm film thickness, RESTEK, USA) and Rxi-17ms (2 m x 0.25 mm x 0.25 μm film thickness, RESTEK, USA), as the first and second dimension columns, respectively. High-purity helium (99.9999%) was used as the carrier gas at a flow rate of $1.4 \, mL \, min^{-1}$. 1 μL of sample was injected with a split ratio of 10:1 at 230 °C. For the first dimension, the chromatographic conditions were: initial temperature 85 °C, 2 min isothermal, 15 °C min up to 330 °C, 2 min isothermal. For the second dimension, the oven was 5 °C higher than the temperature in the first dimension column and the modulation time was set at 4 s for all the run, maintained at 15 °C relative to second oven. The MS data were acquired in TIC (total ion current) mode from m/z 55 to 550 with an acquisition rate of 200 spectra per second and with an extraction frequency of 32 kHz. Transfer line was kept at 280 °C. Mass

spectral assignment was performed by matching with NIST MS Search 2.2. Libraries, implemented with the MoNa Fiehns Libraries. The masses used for the quantification of malic acid and fumaric acid were 232.12 m/z and 245.04 m/z respectively.

3.5.4   Sequencing of the *ldh* and *fumC* cassettes

Sequencing analysis of the *ldh* and *fumC* cassettes was performed on single colonies isolated from previously restreaked samples of the populations in BG-11 agar plates. Colony PCR with Herculase II Fusion DNA Polymerase (Agilent Technologies) was used to amplify the sequence encoding for either the *ldh* gene and the upstream P_{trc} promoter or the *fumC* gene and the upstream P_{cpcBA} promoter. After PCR product purification (Stratec molecular), fragments were sent for sequencing to Macrogen Europe (The Netherlands) using the primers listed in Table 3.2 (shown at the end of this Chapter). The sequenced genes were aligned to the nucleic acid reference sequence by using Ugene bioinformatic software [201] with default settings. The translation analysis was performed by using Translate-ExPASy bioinformatic tool [202] to translate the nucleotide sequence into amino acid sequence. The latter was then aligned to the amino acid reference sequence with the ExPASy tool SIM (Gap open penalty: 12, Gap extention penalty: 4, Comparison matrix: BLOSUM62).

3.6   Data analysis and statistics

In all the following computations, uncertainty was quantified according to the law of propagation of uncertainty (Guide to the expression of uncertainty in measurement).

3.6.1   Cell diameters

Since at the beginning of the batch cultivation the cell dimension was largely variable because of rapid cell division, the cell size was calculated as the arithmetic mean of the average diameters measured in the steady phase (from $\sim$ 136 h cultivation onward). Expanded uncertainties (coverage probability 99%, coverage factor 2.90, degrees of freedom 17), i.e. the intervals which contain the measurands with a probability of 99%, were calculated according to the experimental data. The significance of differences observed between the engineered strains and the control strain was assessed by t-test. The cell volume ratio, representing the ratio between the volume occupied by the cells and the total broth volume, was calculated multiplying the cell number per ml by the average cell volume.

3.6.2   Measurements of intracellular metabolites

The significance of differences observed in intracellular concentrations of metabolites of $\Delta me \Delta mdh$ and $\Delta me \Delta mdh \Delta NSI::fumC$ strains was assessed by t-test. Expanded

uncertainties (coverage probability 95%, coverage factor 3.18, degrees of freedom 3), i.e. the intervals which contain the measurands with a probability of 95%, were calculated according to the experimental data.

3.6.3   Growth rate

The growth rate μ of the different strains was calculated assuming an exponential growth by

$$\mu = \frac{log(x_1) - log(x_2)}{t_1 - t_2} \,, \tag{3.2}$$

being x_1 and t_1 (x_2 and t_2) the absorbance value and the time instant, respectively.

3.6.4   Productivities

The productivities Δq_p of the several strains during the batch cultivations were calculated by

$$\Delta q_p = 2\frac{p_2 - p_1}{(x_1 + x_2)(t_2 - t_1)} \,, \tag{3.3}$$

being t_1, p_1 and x_1 (t_2, p_2 and x_2) the time instant, the product concentration and the dry weight concentration (obtained from the absorbance values through a conversion factor of 148 mg/L/OD$_{730}$ as determined by [197]) of the first (second) sample, respectively.

3.6.5   Product yield from biomass

The maximum yield of product from biomass $Y_{p/x}$ of the strains during batch cultivation has been calculated by

$$Y_{p/x} = \frac{\Delta q_p}{\mu} \,, \tag{3.4}$$

being Δq_p and μ the productivity and the growth rate in the exponential growth phase, respectively.

3.6.6   Carbon partitioning

The carbon partitioning was estimated assuming that the incoming carbon is conveyed towards the formation of product(s) and biomass, assuming an elemental composition of the biomass of $C_4H_7O_2N$ according to [47]. The carbon partitionig in a product was obtained as the ratio between the productivity of that product and the sum of all productivities (including the one of biomass), expressed in carbon-moles,

$$C\% = \frac{\Delta_C q_{p,1}}{\Delta_C q_X + \sum_i \Delta_C q_{p,i}} \,, \tag{3.5}$$

being $\Delta_C q_X$ the biomass carbon productivity and $\Delta_C q_{p,i}$ the carbon productivity of the i-th product.

3.6.7 Generation counting

The count of the number of generations in the serial propagation experiment was calculated starting from the time-varying doubling-time, denoted by the symbol $\mathrm{DT}(\tau)$, with $\tau \in (0, T)$ the time instant and T the experiment duration. Precisely, the number of generations $\mathscr{G}(t)$ occurred after a time t was computed as

$$\mathscr{G}(t) = \int_0^t \mathrm{DT}(\tau)^{-1} d\tau . \qquad (3.6)$$

The inverse of the doubling time was estimated starting from the absorbance measurements at 730 nm performed every $\sim 24\,\mathrm{h}$ according to relation

$$\frac{1}{\mathrm{DT}} = \frac{1}{t_2 - t_1} \log_2 \left(\frac{x_2}{x_1} \right) , \qquad (3.7)$$

being t_1 and x_1 (t_2 and x_2) the time instant and the absorbance value of the first (second) sample, respectively. The numerical evaluation of the integral in (3.6) was performed adopting the composite rectangle rule:

$$\mathscr{G}(t) = \sum_i \Delta t_i \frac{1}{\mathrm{DT}_i} , \qquad (3.8)$$

being Δt the time interval duration between two consecutive evaluations of DT, and the pedix i indicates the intervals in which DT has been evaluated and that preceeds t.

Table 3.1: List of plasmids and strains used in this study

Plasmids and strains	Description	References
pFL-AN	BioBrick "T" vector with AvrII and NheI restriction site on each side	[82]
pWD42	Amp^{r}Km^r, containing the selection cassette *mazF*	[196]
pWD060	pFL-AN derivative, Amp^r containing *fumC* upstream and downstream homologous regions	This study
pWD061	pFL-AN derivative, Amp^{r}Km^r containing the selection cassette *mazF* flanked by *fumC* upstream and downstream homologous regions	This study
pWD084	pFL-AN derivative, Amp^r containing *zwf* upstream and downstream homologous regions	This study
pWD085	pFL-AN derivative, Amp^{r}Km^r containing the selection cassette it mazF flanked by *zwf* upstream and downstream homologous regions	This study
pWD71	pFL-AN derivative, Amp^r containing *mdh* upstream and downstream homologous regions	This study
pWD72	pFL-AN derivative, Amp^{r}Km^r containing the selection cassette *mazF* flanked by *mdh* upstream and downstream homologous regions	This study
pWD73	pFL-AN derivative, Amp^r containing *me* upstream and downstream homologous regions	This study
pWD74	pFL-AN derivative, Amp^{r}Km^r containing the selection cassette *mazF* flanked by *me* upstream and downstream homologous regions	This study
pWD05	pFL-AN derivative, Amp^r containing *sll1314* upstream and downstream homologous regions	This study

Table 3.1: (continue)

pWD06	pFL-AN derivative, Amp^{r}Km^r containing the selection cassette *mazF* flanked by *sll1314* upstream and downstream homologous regions	This study
pHKH001	Amp^{r}Km^r, integration vector disrupting *slr0168* in *Synechocystis* genome	[128]
pBB1	pHKH001 derivative, Amp^{r}Km^r containing the expression cassette composed by cpcb promoter, *fumC* from *E. coli* and His-tag flanked by the upstream and downstream homologous regions to the *slr0168*	This study
Synechocystis sp. PCC 6803	*Synechocystis* sp. PCC 6803 wild type, glucose tolerant	This study
Δ*fumC*	*Synechocystis* sp. PCC 6803 *fumC* gene knock out mutant	This study
Δ*fumC*Δ*zwf*	*Synechocystis* sp. PCC 6803 *fumC* and *zwf* double genes knock out mutant	This study
Δ*me*	*Synechocystis* sp. PCC 6803 *me* gene knock out mutant	This study
Δ*mdh*	*Synechocystis* sp. PCC 6803 *mdh* gene knock out mutant	This study
Δ*me*Δ*mdh*	*Synechocystis* sp. PCC 6803 *me* and *mdh* double genes knock out mutant	This study
Δ*NSI::fumC*	*Synechocystis* sp. PCC 6803 *fumC* overexpressing mutant	This study
Δ*me*Δ*mdh*Δ*NSI::fumC*	*Synechocystis* sp. PCC 6803 *me* and *mdh* gene knock out, *fumC* overexpressing mutant	This study
SAA023	*Synechocystis* sp. PCC 6803 expressing codon optimized *L-ldh* gene from *L. lactis*	[47]
Δ*me*Δ*mdh*Δ*sll1314*	*Synechocystis* sp. PCC 6803 *me*, *mdh* and *sll1314* triple genes knock out mutant	This study

Table 3.2: List of primers used in this study

Primer name	Sequence (5'-3')
fumC-up-Fwd	GAGCAGACGTTCACATCG
fumC-up-Rev	CAATCATCTGCTCTGGAACGtctagaCATACTGTCG-GTTTCAAGGC
fumC-down-Fwd	GCCTTGAAACCGACAGTATGtctagaCGTTCCAGAGCAGAT-GATTG
fumC-down-Rev	CCTAGATTAGGACCTGTCAGC
fumC-seq	AACCATTGTCCAAGGTCTGCG
zwf-up-Fwd	TTCGCCTCAATCGCATTC
zwf-up-Rev	GCGACGGCCATCTTTATTactagtTCTTGACG-GAGTCCAGTG
zwf-down-Fwd	CACTGGACTCCGTCAAGAactagtAATAAAGATGGC-CGTCGC
zwf-down-Rev	ATCTAACACTGCCAGCGT
zwf-seq	TAGCCCAGTCTTATCAGG
mdh-up-Fwd	AGTTCCCACGGTGGATTTGA
mdh-up-Rev	CAGCAAAATGTCGCCAACGACTAGTGAGTGGAA-GATATTCTCGAAGTGC
mdh-down-Fwd	GCACTTCGAGAATATCTTCCACTCACTAGTCGTTGGCGA-CATTTTGCTG
mdh-down-Rev	CAGGCTTTGTAACTGGTGGA
me-up-Fwd	TGAGTCTTATATCCCGTCCGT
me-up-Rev	ACTGCACTGGCTACGGTAGTTCTAGACTGACGC-TATAACTCGGATTGG
me-down-Fwd	CCAATCCGAGTTATAGCGTCAGTCTAGAACTACCG-TAGCCAGTGCAGT
me-down-Rev	CAACTCAGCATGGATATTAAGCACG
me-seq	ATGGTAGGACACCTTCTCCA
mdh-seq	TCGCACAGTTCGTAGGCAA
fumC_ecoli_Fwd	GCCATATGAATACAGTACGCAGCGA
fumC_ecoli_Rev	ACGGATCCTTAACGCCCGGCTTTCATA
fumC_ecoli_Seq	GCTGGGTAGCGATGCTC
phkh_H1seq_F	CCTCTGGTTAGCCACCA
phkh_Kanseq_R	TTGAGACACAACGTGGC
Pcpcb_rev	ATATGGCCGCTGCTGTG
H1_Fwd	TGTCGCCGCTAAGTTAGA
LDH_Rev_3	GTAGGTCAAGATGTCCACGG
LDH_Rev_2	CATCTTGGAACACGGACACG
Kan_Rev	TCCCGTTGAATATGGCTC

Table 3.2: (continue)

sll1314-up-Fwd	TACTGGGATTGAGAGGCT
sll1314-up-Rev	TCAGAGATTGAGCTTGGGAactagtATGCCCTCGGC-TAATAGT
sll1314-down-Fwd	ACTATTAGCCGAGGGCATactagtTCCCAAGCT-CAATCTCTGA
sll1314-down-Rev	GACGATTTTTCCCGTGGT
sll1314-seq	AGAGGCAGCCATAAATACC

Chapter 4

Results and Discussion

4.1 General introduction

Cyanobacteria-based MCFs are gaining more and more interest in the scientific community due to the possibility to directly convert CO_2 into a plethora of C-based compounds through a light-driven process. Several proof-of-concepts for the exploitation of cyanobacterial metabolism leading to the production of commodity chemicals, plastic precursors, biofuels and pigments have already been shown [41]. The most common engineering approaches quite often rely on the overexpression of native pathways or the introduction of heterologous ones that divert the carbon resources needed for the growth of the biomass towards the formation of the desired product, imposing a high fitness burden on the production strain. Genetic instability can compromise the feasibility of a scaled-up process leaning on such engineered organisms. As previously reported, spontaneous mutations affecting the correct transcription or translation of the inserted genes can arise in the population conferring an evolutionary advantage to the mutated clones which will eventually take over the culture, thus causing a drop in the productivity [45, 162]. For this reason, it is of outstanding importance to develop strategies that can guarantee a stable productivity over long periods of cultivation. A possible solution is the growth-coupled production approach that consists in the design of synthetic pathways in which the cell fitness and the target product formation are aligned [203] [156]. Indeed, when the synthesis of product and biomass are obligatorily coupled, non-producer mutants spontaneously emerging in the population are outcompeted by the fitter producing strain according to Darwinian selection [204]. Attempts to devise growth-coupled strategies have been built on the idea of linking a product-forming pathway to the capacity of the cell to regenerate energy and/or redox co-factors. This principle has been proposed also for photoautotrophs [177] with limited applications in the laboratory [174]. This limitation could be related to the extremely high number of genetic modifications necessary to achieve a strict coupling between COI production and regeneration of cofactors, due to the occurrence in cyanobacteria of alternative electron flows around PSI and PSII to finely tune the level of reducing

equivalents [174].

Recently an approach to design growth-coupled production strategies has been developed [142]. Instead of using energy or redox regeneration, this method is based on the direct stoichiometric coupling of the anabolic pathways necessary for the formation of the biomass to the synthesis of the target compound(s). By means of the algorithm FRUITS (Find Reactions Usable In Tapping Side-products), it is possible to analyze existing genome-scale metabolic models and identify side-products that can be coupled to cell growth by the deletion of their re-utilization pathways. In particular, if applied to *Synechocystis* sp. PCC 6803 (hereafter, *Synechocystis*) growing under photoautotrophic conditions, FRUITS predicts nine candidate compounds to be coupled to growth with a maximum of four gene deletions. This approach has been previously validated with the production of acetate [142]. In this work, the focus has been shifted, first, towards another product of the FRUITS list – fumarate – and, afterwards, towards a downstream metabolite of the fumarate pathways, namely malate. Stable over-producers strain of *Synechocystis* have been engineered for the production of both molecules based on the implementation of the above-mentioned principles.

4.2 Fitness-coupled production of fumarate in *Synechocystis* sp. PCC 6803

Fumarate, a dicarboxylic acid with 4 atoms of carbon, is a biotechnologically interesting compound with a range of applications in multiple fields. Fumarate can be employed as acidity regulator in the food industry [205] or as a building block for polymer production [206]. Industrial production of fumarate is mainly derived via chemical synthesis from petrolchemical sources, therefore an alternative sustainable process to obtain this compound would be advisable. Simulation performed with the algorithm FRUITS predicted that fumarate can be produced in a growth-coupled fashion and in 4 fold that of the WT [207, 142].

An evident inconvenience of this (or any) growth-coupled production strategy is that if cells do not grow, they do not produce. Particularly at the industrial scale, it is advisable the usage of natural solar radiation as source of light and energy to sustain cyanobacterial growth [15]. This would imply that the cultures are subjected to an oscillating day-night cycle. Thus, during a significant amount of time, cyanobacteria will be in the dark, a condition where no growth is expected. Here, a combination of different strategies to align genetically engineered product formation with microbial
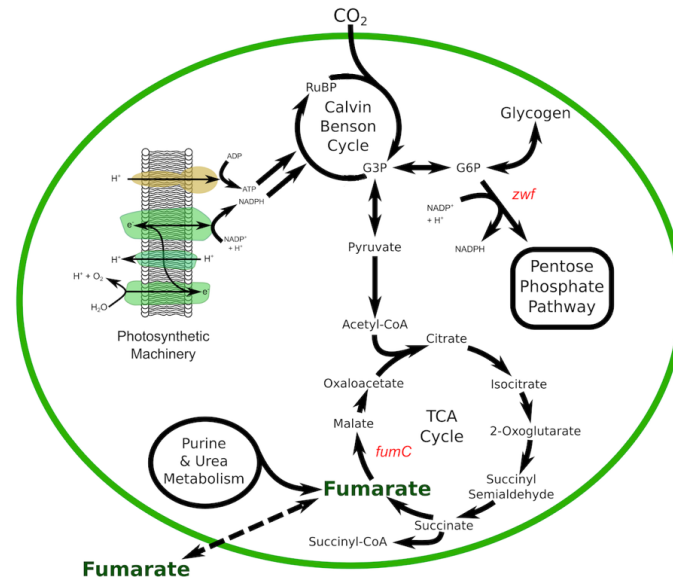
Figure 4.1: Schematic overview of the metabolism surrounding fumarate in *Synechocystis*. During day-time fumarate is produced as part of the purine and urea metabolism. Removing the FumC blocks the reutilization of fumarate, causing its accumulation and eventually leaking out. At night-time *Synechocystis* uses the oxidative pentose phosphate pathway (OPPP) to generate energy-carriers from glycogen. Removal of the *zwf* gene disables the OPPP and forces the utilization of the disrupted TCA cycle. Figure retrieved from Du *et al.* (2019), with permission.

fitness is shown; precisely, product formation is here coupled to the intrinsic abilities of cyanobacteria to adjust their metabolism to suit the environmental conditions they experience (e.g. light-darkness in this case).

4.2.1 Day-time production of fumarate

The analysis of the *Synechocystis* GSMM, constrained to simulate photoautotrophic growth [174], reveals that fumarate is produced as a by-product of specific anabolic reactions within purine- and urea metabolism and is re-assimilated through the TCA cycle via the activity of FumC (fumarase) (Figure 4.1). If the only fumarate assimilation pathway is removed, by the construction of a *fumC* deletion strain, FRUITS predicts that fumarate will accumulate at a yield of 0.848 mmol fumarate per gram of dry weight. Here, this prediction has been tested by constructing a Δ*fumC Synechocystis* mutant (Figure 4.2).

Under constant illumination in batch cultivation in photobioreactor the WT and the Δ*fumC* strain grew similarly during the exponential growth phase. The WT reached a slightly higher optical density after entering stationary phase (Figure 4.3A). Not surprisingly, there was no extracellular fumarate production in *Synechocystis* WT, in contrast,

ΔfumC   WT

2.5 kb ⟶

1.0 kb ⟶

H1   *fumC*   H2

H1   H2

Figure 4.2: PCR confirmation of the markerless deletion of the *fumC* gene in *Synechocystis*. By using primers pairing with the up- and downstream regions flanking the native gene, the PCR product of the knock-out mutants has a size of about 1.2 kb. The WT band for the *fumC* gene using the same primers is about 2.5 kb.

the Δ*fumC* strain excreted significant amounts of fumarate throughout the cultivation (> 1 mM final concentration at about 200 h of cultivation; Figure 4.3A). These results very nicely match the *in silico* prediction that disrupting *fumC* will result in fumarate accumulation. While undoubtedly promising, these initial simple growth experiments do not assure that biomass and fumarate formation are strictly coupled. The strict stoichiometric coupling, which we are striving to engineer, implies that at different growth rates a linearly proportional change in the biomass specific production rate of fumarate is obtained.

4.2.2   Fumarate production rate is proportional to growth rate

To test whether fumarate production and growth rate strictly vary in parallel in the Δ*fumC* strain, 12 independent photonfluxostat experiments at different, yet constant, growth rates were performed [197]. This was achieved by dosing the biomass specific light flux to intensities ranging from 30 to 100 µmol photons/m^2/s/OD. From all cultivations maintained at a specific growth rate, samples were taken at multiple times during the cultivation, to quantify extracellular fumarate concentration. Fumarate productivities were subsequently calculated and plotted against growth rate 4.3B). The results obtained indicate that fumarate productivity is indeed proportional to growth rate, implying that both physiological traits are strictly coupled. Furthermore, the comparison of the linear fit between the rate of fumarate productivity and growth rate, based on
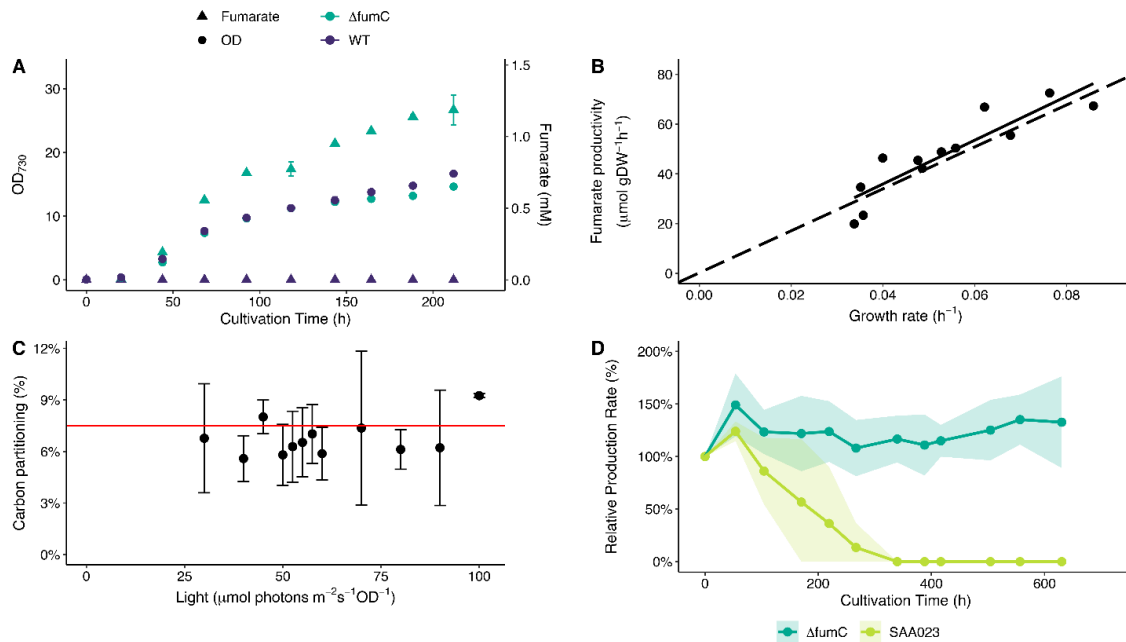
Figure 4.3: Stable fumarate production in *Synechocystis*. (A) Cell growth (circles) and extracellular fumarate production (triangles) of both the WT (purple) and the Δ*fumC* (dark green) strain in a Multi-Cultivator illuminated with constant light for over 200 h. (B) A linear relationship between growth rate and biomass specific fumarate productivity. Each point represents a single observation, and the solid line is a linear fit of all experimental data points. The dashed line is based on *in silico* FBA simulations of the GSMM of *Synechocystis*, using biomass maximization as the objective function. (C) Carbon partitioning of fumarate production versus biomass at different photonfluxostat light regimes. The red line is based on *in silico* FBA simulations. (D) Stability test of fumarate (dark green) and lactate (light green, using strain SAA023 [47]) production during prolonged turbidostat cultivation under continuous illumination at $OD_{730} = 0.6$. SAA023 is a lactate producing *Synechocystis* mutant, expressing the lactate dehydrogenase from *Lactococcus lactis* at the *slr0168* genomic locus. Productivity at corresponding time points was normalized based on the average productivity at the first time point (set to be 100%). The shade area indicates one standard deviation from 4 biological replicates. Error bars indicate the standard deviations (n ≥ 2). If an error bar is not visible, it is smaller than the size of the symbol. Figure retrieved from Du *et al.* (2019), with permission.

our experiments, with the outcome of the simulations using FBA [28] on the metabolic network reconstruction of *Synechocystis* was performed (Figure 4.3B). It is important to highlight that the modelling parameters were not tweaked and were taken directly from the original report [174]. Still, both sets of data match strikingly well, corroborating the hypothesis that fumarate production and growth rate are strictly coupled in the

$\Delta fumC$ strain.

The carbon partitioning towards fumarate in the $\Delta fumC$ strain during the multiple cultivations carried out was calculated based on the average optical density and fumarate concentration, between each two subsequent sampling points (Figure 4.3C). Optical density was converted to gram of dry biomass using a conversion factor of 148 mg/L/OD$_{730}$ as determined in a previous report [197]. The plotted carbon partitioning is an average of individual values obtained for each time interval with standard deviation. No significant changes in carbon partitioning irrespective of the biomass specific light flux were observed (Figure 4.3C). This indicates that irrespective of the growth rate, as long as cells are sufficiently illuminated, the fumarate yield on biomass is constant. This result also supports theoretical predictions stating that fumarate production is only affected by environmental conditions to the extent that the latter affect growth rate. In other words, fumarate production is stoichiometrically and obligatorily coupled to cell growth. It is important to note that the carbon partitioning values reported here are comparable with most of those obtained using more conventional metabolic engineering strategies for a wide variety of products [41].

4.2.3   Stability of fumarate production by the $\Delta fumC$ strain

The $\Delta fumC$ strain has been shown to produce fumarate in a growth-coupled fashion, however this does not prove its (improved) phenotypic stability, compared to traditional metabolic engineering approaches. As explained above, the root of the instability comes from Darwinian selection for fitter (i.e. faster growing under the selected conditions) strains and the occurrence of random mutations in the genome. For cyanobacterial cell factories, production competes directly with fitness, thus mutations resulting in the suppression or elimination of the production pathway(s) are selected. $\Delta fumC$ strain on the other hand integrates fumarate production with biomass production, using an evolutionary more stable approach. This approach is more stable for two reasons: first, fumarate production was enabled via the removal of the *fumC* gene, a strategy which is stable as long cells do not re-evolve a new fumarate assimilation pathway - an event which is expected to be unlikely even on the long time-scales potentially deployed in industrial settings. Second, detrimental mutations impacting the production rate can only occur in pathways that will also lower fitness, hence evolutionary pressure will counter-select non-producing mutants.

Conditions in which cells are under strong selection pressure for faster growth and in which the propagation bottlenecks are small, are predicted to result in the fastest drop in productivity [208]. Such conditions are best met under turbidostat cultivation [198], and so these cultivations provide the harshest test ground to assess the stability of the production strains. $\Delta fumC$ strain was cultivated under turbidostat conditions at its maximal growth rate, with no light limitation (i.e. 100 μmol photons/m^2/s, with a working OD$_{730}$ of 0.6), for a period of over 600 hours. During this period, no significant

changes in production rate have been observed (Figure 4.3D)—confirming the stability of our fumarate producing strain. As a control, it was used a similar cell factory, engineered using classical approaches, for the production of lactate [47], which was grown under the same conditions. Lactate production in this strain was achieved by the heterologous expression of lactate dehydrogenase from *Lactococcus lactis*, yielding an initial carbon partitioning comparably to the one here reported for fumarate [47]. As theory would predict, lactate production was lost within 5 to 10 days for a culture of this strain (Figure 4.3D). This result reinforces the stringency with which this regime selects for fitter cells, which - when using the novel engineering method here presented-means the producing ones.

4.2.4 Night-time production of fumarate

In order to address night-time fumarate production, *Synechocystis* GSMM has been queried again. Night-time metabolism was approximated by simulating chemoheterotrophic conditions under constrained glycogen utilization in the absence of light [209]. As for the objective function, maximization of ATP consumption was initially chosen, as *Synechocystis* does not grow during the night but is still metabolically active, presumably to cover cellular maintenance costs [210, 211]. However, these initial simulations predicted that there would be no fumarate production for a $\Delta fumC$ strain under night-time conditions. This prediction is in contrast to the experimentally measured night-time fumarate production rates for the $\Delta fumC$ strain (Figure 4.5A). As mentioned previously, fumarate is produced as a by-product of anabolic reactions. The data here shown suggest that although *Synechocystis* does not grow at night, it still has residual anabolic activity. For this reason the maximization of a heterotrophic growth, which also accounts for ATP consumption, was set as the objective function, to simulate a qualitative proxy for night-time metabolism.

In the interest of further increasing the night-time production of fumarate, the algorithm OptKnock [180] has been used to identify gene deletions that would redirect night-time metabolic flux towards fumarate production (Table 4.1). The primary predicted gene deletion is *slr1843*, or more commonly known as the *zwf* gene. The product of the *zwf* gene catalyses the first reaction in the oxidative pentose phosphate pathway (OPPP) (Figure 4.1). FBA predicts for the $\Delta fumC$ strain under these night-time conditions, the OPPP as the primary mode for the production of reducing equivalents [41, 212, 213]. Additionally, the OPPP is predicted to provide precursors for glycine production. Therefore, simulations of a $\Delta fumC\Delta zwf$ double mutant predict that night-time fumarate production will increase for potentially two reasons: 1) fumarate is produced as an end-product of the TCA cycle which provides energy carriers and 2) fumarate is produced as a by-product of L-proline degradation as alternative pathway for the production of glycine precursors. Of these two sources, the TCA cycle is predicted to be the predominant contributor, supplying 73% of flux associated with the increase in night-time fumarate production. To the experimentally validate this *in silico* prediction
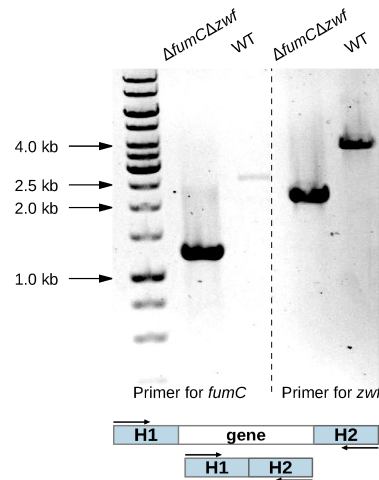
Figure 4.4: PCR confirmation of the markerless deletion of the *zwf* gene on the background of the Δ*fumC* strain of *Synechocystis*. By using primers pairing with the up- and downstream regions flanking the native gene, PCR products of the knockout mutants have a size of 1.2 kb for the deletion of *fumC* and 2.0 for *zwf*. The WT bands are 2.5 and 4.0 kb for *fumC* and *zwf*, respectively.

a Δ*fumC*Δ*zwf* strain has been engineered by markerless deletion on the background of the Δ*fumC* strain. Full segregation of the double knock-out mutant was assessed by PCR analysis (Figure 4.4).

The production of fumarate by the Δ*fumC*Δ*zwf* strain was tested in a 12h-12h sinusoidal day-night rhythm and it was compared to the performance of the Δ*fumC* strain. During this cultivation the photonfluxostat mode was used to adjust light intensity to biomass, in order to extend the range during which growth is stable. This allowed to

Table 4.1: OptKnock simulations of fumarate production rates in night-time regime and of growth rates in day-time of different strains. Simulations were performed simulating heterotrophic growth on glucose under night-time conditions in the Δ*fumC* and in the possible derivative strains.

Strains	Night-time fumarate yield (mmol gDW^{-1})	Photoautotrophic growth-rate (h^{-1})
Δ*fumC*	0.848	0.050
Δ*slr1843*	3.17	0.050
Δ*slr1843*Δ*slr2132*	9.23	0.050
Δ*slr1843*Δ*slr2132*Δ*slr0394*	12.5	0

Figure 4.5: Stable fumarate production around the circadian clock. (A) Cell growth (circles), extracellular fumarate production (triangles), and (B) fumarate productivity of both the $\Delta fumC$ (dark green) and the $\Delta fumC\Delta zwf$ (green) strain in a batch Multi-Cultivator under the 12-h-day/12-h night cycle with a constant light intensity over biomass ratio of 100 µmol photons/m^2/s/OD. OD$_{730}$ and fumarate concentrations were measured at every perceived dawn and dusk. Fumarate productivity was calculated separately for each day and night period, using the fumarate concentration differences, while both dividing by the average OD$_{730}$ and the time interval between dawn and dusk. Cell dry weight was calculated based on a conversion factor of OD$_{730}$ into 148 mg/L/OD$_{730}$ [197]. The error bars indicate the standard deviations of four replicates for the $\Delta fumC$ and three replicates for the $\Delta fumC\Delta zwf$ strain. If an error bar is not visible, it is smaller than the size of the symbol. Figure retrieved from Du *et al.* (2019), with permission.

collect multiple samples from similar conditions, without the complications of a turbidostat. The biomass density and fumarate concentration were measured daily at the beginning and end of each day period, so that production rate of fumarate for day and night could be calculated separately.

After about 100 hours of cultivation, $\Delta fumC$ strain reached a slightly higher biomass density (Figure 4.5A), while the $\Delta fumC\Delta zwf$ strain produced slightly more fumarate (Figure 4.5A), suggesting more carbon was diverted into fumarate by $\Delta fumC\Delta zwf$. After calculating the specific production rate of fumarate for both strains in day and night separately (Figure 4.5B), it emerged that both strains produced fumarate at similar rates during the day (two-sided t-test, H0: $\Delta fumC = \Delta fumC\Delta zwf$ p = 0.2377). During the night, however, $\Delta fumC\Delta zwf$ turned out to produce fumarate at more than twice the rate of $\Delta fumC$ (Figure 4.5B). While $\Delta fumC$ is designed to only produce fumarate in a growth coupled fashion and no significant growth was observed during the night,

fumarate production was observed in $\Delta fumC$ during the night (Figure 4.5B). As discussed before this finding supports the idea that anabolic reactions are active during night [182]. The production ability of the $\Delta fumC\Delta zwf$ strain during dark periods confirms the model predictions according to which anabolic reactions are active during the night. One explanation may be found in *Synechocystis* preparing for the day. A more detailed study of the night-time behaviour of these strains may reveal how these reactions are regulated.

There are no experimental indications of phenotype instability in the $\Delta fumC\Delta zwf$ fumarate producing strain, however it is expected to be as stable as the $\Delta fumC$ strain, since both strains were generated using the same metabolic engineering approach, that is by gene deletions.

4.2.5   Conclusions

A new dual strategy cyanobacterial cell factory for the production of fumarate, by exploiting day- and night-time metabolism, has been proposed in the present study. Using the available GSMM for *Synechocystis*, and the FRUITS and OptKnock algorithms to design specific mutation, fumarate accumulation was achieved and resulted to be coupled to growth, during the day, and to fitness, during the night, by introducing only two knockouts. This is, to the best of the authors' knowledge, the first cyanobacterial cell factory exploiting day- and night-time metabolism, in the same host, for the production of fumarate. When compared to other cyanobacterial production hosts constructed using conventional metabolic engineering strategies, our day-time specific productivity of fumarate (0.060 µmol/gDW/h) comes close to the one published for the production of butanol (0.062 µmol/gDW/h)[214, 41]. This ranks our strain in the middle among all the cyanobacterial production hosts with two very important advantages: (i) it has been proven to be stable and (ii) it also displays night-time production. Moreover, the adopted approach has been shown to be more stable over time when compared to a cell factory constructed using conventional metabolic engineering strategies. This achievement demonstrates it is possible to obligatory couple production of fumarate to fitness, even in conditions without net growth. More insight into day- and night-time metabolism will help to identify other pathways that can be exploited with similar approaches. Although night-time production is relatively small, compared to day-time production, in industrial settings, where these cell factories are to be implemented, similar environmental dynamics are likely to be expected [182] and the cell factory here reported demonstrates avenues to exploit these dynamics. This study reports the first truly sustainable method to produce fumarate directly from CO_2, with final production parameters which are the highest for a fitness-coupled method using a photoautotrophic cell factory. The approach taken here is applicable to other production systems and of particular relevance to production processes that while striving for maximum production, also need to be robust against genetic drift and need to cope with environmental fluctuations, such as the ones exploited here for day and night.

4.3   Stable malate production in *Synechocystis* sp. PCC 6803

This section is the basis of a manuscript in preparation: Battaglino, B., Du, W., Jongbloets, J.A., Pagliano, C., Re, A., Saracco, G., Branco dos Santos, F. Stable malate production in cyanobacterium *Synechocystis* sp. PCC 6803

Malate is a C_4-dicarboxylic acid with a variety of applications, ranging from the food and feed industry, where it is used as flavoring agent and acidulant [215], to the pharmaceutical and biopolymeric fields (e.g. plasticizer, surface coating, polymalate) [216]. Despite several fermentative processes to yield malate and its derivatives have been investigated [217, 218], malic acid is currently mainly produced chemically by hydration of maleic anhydride which is obtained by oxidising n-butane [219]. For this reason sustainable production process to respond to the increasing demand of this compound would be necessary.

In *Synechocystis*, the precursor of malate is fumarate, a by-product of the arginine and urea anabolic pathway, which is subsequently re-cycled inside the TCA cycle (Figure 4.6a). As already predicted by *in silico* simulations based on FRUITS algorithm [142] and demonstrated in [220], fumarate is a growth-coupled compound, i.e. its production is stoichiometrically bound to the formation of biomass. Here, we demonstrate that, by exploiting a strict growth coupled compound, such as fumarate, it is possible to drive the accumulation of its first derivative in the TCA cycle, that is malate. We showcased the feasibility of the metabolic engineering strategy adopted to stabilize this product formation resulting in the first report of stable cyanobacterial conversion of CO_2 into malate.

4.3.1   Theoretical approach

The malate intracellular pool in *Synechocystis* derives from the hydration of fumarate catalyzed by the FumC enzyme. Malate utilization inside the TCA cycle is mediated by the malic enzyme (Me) and by the malate dehydrogenase (Mdh) which convert malate into pyruvate and oxaloacetate, respectively (Figure 4.6a). Based on FVA of the GSMM of *Synechocystis* metabolism iJN678 [174], under light-limited photoautotrophic growth, malate is predicted to accumulate if the enzymatic reactions responsible for the consumption of malate are deleted (Figure 4.6). In particular, FVA predicted that single knock-out of *me* and *mdh* would neither enhance malate accumulation nor affect *Synechocystis* growth. On the other hand, the double deletion of the two target genes would induce the accumulation of malate with small slowdown effect on the cell growth. The results of the simulations in terms of growth rate and malate and fumarate yields are reported in Table 4.2, together with the experimental measurements. In the case of the double knock out mutant $\Delta me\Delta mdh$, *in silico* simulations predict malate or fumarate production, for a total amount of 0.860 mmol gDW^{-1}. In other words, each compound
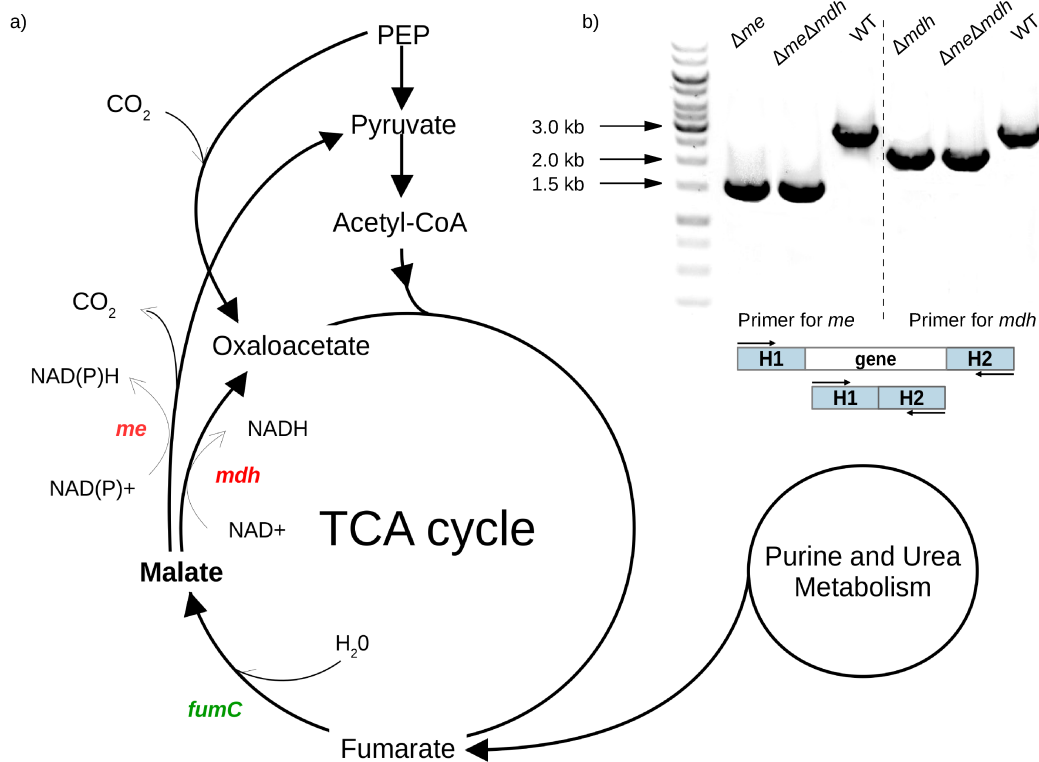
Figure 4.6: Overview of the malate pathway in *Synechocystis* and generation of mutants. a) In red are indicated the genes knocked-out and in green the overexpressed one in this study. b) PCR confirmation of the markerless deletions of *me* and *mdh* genes in the constructed strains Δme, Δmdh, $\Delta me\Delta mdh$ of *Synechocystis*. By using primers pairing with the up- and downstream regions flanking the native gene (about 1 kb each), the PCR products of the knockout mutants have a size of 1.5 kb for Δme and 1.8 for Δmdh. The WT bands are 2.8 and 2.9 kb for *me* and *mdh*, respectively.

can assume a value between 0 and 0.860, with the additional constraint that the maximum value of the sum of the two is equal to 0.860.

In order to experimentally test these model predictions, we engineered three deletion mutants, namely Δme, Δmdh and $\Delta me\Delta mdh$ (Figure 4.6b). WT *Synechocystis* was subjected to two consecutive rounds of transformation to remove by markerless deletion the *me* and *mdh* genes.

4.3.2 Characterization of the deletion mutants

The engineered strains and the WT were cultured photoautotrophically under continuous light in the Multi-Cultivator. Δmdh grew similarly to the WT until the end of the experiment (exponential growth rate = $0.055\,\text{h}^{-1}$) , while Δme and $\Delta me\Delta mdh$

Table 4.2: Simulated and measured growth rate and yields for the WT and the deletion mutants. The experimental values of both yield and growth rate are referred to the exponential growth phase, according to data shown in Figure 4.7 and 4.8). The ÷ denotes the range of values allowed, whereas between brackets is reported the standard deviations referred to the last digits of the quoted value.

Strains	Growth rate (h^{-1})		Malate yield (mmol gDW^{-1})		Fumarate yield (mmol gDW^{-1})	
	Model	Measure	Model	Measure	Model	Measure
WT	0.052	0.055(1)	0	0	0	0
Δme	0.052	0.052(0)	0	0.067(19)	0	0.274(14)
Δmdh	0.052	0.055(0)	0	0	0	0
$\Delta me\Delta mdh$	0.050	0.050(1)	0 ÷ 0.860	0.607(91)	0 ÷ 0.860	0.557(2)

showed a slower growth in the exponential phase (0.052 and 0.050 h^{-1}, respectively) compared to the WT (Figure 4.7a, Table 4.2). A similar slowdown effect on growth, due to the disruption of the gene encoding for Me, was observed by Bricker and co-workers [221]. Notably, the Δme and $\Delta me\Delta mdh$ reached higher optical density once entering the stationary phase compared to the other strains (Figure 4.7a). However, cell size measurements revealed that this phenomenon was due to an increase of cellular dimension of Δme and $\Delta me\Delta mdh$ rather than to an actual major number of cells (Figure 4.7b and 4.7c). A linear correlation (Pearson correlation coefficient = 0.93) between the cell volume ratio, that is the volume occupied by the cells over the total volume of broth, and the OD$_{730}$ values was found (Figure 4.7c). This correlation indicates that the measurement of the optical density alone is not always a good parameter for growth estimation, since it depends on both the number of cells and their size, as also observed by Huokko and co-workers [222]. An increase in cell size has been recorded for other microorganisms, such as *E. coli*, engineered for malate production [154]. This phenomenon is likely due to some inteference effect on the metabolism of the cell mediated by the intracellular accumulation of malate and fumarate which may alter the redox balance (both Me and Mdh generate reduced cofactors) or exert a certain toxicity due to the acid nature of the two metabolites.

Comparison of fumarate and malate extracellular production between the WT and the engineered strains allowed to assess the impact of deleting *me* and *mdh* on the metabolism of *Synechocystis*. As expected from previous works, which investigated the secretion of organic metabolites by *Synechocystis* grown under photoautotrophic conditions [223], neither fumarate nor malate were detected in significant amount in the extracellular broth of WT. In contrast to *in silico* analysis, which predicted a null malate yield for Δme (Table 4.2), this mutant was able to accumulate modest amount of malate, indicating that the conversion of malate into oxaloacetate by the Mdh is less effective than the consumption of malate into pyruvate mediated by the Me. This result
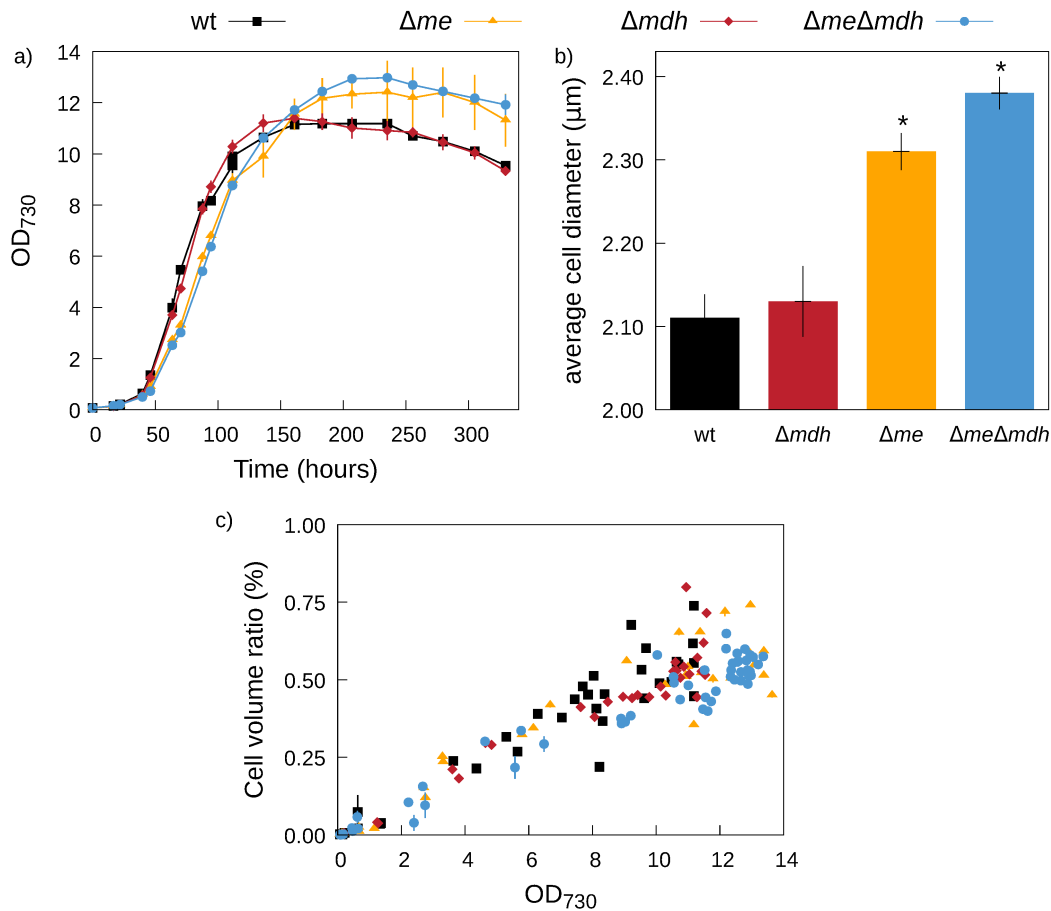
Figure 4.7: Phenotypic characterization of WT and knockout mutants Δme, Δmdh and $\Delta me\Delta mdh$ of *Synechocystis* cultivated under continuous light in photobioreactor. a) Growth curves of the different strains. b) Average cell diameter of the different strains measured in the steady phase starting from $\sim$ 136 h cultivation onward. c) Variation of the cell volume ratio with respect to the OD_{730} values. The values are mean and uncertainties of at least two biological replicates (n=6 for the $\Delta me\Delta mdh$ strain). *p < 0.05 according to Student's t-test for statistical comparison of data.

is partially in agreement with ^{13}C flux analysis [223, 224, 144] showing that during continuous illumination, similar to that of our set-up, the high levels of ATP generated photosynthetically inhibit the pyruvate kinase, which converts PEP into pyruvate (Figure 4.6a), inducing cells to convert malate for supplying the necessary pyruvate. In this context, indeed, the higher activity of Me compared to Mdh could be functional to provide pyruvate, thus compensating the bottleneck through the pyruvate kinase. In accordance with model predictions (Table 4.2), both fumarate and malate were released in the extracellular broth by $\Delta me\Delta mdh$ strain in higher yields compared to the single mutant Δme (Figure 4.8a and 4.8b). The maximum titers of malate and fumarate
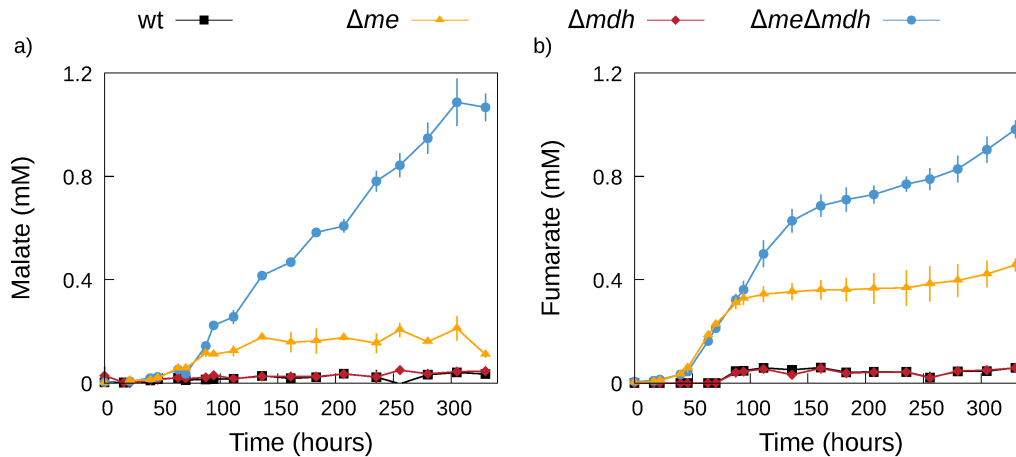
Figure 4.8: Extracellular production of malate a) and fumarate b) for WT, Δme Δmdh and $\Delta me\Delta mdh$ strains under continuous illumination in photobioreactor. Values are mean and standard errors of at least two biological replicates. Values below the detection limit of the analytical techniques (i.e., 2 µM for malate and 20 µM for fumarate) are reported as zero in the panels

observed in the $\Delta me\Delta mdh$ strain were 1 mM and 1.2 mM, respectively, after 14 days of cultivation (Figure 4.8a and 4.8b).

4.3.3   Improving malate accumulation by *fumC* overexpression

The $\Delta me\Delta mdh$ strain was the mutant with the highest malate production (Figure 4.8a), however, the presence of a considerable amount of fumarate in the culturing broth (Figure 4.8b) indicates that the conversion of fumarate into malate catalyzed by the FumC might be limited. To overcome a possible enzymatic bottleneck due to restricted access to the substrate and/or low expression of FumC and ensure the highest conversion of fumarate, *fumC* gene from *E. coli* was integrated into a neutral site (NSI) in the genome of *Synechocystis* WT and in the $\Delta me\Delta mdh$ strain in order to obtain *fumC* overexpressing mutants (Figure 4.9). Full segregation of the two strains, $\Delta NSI::fumC$ and $\Delta me\Delta mdh\Delta NSI::fumC$, was confirmed by PCR analysis with primers that pair to the up- and downstream homologous regions of the target locus (Figure 4.9 and Table 3.2).

The fumC overexpressing strains were cultured photoautotrophically under continuous light in the Multi-Cultivator in the same conditions as the deletion mutants. The growth curve of $\Delta NSI::fumC$ was similar to that of the WT, whereas $\Delta me\Delta mdh$ $\Delta NSI::fumC$ showed a slower growth during the exponential phase compared to the $\Delta NSI::fumC$. Conversely, $\Delta me\Delta mdh\Delta NSI::fumC$ grew similarly to the $\Delta me\Delta mdh$ in the first stages of growth, reaching the steady state earlier than the double mutant (Figure 4.10a). Concerning malate and fumarate extracellular production, the overexpression of *fumC* alone in *Synechocystis* was not sufficient to enhance the secretion
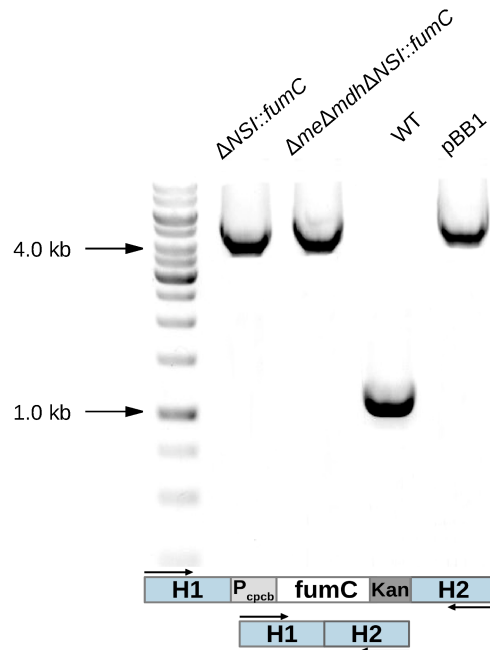
Figure 4.9: PCR confirmation of the integration of the *fumC* gene into a neutral site (NSI) in *Synechocystis* WT and in the $\Delta me \Delta mdh$ strain. By using primers pairing with the up- and downstream regions flanking the neutral site, the PCR products of the knock-in mutants have a size of 4 kb. WT genomic DNA and the integration vector pBB1 have been used as negative and positive control, respectively.

of detectable quantities of neither of the two compounds (Figure 4.10b). On the other hand, $\Delta me \Delta mdh \Delta NSI::fumC$ was capable to release in the extracellular environment a higher titer of malate and a lower titer of fumarate compared to the $\Delta me \Delta mdh$ strain determining a higher molar ratio of malate over fumarate in the extracellular broth throughout the entire cultivation (Figure 4.10c). When analyzing the malate productivity, the highest productivity was observed during the exponential phase for both the $\Delta me \Delta mdh \Delta NSI::fumC$ and $\Delta me \Delta mdh$ strains (Figure 4.10d). In this growth phase, the malate productivity of the over-expressing triple mutant was significantly higher than that of the double deletion mutant, once more indicating an improved ability of conversion of fumarate into malate in the $\Delta me \Delta mdh \Delta NSI::fumC$ mutant.

4.3.4   Measurement of intracellular metabolites

Carriers for the transport of C_4-dicarboxylic acids across the membrane of *Synechocystis* have not been identified, yet. Fumarate and malate are expected to be completely dissociated given their pKa values (4.17 and 2.88 for fumarate and 4.83 and 3.40 for malate) [225] and the intracellular pH of 7.5 [226]. For this reason, passive diffusion
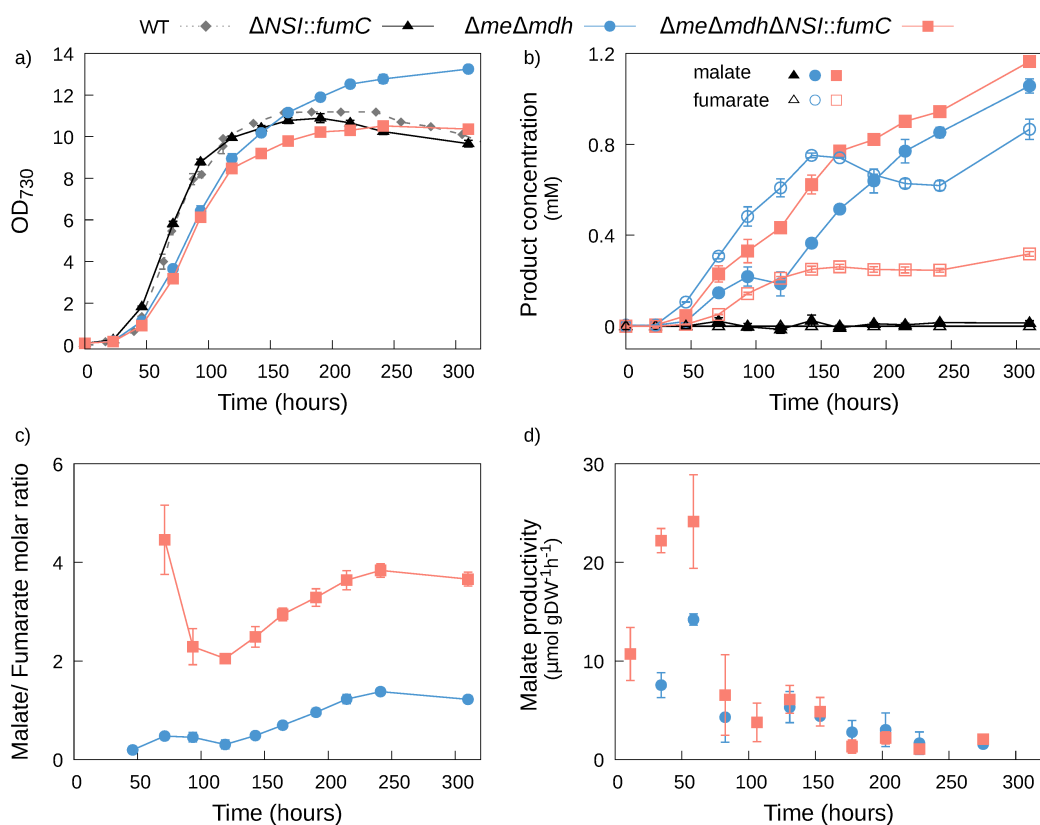
Figure 4.10: Characterization of *fumC* overexpressing strains of *Synechocystis* compared to the WT and to the double knockout Δ*me*Δ*mdh* cultivated under continuous light in photobioreactor. a) Growth curves and b) extracellular production of malate and fumarate of the different strains. Variation of c) malate/fumarate molar ratio and d) malate productivity of Δ*me*Δ*mdh* and Δ*me*Δ*mdh*Δ*NSI::fumC* strains. Values are mean of at least two biological replicates. Error bars are standard errors of the mean in panel a) and b), and combined standard uncertainty in panel c) and d). Concentration values below the detection limit of the analytical techniques used (i.e., 2 μM for malate and 20 μM for fumarate) are reported as zero in panel b). Malate/fumarate molar ratios are not reported whenever either malate or fumarate concentration falls below the detection limit.

of malate and fumarate is unfeasible due the hydrophobic nature of the membrane and the presence of these metabolites in the cultivation broth suggests the existence of a protein-mediated efflux. In order to investigate the actual conversion of fumarate into malate catalyzed by the *fumC* and possible transporter effects on the efflux of these metabolites across the membrane, the intracellular concentration of the two metabolites was measured in the WT, Δ*me*Δ*mdh* and Δ*me*Δ*mdh*Δ*NSI::fumC* and compared to their extracellular counterpart (Figure 4.11).
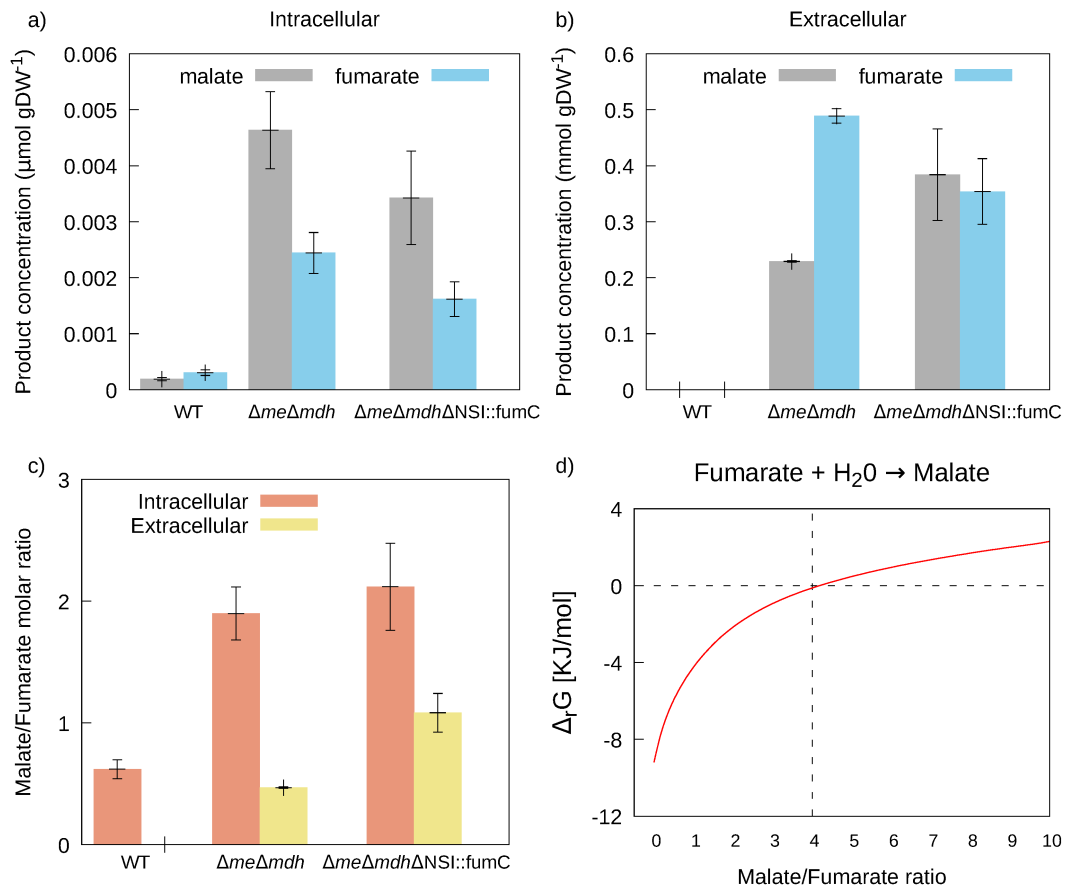
Figure 4.11: Malate and fumarate levels inside and outside the cell of different strains. Intracellular a) and extracellular b) concentration of malate and fumarate in the engineered and WT strains. c) Intracellular and extracellular molar ratio of malate/fumarate in the different strains. Error bars in a) and b) are the expanded uncertainties (n=3), error bars in c) are the combined standard uncertainties. d) Variation of the Gibbs reaction free energy for increasing molar ratio of malate/fumarate calculated through eQuilibrator (pH =7.0, ionic strength = 0.1 M, temperature = 25 °C) [227].

For these measurements, samples were cultivated in flask (see Material and Methods section for details) and collected in the exponential growth phase (i.e., OD_{730} = 1), at which the recombinant strains had shown the maximum extracellular malate productivity in batch cultivation in Multi-Cultivator (Figure 4.10d). In parallel, extracellular concentrations of the two metabolites, were recorded as well.

Intracellular concentrations of malate and fumarate were significantly higher in the engineered strains compared to the WT (Figure 4.11a). Intracellular amount of fumarate and malate were 3.03×10^{-4} and 1.88×10^{-4} $\mu mol\, g^{-1}$ of cell dry weight, respectively

for the WT. In the $\Delta me \Delta mdh$ and $\Delta me \Delta mdh \Delta NSI$::*fumC* strains the intracellular concentrations of malate were ~ 20 times higher compared to the WT (4.64×10^{-3} and 3.43×10^{-3} μmol g^{-1} of cell dry weight, respectively), whereas those of fumarate were one order of magnitude higher compared to the WT (2.44×10^{-3} and 1.62×10^{-3} μmol g^{-1} of cell dry weight, respectively)(Figure 4.11a).

$\Delta me \Delta mdh$ and $\Delta me \Delta mdh \Delta NSI$::*fumC* showed an intracellular malate/fumarate molar ratio 4 times higher compared to the WT (Figure 4.11c). Interestingly the intracellular molar ratio was similar in the two mutants and attested around a value of 2, which, apparently, represents the homeostatic condition for the engineered strains. This ratio results in accordance with thermodynamic analysis indicating that the conversion of fumarate into malate (i.e., forward reaction) is favored up to an intracellular malate/fumarate molar ratio of 4 (Figure 4.11d), and confirms the favorable outcome of the metabolic engineering strategy adopted. On the other hand, extracellular malate/fumarate molar ratio was two times higher in the $\Delta me \Delta mdh \Delta NSI$::*fumC* than in the $\Delta me \Delta mdh$ strain (Figure 4.11c). Considering the similar intracellular malate/fumarate ratio shown by the two mutants (Figure 4.11c), the higher extracellular amount of malate in the $\Delta me \Delta mdh \Delta NSI$::*fumC* (Figure 4.11b) might result from an enhanced secretion adopted by this mutant to keep constant the intracellular malate/fumarate homeostatic ratio of 2.

Characterization of the carriers for C_4-dicarboxylic acids would be desirable in order to elucidate the mechanisms of transport across the membrane and ameliorate the excretion of these target compounds.

4.3.5 Genetic stability of malate production of the engineered strains

The engineering approach adopted to build the $\Delta me \Delta mdh$ strain is based on the deletion of the two consumption pathways of malate. This strain is therefore expected to be stable because the evolution time required to re-evolve the deleted enzymatic capabilities is longer than time-scales commonly adopted in industrial applications [165, 166]. Most importantly, malate production should be stably maintained on the grounds that its precursor, fumarate, is a growth-coupled metabolite. On the other hand, there are no indications that the productivity of $\Delta me \Delta mdh \Delta NSI$::*fumC* will remain stable over several generations. Indeed, in this over-expressing mutant, more cellular resources are involved in the synthesis of FumC, thus introducing a protein burden to the cell absent in the double knock-out strain.

Genetic stability of the most productive strains, namely $\Delta me \Delta mdh$ and $\Delta me \Delta mdh \Delta NSI$::*fumC*, was assessed through a serial propagation experiment in which the cultures were kept in an exponential growth (OD_{730} between ~ 0.6 and 1) over a period of ~ 2 months to assure a constant selective pressure [208]. As a control strain, we used SAA023, a lactate producing mutant of *Synechocystis* engineered according to a
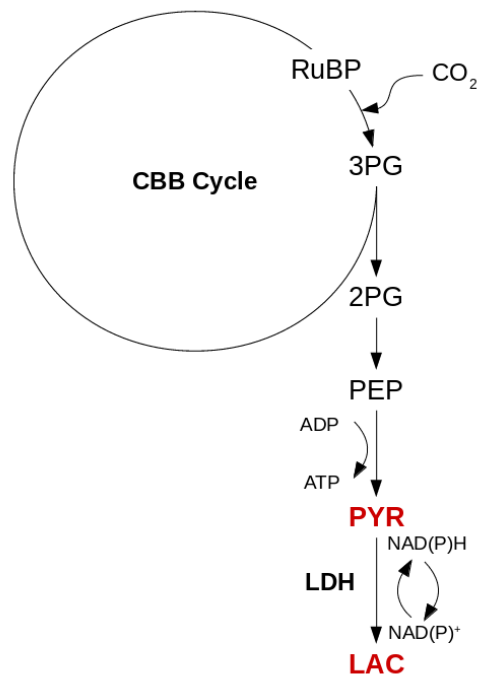
Figure 4.12: Schematic representation of engineered lactate production pathway in the SAA023 mutant of *Synechocystis*. In this strain, the LDH enzyme from *L. lactis*, converting PYR into LAC, has been inserted in the genome of *Synechocystis*. CBB: Calvin–Benson–Bassham cycle, RuBP: ribulose 1,5-bisphosphate, 3PG: 3-phosphoglycerate, 2PG: 2-phosphoglycerate, PEP: phosphoenolpyruvate, PYR: pyruvate, LAC: lactate, LDH: lactate dehydrogenase.

classic metabolic engineering method. The SAA023 strain carryes the L-lactate dehydrogenase (L-LDH) enzyme that converts pyruvate into L-lactate [47] (Figure 4.12) and it has already been shown to be unstable during prolonged culturing since spontaneous revertants with mutations in the *ldh* cassette become dominants after few generations [162]. The genetic instability of this strain is associated to the metabolic engineering strategy used, that imposes a high trade-off between biomass growth and product formation, because an essential metabolite of the central metabolism, such as pyruvate, is depleted [162].

Along the experiment, a number of generations between 42 and 50 of each cultures has been monitored. $\Delta me\Delta mdh$ and $\Delta me\Delta mdh\Delta NSI::fumC$ accumulated malate in the extracellular environment until the end of the serial propagation (Figure 4.13a), albeit with some fluctuations along time, whereas a clear drop in lactate extracellular productivity was recorded for the SAA023 strain (Figure 4.13b). To check whether this decrease in lactate was due to the presence of mutations in the *ldh* cassette, the gene encoding for
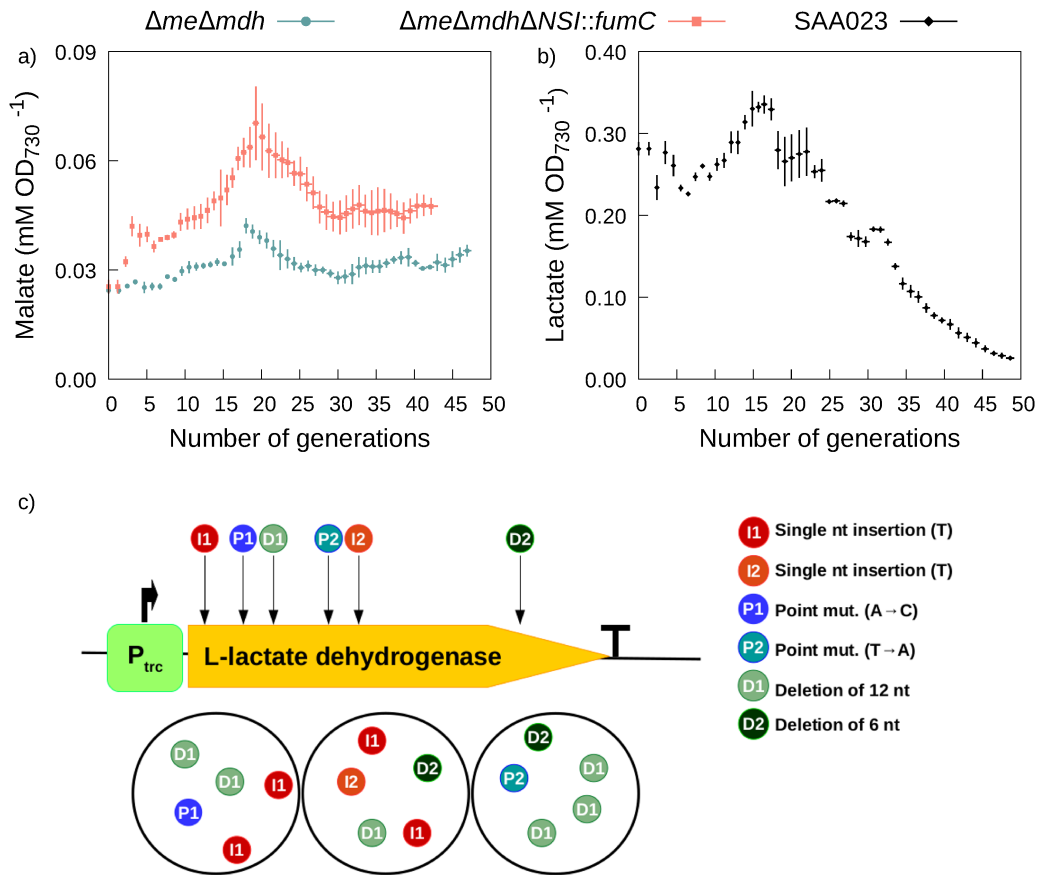
Figure 4.13: Testing the genetic stability of malate and lactate production in different mutant strains of *Synechocystis* during the serial propagation experiment. a) Malate production normalized by the OD_{730} of $\Delta me\Delta mdh$ and $\Delta me\Delta mdh\Delta NSI::fumC$ strains. b) Lactate production normalized by the OD_{730} of SAA023 strain. c) Mutations (and their positioning) found after sequencing of the *ldh* cassette in colonies of SAA023 deriving from the last generation observed. The distribution of the mutations amongst the three experimental populations is reported in the circles. In panel a) and b), the values are mean of three biological replicates, the y error bars are combined uncertainties, the x error bars are standard errors.

the LDH and the upstream promoter sequence were amplified from 15 single colonies (5 from each of the 3 biological replicates) and subjected to Sanger sequencing. Mutations in the *ldh* cassette were found in all the analysed sequences. These mutations included insertions, deletions of nucleotides and single point mutations (Figure 4.13c and Table 4.3). In particular, the most abundant mutation was a deletion of a region composed by the repetition of 6 nucleotides, for a total length of 12 bases, which leads

to a truncated polypeptide (Table 4.3). Since this mutation occurred in all the three independent analyzed populations, the region involved is likely a 'mutational hot spot' of the *ldh* gene, that is a region where the duplication machinery is more prone to make mistakes. A similar mutation pattern was also observed in the *efe* gene expressed in *Synechocystis* [45]. Interestingly, the detected mutations only affect the correct translation of the LDH protein and not the transcription of the *ldh* (because no mutations involved the promoter). Since these mutations target primarily the activity of the protein rather than its synthesis, it is likely that the expression per se is not a trade off point with growth rate. On the other hand, no mutations were found in the *fumC* cassette.

Compared to that of lactate, the accumulation of malate was stably maintained for more than 45 generations by Δ*me*Δ*mdh* (Figure 4.13a), thus suggesting that the production of malate does not seem to be a burden for the cell. Hence, strategies aiming at aligning fitness and product formation instead of "stealing" central C-compounds necessary for growth – as pyruvate, – are once again confirmed to be promising [142, 220]. Besides this, the overexpression of FumC did not seem to be an unsustainable cost in terms of protein resources for the economy of the cell, since no decrease in the growth rate (Figure 4.10) and no losses in malate production (Figure 4.13a) were recorded for Δ*me*Δ*mdh*Δ*NSI::fumC* strain over more than 40 generations and therefore no selective pressure is active against this introduced trait.

Table 4.3: Translation analysis related to the mutations found in the sequenced *ldh* cassettes.

Mutation type	Position (from ATG)	Translation analysis	Frequency
Deletion of 12 nucleotides	190-201	missing aa 65-68	6 out of 15
Point mutation (A to C)	180	K61Q	1 out of 15
Point mutation (T to A)	293	N98K	1 out of 15
Single nucleotide insertion (T)	132	translation of 46 aa	4 out of 15
Single nucleotide insertion (T)	305	translation of 60 aa	1 out of 15
Deletion of 6 nucleotides	711-717	missing aa 238 and aa 239	2 out of 15

4.3.6   Conclusions

The feasibility of a metabolic engineering strategy aiming at exploiting a strict growth-coupled compound, fumarate, to drive the accumulation of a downstream metabolite, malate, has been here proved. By implementing this strategy a strain of *Synechocystis* able to accumulate a significant amount of malate, namely Δ*me*Δ*mdh*, has been engineered. The conversion of fumarate into malate has been further improved by overexpressing FumC in the Δ*me*Δ*mdh* strain. The synthesis of extra amount of

FumC did not compromise the fitness of the microorganism and did not cause losses in malate productivity due to genetic instability. These results indicate that the strategy here proposed could be in principle applied to any compounds deriving from a growth coupled metabolite, as long as the latter results as a by-product of the anabolism and the reaction is thermodynamically favorable.

4.4   Exploring malate and fumarate export mechanism

Knowledge about transport systems in *Synechocystis* sp. PCC 6803 is lacking. Data concerning the crossing mechanisms of the plasma membrane by different classes of compounds, including organic acids such as fumarate, malate, succinate and acetate, are largely missing [228]. Nevertheless, understanding the extracellular transport system of a microbial host represents an important goal for the industrial feasibility of any microbial cell factory. Indeed, the ability of an engineered organism to release the target compound(s) in the extracellular environment can prevent the economic burden related to the extraction step in the downstream process. In addition, toxic effects – such as osmotic pressure and pH stress – due to the intracellular accumulation of high concentrations of a certain compound could be avoided, allowing a more efficient microbial cultivation. Finally, elucidating the transport mechanisms would allow the fine tuning of the efflux process, thus removing possible bottlenecks.

Even though their transporter(s) has not been identified, the detection of extracellular amounts of malate and fumarate in the engineered strains $\Delta fumC$, Δme, $\Delta me\Delta mdh$, and $\Delta me\Delta mdh\Delta NSI::fumC$ of *Synechocystis* suggests the presence of a native transport system. Malate and fumarate are dicarboxylic acids with 4 atoms of carbon showing similar chemical properties and structure. The mechanism responsible for their secretion is therefore expected to be similar. Given the intracellular pH of *Synechocystis* (estimated ~7.5-7.7) [226], fumarate and malate are completely dissociated inside the cell. Fumarate pKa1 and pKa2 are 4.17 and 2.88, whereas malate pKa1 and pKa2 are 4.83 and 3.40 at standard conditions (T= 25 °C, ionic strength = 0.1 M), respectively [225]. Passive diffusion of the ionized forms of malate and fumarate across the membrane is not favorable due to the hydrophobic nature of the latter, suggesting the existence of a protein-mediated efflux. Several secondary transporter families are involved in C_4-dicarboxylate transport, including uptake, exchange and efflux, in many bacteria. Most of these protein carriers show promiscuous activity: they can accept diverse C_4-dicarboxylic acids (succinate, fumarate, malate) and C_4-dicarboxylic amino acids (aspartate) as substrates with different Kd values for each substrate [229]. DcuAB carriers seem to be related to the uptake and exchange of C_4-dicarboxylates in anaerobic and facultative anaerobic bacteria capable of fumarate respiration. DcuC transporters, as well as DcuAB, are expressed during anaerobic growth conditions, but they were primarily associated to the efflux. DctA transporters mainly work as H^+ or Na^+-C_4-dicarboxylate symporters and they are involved in the uptake of C_4-dicarboxylates in aerobically growing bacteria [230]. TRAP (tripartite ATP-independent periplasmic) transporters, firstly characterized in the purple bacterium *Rhodobacter capsulatus*, represent a family of permeases for organic acids widely distributed among Gram-negative bacteria. They consist of two integral membrane proteins (DctM and DctQ) and a soluble periplasmic substrate-binding protein (DctP) and use a proton gradient as electrochemical driving force to drive the transport [231, 232].

4.4.1 Homology search for C$_4$-dicarboxylate transporters in *Synechocystis*

Since there are no information available about C$_4$-dicarboxylate transporters in *Synechocystis*, bioinformatics homology search using sequences from known C$_4$- dicarboxylic acid transporters from other organisms was carried out by the Amsterdam-IGEM team 2017 to identify suitable targets that may encode components of a dicarboxylic acid transporter (http://2017.igem.org/Team:Amsterdam/Export, accessed 07/06/2019). Both targeted and untargeted searches were performed. The former was addressed to known, phylogenetically closely related transporters, protein motifs and conserved domains whose sequences were used as a template for the alignment, whereas the latter was used to profile large groups of sequences (including putative identifications) and find distant homologous relationships between proteins. In phylogenetically closely related cyanobacteria, such as *Synechococcus* and *Nodularia spumigena* [36], C$_4$-dicarboxy-late transporter (domain)s have been identified. In particular, in *Synehcococcus*, a DctM domain was found, whereas in *N. spumigena*, a DcuC transporter was putatively identified based on sequence homology studies.

Two suitable targets, locus *sll1103* and locus *sll1314*, were identified as putative C$_4$-dicarboxylic acid transporters in *Synechocystis. Sll1103* is mapped to the conserved domain of DctM (pfam06808), with an E-value of 2.5 E-44, whereas *sll1314* is mapped to the conserved domain of DctP (TIGR00787) with an E-value of 3.3 E-106. To find indications about the actual function of the translated products from the two loci, the similarity at the protein level between these two putative domains and their corresponding counterpart in phylogenetically close microorganisms, has been assessed by amino acid sequence alignment (Pairwise sequence alignment though Needle EMBOSS algorithm with default settings [233]). The DctM subunit of *Synechocystis* (UniProtKB P74224) shares 62.7% amino acid identity to the DctM subunit from *Synechococcus* sp. WH8016 (UniProtKB J4IQ13) (Appendix B, Figure A.1) and 19.6% to DcuC from *N. spumigena* (UniProtKB A0ZHV0) (Appendix B, Figure A.2). The DctP subunit of *Synechocystis* (UniProtKB P73589) shares 61.9% amino acid identity to the DctP from *Synechococcus* sp. PCC 7502 (UniProtKB K9SU31) (Appendix B, Figure A.3). The *sll1314* locus probably encodes a periplasmic substrate-binding protein, as also suggested in the proteomic study by Fulda and co-workers [234].

4.4.2 Role of *sll1103* and *sll1314* loci in *Synechocystis*

To experimentally prove the function *in vivo* of *sll1103* and *sll1314*, two knock-out mutants of these putative genes on the background of the Δ*fumC* strain have been constructed and phenotypically characterized by the Amsterdam-IGEM team 2017 (http://2017.igem.org/Team:Amsterdam/Export, accessed 07/06/2019). To study the possible involvement of *sll1103* and *sll1314* in fumarate efflux, Δ*fumC*Δ*sll1103* and Δ*fumC*Δ*sll1314* were grown and tested in comparison to the Δ*fumC* strain. Whereas no variations in
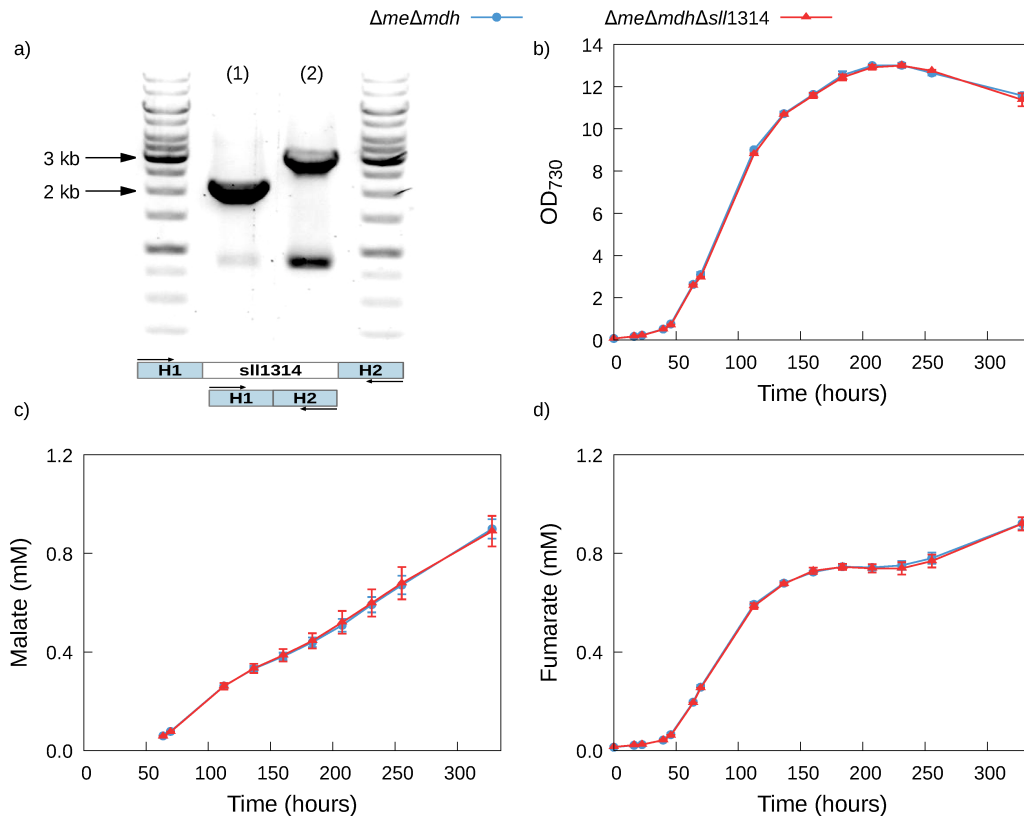
Figure 4.14: Characterization of $\Delta me\Delta mdh\Delta sll1314$ knockout mutant of *Synechocystis*. a) PCR confirmation of the markerless deletions of *sll1314* gene in the constructed strain $\Delta me\Delta mdh\Delta sll1314$ of *Synechocystis*. By using primers pairing with the up- and downstream regions flanking the native gene ($\sim$ 1 kb each), the PCR product of the knock-out mutant has a size of about 2 kb (1). The WT band for the *sll1314* locus is 3 kb (2) b) Growth curve of the $\Delta me\Delta mdh$ and $\Delta me\Delta mdh\Delta sll1314$ strains cultivated under continuous light in photobioreactor. Extracellular production of malate c) and fumarate d) for $\Delta me\Delta mdh$ and $\Delta me\Delta mdh\Delta sll1314$ mutants. Values are mean and standard errors (n=4).

the outer concentration of fumarate were recorded for the $\Delta fumC\Delta sll1103$ mutant, the $\Delta fumC\Delta sll1314$ strain showed a 31% decrease in the fumarate extracellular concentration after 49 h of cultivation under continuous light. *Sll1314* is possibly encoding for a component of the fumarate transport system, however, since the extracellular transport of the compound was not completely abolished, *sll1314* is likely not the only efflux carrier for fumarate.

Based on these preliminary results, we wanted to further investigate the role of *sll1314*, and in particular, its selective properties, by engineering a markerless knock-out mutant on the $\Delta me\Delta mdh$ background. We hypothesized that if the protein encoded by

sll1314 was also capable of binding malate, a variation in the extracellular concentration of the latter would occur. If not, decreasing the ability of the $\Delta me\Delta mdh$ strain to export fumarate would increase the intracellular accumulation of malate, since the fraction of fumarate not-excreted would remain inside the cell where it is accessible to the FumC enzyme which converts it into malate.

4.4.3 Phenotypic characterization of $\Delta me\Delta mdh\Delta sll1314$ knock-out mutant of *Synechocystis*

Full segregation of $\Delta me\Delta mdh\Delta sll1314$ strain was confirmed by PCR analysis with primers that pair to the up- and downstream homologous regions of the target locus (Figure 4.14a). The markerless triple deletion mutant and the $\Delta me\Delta mdh$ were cultured in a Multi-Cultivator photobioreactor under continuous light illumination (120 µmol photons/m^2/s) and the extracellular concentrations of malate and fumarate were measured at different time intervals. The two strains showed an identical growth behavior (Figure 4.14b). Malate and fumarate extracellular concentration measurements did not show significant differences between the two strains (Figure 4.14c and 4.14d). The knockout of the *sll1314* gene did not seem to interrupt the export of fumarate and malate in the $\Delta me\Delta mdh$ strain. The trend of the extracellular concentration of both compound throughout the whole experiment suggests that the putative protein codified by *sll1314* locus is not primarily involved in the fumarate and malate export.

4.4.4 Conclusions

The deletion of the *sll1314* gene, which likely codifies for the soluble periplasmic substrate-binding protein of a TRAP transporter, was not sufficient to stop neither malate nor fumarate export in the *Synechocystis* strain $\Delta me\Delta mdh\Delta sll1314$. Further characterizations of the native C_4-dicarboxylate carriers of *Synechocystis* are needed in order to elucidate the mechanism underlying the transport mechanism of malate and fumarate and, ultimately, to improve the productivity of the engineered strains presented in this study. Alternatively, the introduction of heterologous carriers, such as the 00582-Lr from *L. rhamnosus* 705 or the DcuB from *E.coli* [235], could be a feasible strategy to increase the efflux of dicarboxylic acids.

Chapter 5

Retro-mutants dynamics modeling

The content of this Chapter forms the basis of a manuscript in preparation: Battaglino, B., Arduino, A., Pagliano, C. Mathematical modeling study of the dynamics of a retro-mutant population of photosynthetic microorganisms.

5.1 Introduction

The genetic instability of the engineered strains is nowadays one of the major constraints to the spreading of large-scale MCF processes. The loss of productivity and yield has been reported for many engineered microorganisms [162, 45, 160, 159] and has been mainly associated to the arising inside the population of revertant mutants which have mutated the genes responsible for the formation of the target compound(s). The producing cells often experiment detrimental effects on the fitness due to the presence of heterologous pathways that alter the carbon flux or interfere with the resource allocation inside the cell [208].

The effective genetic stability of an engineered strain can be assessed through an evolution experiment in which the microorganisms are subjected to long periods of culturing under laboratory conditions in order to select and characterize the possible arising of retro-mutants with an expected increased fitness, as reported in the previous sections 4.2 and 4.3. These experiments often result time- and resource-consuming, therefore alternative strategies that allow to predict the population dynamics of retro-mutants are advisable. One possibility is the design of a mathematical model describing the onset of genetic instability inside a population.

In order to devise such a mathematical model, two main points were considered: i) the intrinsic biological properties of photosynthetic microorganisms and ii) the evolution of finite populations, resulting into an innovative combination of classic literature approaches [236, 237]. In particular, the proposed model takes into account the effect

of light availability on the growth of photosynthetic microorganisms, such as the light-limitation, determining sub-optimal growth, and light-excess, leading to photoinhibition. The model could be used to search for the optimal constraints that the cultivation system should satisfy to guarantee the longest stability, given the genetic and metabolic characteristics of the engineered strain.

The developed deterministic model has been validated by comparing its results with those obtained with a stochastic one. The latter is more expensive from the computational point of view, but is often preferred because of its capability to reproduce the aleatoric nature of the population evolution and dynamics, so its solution is used as a reference.

5.2   Microbial growth and evolution

Evolutionary dynamics in populations depends on mutations and their effect on phenotype, that is on the fitness of the organism. In microbial evolution experiments, the starting point usually consists of a monoclonal population with no recombinant capability, therefore, ideally without initial heterogeneity. In this situation the only source of variability is given by the spontaneous mutations arising in the population on which the natural selection will act [238, 164]. The sequencing technologies together with innovative experimental procedures (such as marker divergence studies) allowed to detect these mutations and to gain useful information about the dynamics of adaptation in microbial populations[238]. On the other hand, theoretical models of evolution generally consider the relative fitness advantages of different mutants in a population of a given size (N) [239]. The population under examination could be either a haploid population (one copy of each gene per individual) or a polyploid population (more than one copy of each gene per individual). Moreover, the individuals in the population may reproduce asexually or sexually. Here, we will focus on a haploid asexually reproducing population, in which only one type of mutation can occur (i.e. no clonal interference). Several deterministic models describing a variety of microbial evolution dynamics are present in the literature. For instance, Luria and Delbruck developed a model, validated by experimental data, which allowed to understand that the arising of virus-resistant bacteria is independent from the presence of virus, but is determined only by the mutation rate of bacteria. The resistance trait does not alter the growth rate of the mutants but confers a selective advantage when virus are present [240]. Other mathematical models have been developed to describe the antibiotic resistance phenomena [241, 242]. Many stochastic models of an evolving population have been proposed, being the Fisher-Wright model [243] and the Moran model [244, 245] the most known. These models, however, usually consider a constant population size which does not allow to take into account the effect of the environment on the population, as also pointed out in [239]. Here, a deterministic model describing the population dynamics when a producing strain is susceptible to suppression is proposed. A variant of the Moran process, with varying size N, is

presented below and used to validate the developed deterministic model.

5.2.1 Deterministic model

The growth model of a generic population can be written employing the Malthus equation

$$\frac{dN}{dt} = \mu N - DN,\tag{5.1}$$

being N the population size, μ the net growth rate and D the possible dilution rate in case of chemostat cultivation mode.

The modeling of an engineered producing population is inevitably more complex than that described by the Malthus equation. Precisely, the model needs to reproduce the following phenomenological observations:

- the synthesis of a product can be burdensome for the producing population p, whose growth rate is consequently affected;

- the probability of the arising of retro-mutants w that loose the production traits is not negligible, whereas the re-evolution of the deleted traits or the spontaneous development of the inserted traits is almost impossible, in a relatively short time-scale.

Consequently, the total number of individuals into the population is $N = w + p$, whose growth can be described by the following system of equations, adapted from [237]

$$\begin{cases} \dfrac{dp}{dt} = \underbrace{\mu_+(1-\rho)p}_{\text{growth}} - \underbrace{\mu_+(1-\rho)\tilde{m}p}_{\text{retro-mutations}} + \underbrace{\mu_- p}_{\text{death}} - \underbrace{Dp}_{\text{dilution}} \\[3mm] \dfrac{dw}{dt} = \underbrace{\mu w}_{\text{growth/death}} + \underbrace{\mu_+(1-\rho)\tilde{m}p}_{\text{retro-mutations}} - \underbrace{Dw}_{\text{dilution}} \end{cases}\tag{5.2}$$

In the latter formula p is the producing population size, w is the retro-mutant population size, μ is the retro-mutant population growth rate (where μ_+ is the positive part of μ and μ_- is its negative part)[1], ρ is the production burden, $\tilde{m} = m/\log(2)$ with m the mutation rate per generation, and D the possible dilution rate in case of chemostat cultivation mode. It is worth noting that in 5.1 the population size w equals the total number of individuals N in the culture.

The retro-mutants growth term is the same as in (5.1), whereas the one of the producing population takes into account the production burden by means of a multiplicative factor (for $\mu > 0$). A term modeling the contribution of the retromutations is introduced coupled to the producers growth by multiplying it to the producers growth rate.

---

[1]The function positive part, denoted by $(\cdot)_+$, is equal to its argument when it is positive and is null otherwise. Viceversa for the function negative part, denoted by $(\cdot)_-$.

The death term is explicitly present in the producing population dynamics equation because when μ is negative, the production burden has no role.

If μ is assumed constant and greater than zero and the dilution rate is null, then equation (5.2) simplifies in

$$\begin{cases} \dfrac{dp}{dt} = \mu(1 - \rho)(1 - \tilde{m})p \\ \dfrac{dw}{dt} = \mu w + \mu(1 - \rho)\tilde{m}p \end{cases} \tag{5.3}$$

which can be solved analitically for any initial state of p and w. Indeed, the solution is

$$p(t) = p_0 e^{\mu(1-\rho)(1-\tilde{m})t} \, , \tag{5.4}$$

being p_0 the producing population size at time $t = 0$. Consequently, considering $w_0 = 0$, i.e. no retro-mutants are present in the initial population,

$$w(t) = p_0 \frac{(1 - \rho)\tilde{m}}{\rho + (1 - \rho)\tilde{m}} \left(e^{\mu t} - e^{\mu(1-\rho)(1-\tilde{m})t} \right) \, . \tag{5.5}$$

5.2.2 Stochastic model

The same evolution dynamics can be modeled by a stochastic process whose randomicity recalls the aleatoric nature of the onset of mutations. The stochastic model has been developed on top of the Moran model, which is a simple succession of random operations, called Moran steps, that describe the spontaneous appearance of mono-allelic mutants in a population [246].

The original Moran model assumes that the population size is maintained constant and equal to N individuals. A Moran step advances in time for N^{-1} generation, so that a generation lasts for N Moran steps. Each Moran step consists in:

1. Selection of a duplicating individual.

   In presence of a production burden, impaired probabilities are used to select the duplicating individual according to

   $$P(\text{duplicating producer}) = \frac{p}{N + sw} \, ,$$

   $$P(\text{duplicating retro-mutant}) = \frac{(1 + s)w}{N + sw} \, ,$$

   where $s = \rho/(1 - \rho)$ is the selective advantage, w is the number of retro-mutants and p is the number of producers in the population. If the duplicating individual is a retro-mutant, its offspring will be a retro-mutant; otherwise, it may become a retro-mutant with a certain probability m, called mutation rate.
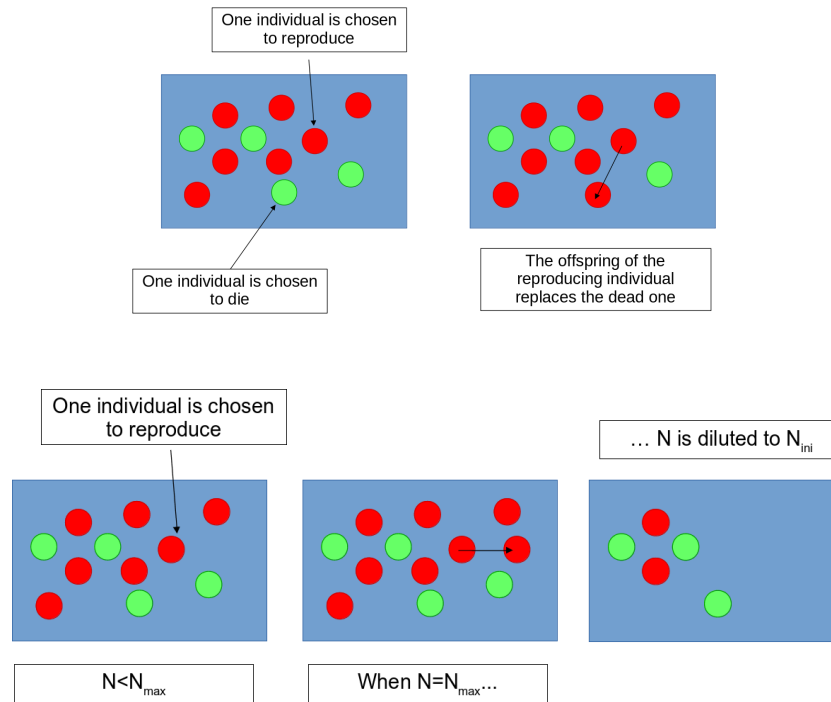
Figure 5.1: Schematic representation of a Moran step (top) and of a Moran variant (bottom).

2. Selection of a removed individual.

   All individuals have the same uniform probability of being removed.

Figure 5.1 (top) shows a schematic sketch of the Moran step. Since the Moran model keeps the population size constant, it can be efficiently used to model an ideal continuous culture system. On the other hand, to model a semi-continuous system, consisting of repeated dilutions, a variant of the Moran process is here proposed. In this case, an original population of N_{ini} individuals grows until the size of N_{max} individuals is reached. Then, the population is suddenly reset to the starting size N_{ini} with a random sampling of the individuals, simulating what happens during dilution.

Thus, the Moran variant model, sketched in Figure 5.1 (bottom), consists of the repetition of the first point of the Moran step (i.e., the selection of a duplicating individual) until the population size N reaches N_{max}. Then, the second point of the Moran step (i.e., the selection of a removed individual) is repeated until the population size N is reset to N_{ini}.

Since in the Moran variant the population size is not constant, each repetition of the selection of a duplicating individual has a different time duration equal to N^{-1} generation. The generations passed between a couple of successive dilutions (g_{d}) could be efficiently computed by relying on few approximations. Rigorously, the number of

73

such generations would be

$$g_d = \sum_{N=N_{\text{ini}}}^{N_{\text{max}}-1} \frac{1}{N} = \left(\sum_{N=1}^{N_{\text{max}}-1} \frac{1}{N} \right) - \left(\sum_{N=1}^{N_{\text{ini}}-1} \frac{1}{N} \right) = H_{N_{\text{max}}-1} - H_{N_{\text{ini}}-1} \,, \qquad (5.6)$$

where H_i is known as the i-th harmonic number. A very accurate approximation of the i-th harmonic number is given by $H_i \simeq \gamma + \log(i)$, where γ is the Euler-Mascheroni constant. Thus,

$$g_d \simeq \log(N_{\text{max}} - 1) - \log(N_{\text{ini}} - 1)\,. \qquad (5.7)$$

The latter equation can still be elaborated by noting that the dilution ratio d is

$$d = \frac{N_{\text{max}} - N_{\text{ini}}}{N_{\text{max}}} \quad \Rightarrow \quad N_{\text{ini}} - 1 = \left(1 - \frac{N_{\text{max}}}{N_{\text{max}} - 1} d \right)(N_{\text{max}} - 1)\,. \qquad (5.8)$$

So, by exploiting the properties of the logarithm,

$$g_d \simeq -\log\left(1 - \frac{N_{\text{max}}}{N_{\text{max}} - 1} d \right) \simeq -\log(1 - d)\,, \qquad (5.9)$$

where the last approximation holds for population size N_{max} sufficiently large.

Here a novel generalization of the Moran process has been presented. Indeed, it is worth noting that the original Moran model can be obtained as a special case of the more general Moran variant model, in which the final population size N_{max} is just one individual more than the initial population size N_{ini}.

5.2.3   Validation of the deterministic approach

In order to make a comparison between the results of the stochastic and the deterministic models, the analitical solution of the deterministic model needs a change of the independent variable from time to generation of producers. Since $t = g \log(2)/\mu/(1 - \rho)$, being g the generation count, then (5.4) and (5.5) rewrite as

$$\begin{cases} p(g) = p_0 2^{(1-\tilde{m})g} \\ w(g) = p_0 \dfrac{(1 - \rho)\tilde{m}}{\rho + (1 - \rho)\tilde{m}} \left(2^{g/(1-\rho)} - 2^{(1-\tilde{m})g} \right) \end{cases} \qquad (5.10)$$

The comparison shows that there is a perfect correspondence between the two approaches (Figure 5.2). The results reported in Figure 5.2 were obtained by assuming a mutation rate per generation m of 10^{-5} and, for the stochastic model, setting a population size $N = 10^8$. The mutation rate, accounting for mutations affecting positively the fitness, was chosen according to [247]. A population size in the order of 10^8 reasonably represents an experimental population into an evolution experiment. For instance, a *Synechocystis* culture with an OD_{730} of 1 corresponds to 10^8 cells per ml.
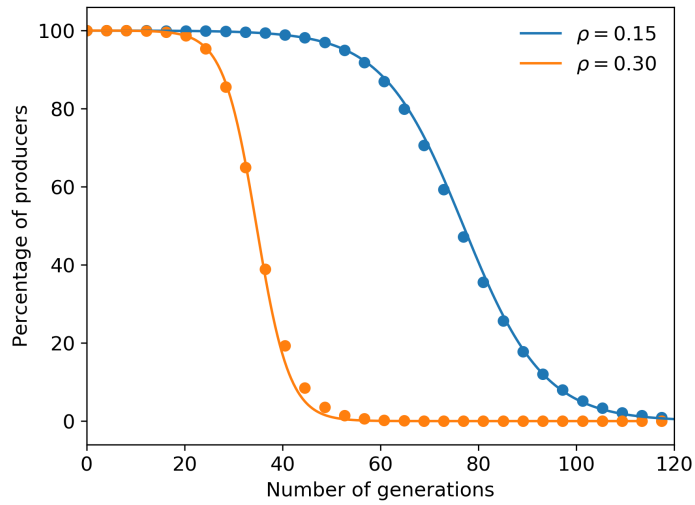
Figure 5.2: Trend of the percentage of producers with increasing number of generations of producers. The analytic solutions of the deterministic model (solid line) and the results of the stochastic model (circles) estimated with production burdens ρ of 15% and 30%, mutation rate m of 10^{-5} per generation, and population size N of 10^8.

Whereas in the deterministic model the counting of the generations of producers is highly accurate, the same does not apply to the stochastic process, since in the latter the contribution of both populations (producers and retro-mutants) are mixed in the generation counting in a not discernable way. For this reason, a calibration of the stochastic model has been performed, allowing to introduce a corrective factor for the generation counting equal to 1.35.

In both models, the percentage of producers inside the population decreases faster, in terms of number of generations, when the production burden ρ is higher (Figure 5.2), as also referred by [165]. Exactly the same trend reported in Figure 5.2 has been obtained by running the Moran variant using the same set of parameters and different values of dilution ratio (data not shown). This fact suggests the negligible effect of the dilution size on the final output.

The output of the stochastic simulations has a deterministic behavior until the population size is sufficiently large ($N > 10^5$) (Figure 5.3). On the other hand, when the population is too small the aleatoric behaviour of the phenomena becomes evident, as indicated by the wider variability associated to the smaller N considered (Figure 5.3). Therefore, for the reason explained above, in realistic operative conditions, where the population size is wide (1 mL of culture at OD_{730} = 1 corresponds to about 10^8 individuals), the deterministic model adequately and fully describes the dynamic behaviour.
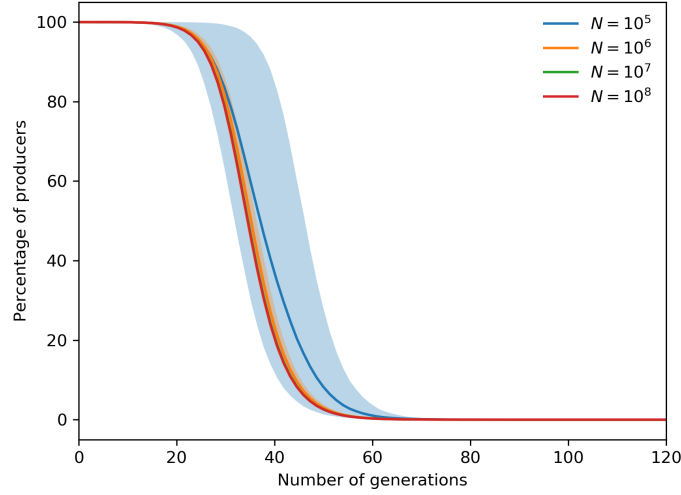
Figure 5.3: Trend of the percentage of producers with increasing number of generations of producers obtained with the stochastic model using different sizes of population. Lines indicate the average values of 5 random Moran runs, whereas the shade area covers from the minimum to the maximum value obtained at each generation ($m = 10^{-5}$, $\rho = 30\%$).

5.3 Evolution of photosynthetic microorganisms

The previous simulations hold only for those microorganisms and cultivation systems that allow the assumption of a constant growth rate. This assumption can be rarely applied to photosynthetic microorganisms, because of the strict non-linear dependancy to the light intensity, which is in turn influenced by the biomass density. For this reason, a more detailed modeling of the growth rate μ present in (5.2) is here described.

5.3.1 Model description

Many models have been proposed in the literature for describing the growth of photosynthetic microorganisms [248, 249, 250]. The simplest approach consists in the adaptation of the Monod model, originally conceived to describe the growth of heterotrophic microorganisms, substituting a substrate-limited growth with a light-limited one [251].

Both intrinsic biological features of the species in exam and physical properties of the cultivation system influence the growth rate of the photosythetic microorganisms. To take into account the contribution of these factors, more complex models have been devised [249]. Concerning the biological properties of photosynthetic microorganisms, some models include peculiar aspects of their growth, such as the light-limitation (e.g. the Tamiya model [252]) and the light-limitation associated with light-attenuation by

cells (e.g. the Grima model [253]). Other models consider both light-limitations and photoinhibition (i.e. the decrease of photosynthesis efficiency at increasing light intensities) [254, 236, 255]. The complexity of the model can be further increased by considering co-limitation of the growth by multiple factors (i.e. N, P, CO_2 and light) [256, 257]. These models usually include many parameters whose experimental determination is often challenging, compromising their real predictivity and applicability. State models aim at describing the major processes of the photosynthesis, photochemistry, energy dissipation and damages of the photosynthetic units [258, 259].

The growth rate is also affected by the geometry of the photobioreactor, the length of the light-path of the cultivation vessel and the biomass density [260].

Here, the Aiba model [236], which takes into account light limitation and photoihibition has been choosen. It describes the variation of the growth rate in function of the light intensity, leading to

$$\mu(I) = c_{\max} \frac{I}{K_s + I + I^2/K_l} - l \, ,$$ (5.11)

where I is the light intensity, l is the maintenance (or carbon loss), $c_{\max}$ is related to the maximum carbon uptake, and K_s and K_l are fitting parameters. The equation term I^2/K_l describes the effect of photoinhibitory light intensities and for very large K_l equation 5.11 falls back in the classic Monod model.

The distribution of the light intensity in the volume of the reactor, in general, is not homogeneous, because light is both absorbed and scattered by the cells themselves through the culturing medium. Light extinction is modeled in first approximation by the Lambert-Beer law

$$I(z) = I_0 e^{-\xi z}$$ (5.12)

being I_0 the light intensity at the surface of the vessel, ξ the extinction coefficient and z the lenght of optical path.

It is worth noting that the extinction coefficient ξ is affected by the biomass density and can be, therefore, estimated as the sum of the contribution from the different subpopulations, as

$$\xi = \varepsilon_w w + \varepsilon_p p + \xi_b$$ (5.13)

where ε_w and ε_p are the specific extinction coefficients of the retro-mutants and the producing cells, respectively, and ξ_b is the extinction coefficient of the background. A proper modeling of the specific extinction coefficient should take into account the photoacclimation phenomena. Indeed, when the cells acclimate to low light intensities they increase their pigments content to enhance their light harvesting capacity, whereas in case of acclimation to high light intensities the opposite response occurs [261, 262, 263]. This adaptation mechanism determines changes in the specific extinction coefficient which can be modeled as proposed in [264].

By assuming that the cell density is homogeneous in the culture volume, it is possible to use the system of equations (5.2) to describe the system evolution. In this case, the

heterogeneity of the light distribution due to the self-shading generated by the biomass itself is implicitly taken into account by averaging the growth rate. At least two limit approximations can be adopted for the averaging:

- Method 1: in the infinite mixing hypothesis, the mixing rate is assumed to be higher than the photosynthetic response to light. In this case, the growth rate is computed by applying (5.11) to the mean light intensity $\bar{I}$.

- Method 2: if the photosynthetic response of the cells to light is significantly faster than the mixing rate, then each cell experience a different light intensity. In this case, the growth rate is computed by averaging every growth rate at the corresponding light intensity.

Clearly, the result of the averaging is dependent on the geometry of the cultivation system which influences the light distribution.

5.3.2   Estimation of parameters

The parameters necessary to perform reliable simulations are here assigned, based on previous literature.

Fitting of the Aiba model

The Aiba model contains the parameters l, c_{max}, K_s and K_l. The model parameters have been assigned by fitting the Aiba model to the data collected during a growth experiment of *Synechocystis* sp. PCC 6803 and reported in [265]. The experiment has been conducted in a flat panel photobioreactor (FMT 150.2/400, Photon Systems Instruments) illuminated by a far light source and aimed at evaluating the growth response to orange-red light at different intensities. The growth rate, the supplied and the transmitted light intensities have been recorded (Table 5.1).

Table 5.1: Measurements of growth rate at increasing orange-red light intensities (636 nm) with acclimation time interval of 24 h (T= 30 °C, pH = 8.0), reported in [265]

Supplied (μmol photons/m²/s)	50	200	300	500	800	950
Transmitted (μmol photons/m²/s)	31.75	140.20	219.00	386.40	631.60	770.50
Growth rate (h^{-1})	0.05	0.11	0.12	0.11	0.10	0.09

The evaluation of maintenance level l in cyanobacteria is still a challenge [266] and even though it is usually assumed to be constant, in reality it varies with light irradiance, because a major metabolic cost could be required to repair damaged components when cells are exposed to high light intensities [259]. Some studies, such as [260], reported a value for l, which however is not yet supported by experimental validation. In

the present work, l has been computed as follow. Because of the nature and the quantity of experimental measurements available from [265], the fitting is possible with infinite values of l. However, we know that in a batch cultivation experiment, given a certain light intensity and no other nutrient limitations than light, the OD will reach a stationary value. Since we observed that this OD value significantly depends on l, we decided to select l as the value for which the OD equals a reasonable value at stationarity (OD = 16), given a certain light intensity (I = 120 μmol photons/m²/s). We started with an initial guess of l and we fitted the other Aiba parameters. Then, a batch reaching the stationary phase has ben simulated and based on the OD value obtained we decided if increase (OD value too high) or reduce (OD value too low) the l value, which was finally set to $0.03\,\mathrm{h}^{-1}$.

The fitting of parameters can be performed with both the limit approximations for growth rate averaging. On the one hand, under the infinite mixing hypothesis the function to be fitted is $\mu(\bar{I})$, being $\bar{I}$ computed as

$$\bar{I} = \frac{1}{\delta} \int_0^\delta I(z) dz = \frac{1}{\delta\xi} \int_{I(\delta)}^{I_0} dI = \frac{I_0 - I(\delta)}{\delta\xi} = \frac{I_0 - I(\delta)}{\log(I_0/I(\delta))}, \qquad (5.14)$$

where Lambert-Beer law (5.12) has been used in the second and forth equalities. In the latter equations δ is the depth of the flat panel vessel. On the other hand, if the photosynthetic response to light intensity is assumed to be faster than the mixing rate, the function to be fitted is the averaged growth rate $\bar{\mu}$ computed as

$$\bar{\mu} = \frac{1}{\delta} \int_0^\delta \mu(I(z)) dz = \frac{1}{\delta\xi} \int_{I(\delta)}^{I_0} \frac{\mu(I)}{I} dI = \frac{1}{\log(I_0/I(\delta))} \int_{I(\delta)}^{I_0} \frac{\mu(I)}{I} dI. \qquad (5.15)$$

Table 5.2: Fitted parameters obtained by applying the two approaches for the approximation of the average growth rate (Method 1 and Method 2) to the experimental data from [265]

Parameters	Method 1	Method 2
c_{max} (h^{-1})	0.219	0.219
K_s (μmol photons/m²/s)	68.24	68.58
K_l (μmol photons/m²/s)	1156.11	1162.08

The fitting curves obtained by applying the two approximation approaches to the experimental data from [265] are reported in Figure 5.4. The curves result to be overlapped, therefore in this case both the methods can feasibly represent the average growth rate inside the photobioreactor. Moreover, the fitted parameters (Table 5.2) are very similar for the two approaches. Therefore, since the first approach is simpler than the second one, it will be utilized in next computations.
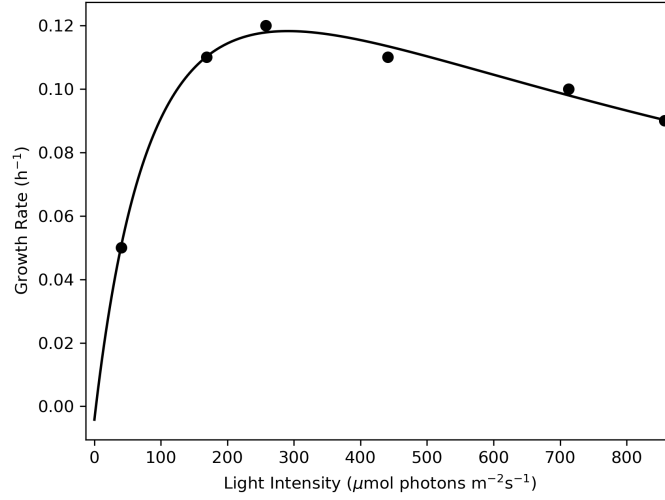
Figure 5.4: Growth rate variation in function of increasing light intensities. The fitting curves obtained by using the two different approximation approaches for averaging the growth rate are represented as solid lines (they are perfectly overlapped), whereas in circles are reported the experimental data from [265].

Evaluation of the extinction coefficient

To estimate the extinction coefficient (5.13), the contribute of the background turbidity, ξ_b, due to the presence of the cultivation medium and of the possible bubbles, is neglected. In addition, the mutation affecting the productivity in the retro-mutants is assumed to have no effects on the cell size and on the specific absorption coefficient, therefore ε_w and ε_p are set as equals. A more accurate model would take into account also these aspects.

Evaluations of the specific extinction coefficient of *Synechocystis* sp. PCC 6803 based on spectroscopic pigments determination have been reported by [264]. This parameter has a maximum value of $0.18\,\mathrm{m^2\,g^{-1}}$ when the cells are acclimated to low light intensities, and a minimum value of $0.045\,\mathrm{m^2\,g^{-1}}$ for biomass without any light absorption, only scattering [264]. Based on the measured values reported in [264] and a maximum light intensity of $120\,\mu$mol photons/m^2/s, the specific extinction coefficient is set constant and equal to $0.16\,\mathrm{m^2\,g^{-1}}$.

5.3.3   Effects of the geometry of the cultivation system

As mentioned before, the self-shading phenomenon depends on the biomass density and on the geometry of the reactor. Calculations for the average light intensity, $\bar{I}$, and for the average growth rate, $\bar{\mu}$, have been done in the previous sections for the case of a flat panel (parallelepiped) bioreactor with far light source. Here, calculations for two
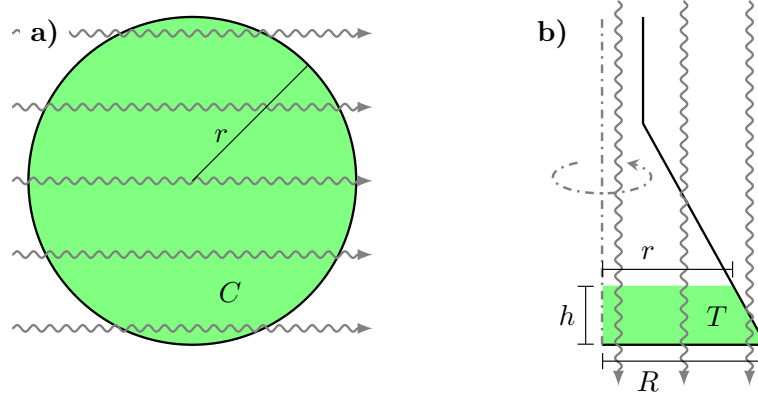
Figure 5.5: Schematic representation of two different geometries of cultivation systems. Cross section of a cylindrical vessel illuminated by a lateral source a) and longitudinal section of an Erlenmeyer flask illuminated by a top source b).

other common geometries—cylindrical vessel and Erlenmeyer flask—will be performed. In order to obtain results of general validity for both limit approximations, the averaging of the generic function of light intensity $f(I)$ is considered for both geometries. The result can be applied to $\bar{I}$ with $f(I) = I$ and to $\bar{\mu}$ with $f(I) = \mu(I)$.

Cylindrical vessel

The average of the function $\bar{f}$ is here calculated for a cylidrical vessel illuminated by a lateral source (Figure 5.5a). The light source is assumed far from the vessel, so that the incident light rays are parallel one to each other. In addition, refraction and scattering effects are neglected, maintaining the light rays parallel also inside the vessel volume.

The computation is based on the integral

$$\bar{f} = \frac{1}{\pi r^2} \int_C f(I) d\vec{x} \,, \tag{5.16}$$

where C is the circular section of the vessel of radius r. This integral can be processed as follows,

$$\bar{f} = \frac{2}{\pi r^2} \int_0^r \left(\int_{-g(x)}^{g(x)} f(I) dy \right) dx = \frac{2}{\xi \pi r^2} \int_0^r \left(\int_{I(2g(x))}^{I_0} \frac{f(I)}{I} dI \right) dx \,, \tag{5.17}$$

being $g(x) = \sqrt{r^2 - x^2}$. When $f(I) = I$, as in the case of infinite mixing assumption, then the integral with respect to the light intensity can be substituted with $I_0 - I(2g(x))$.

Erlenmeyer flask

For the Erlenmeyer flask, the average of the function $\bar{f}$ is calculated assuming a source illumination positioned at the top (Figure 5.5b). The source is assumed far from

the flask, so that the incident light rays are parallel one to each other. In addition, refraction and scattering effects are neglected, maintaining the light rays parallel also inside the flask volume. In this case, the calculations are done in circular symmetry, leading to the integral

$$\bar{f} = \left(\int_T x\,dx\,dy \right)^{-1} \int_T f(I)x\,dx\,dy \,, \tag{5.18}$$

where T is the right trapezoid depicted in Figure 5.5b. The integral at denominator has value $h(r^2 + R^2 + rR)/6$. The other integral on the trapezoid is conveniently splitted in the sum of the integration on a rectangle and a triangle. Integration on the rectangle leads to

$$\int_0^r x\,dx \int_0^h f(I)\,dy = \frac{r^2}{2\xi} \int_{I(h)}^{I_0} \frac{f(I)}{I} dy \,, \tag{5.19}$$

being h and r the height and the short base of the trapezoid, respectively. The integration on the triangle leads instead to

$$\int_r^R \left(x \int_0^{g(x)} f(I)\,dy \right) dx = \frac{1}{\xi} \int_r^R \left(x \int_{I(g(x))}^{I_0} \frac{f(I)}{I} dI \right) dx \,, \tag{5.20}$$

where R is the long base of the trapezoid and $g(x) = h(x - R)/(r - R)$. By combinig the partial results, the following equation is finally obtained

$$\bar{f} = \frac{6}{\xi h(r^2 + R^2 + rR)} \left(\frac{r^2}{2} \int_{I(h)}^{I_0} \frac{f(I)}{I} dI + \int_r^R \left(x \int_{I(g(x))}^{I_0} \frac{f(I)}{I} dI \right) dx \right) \,. \tag{5.21}$$

Please note that, as already shown, the integral with respect to the light intensity can be analitically computed in the case of $f(I) = I$.

5.4   Simulation results

The simulations of the dynamics of retro-mutants can be performed considering different cultivation methods, including batch and semi-continuous cultivations.

In a batch, all resources are provided in finite amount at the beginning of the cultivation with the exception of light which is continuously delivered. In the model here proposed, the first phases of the growth are properly simulated. However, since nutrient depletion is not included, the growth can be described only as long as the resources different from light (i.e., C, P, N) are not in limiting concentrations.

Serial dilution is here intended as a semi-continuous cultivation system in which the OD is kept constant by means of dilutions with different possible ratios. This category, therefore, includes both repeated batch transfer and turbidostat modes. To simulate this operative condition, the effect of dilutions has to be added to the proposed model as follows,

- Let OD_b be the base OD, i.e. the value at which the OD is reduced after each dilution;

- Let OD_c be the cut-off OD value;

- Let T be the time interval between two consecutive OD observations;

- Let t_0 be the instant of the last OD observation and $t_1 = t_0 + T$ the instant of the next observation;

System (5.2) is solved from t_0 to t_1. The OD corresponding to the solution at t_1 is compared to the value OD_c: if it is greater, then the dilution is performed by setting

$$
\begin{cases}
p(t_1^+) = OD_b \; \dfrac{p(t_1^-)}{p(t_1^-) + w(t_1^-)} \\[2ex]
w(t_1^+) = OD_b \; \dfrac{w(t_1^-)}{p(t_1^-) + w(t_1^-)}
\end{cases}
\tag{5.22}
$$

where t_1^- is the left limit and t_1^+ is the right one of the time instant. On the other hand, if the OD is lower than OD_c, then no dilutions are operated. After the OD check and the possible dilution, the procedure is iterated, so that t_1 becomes the new t_0.

A cultivation system such as the turbidostat can be considered a type of serial dilution in which the OD is checked frequently (for instance, $T = 30\,\text{min}$). A serial batch transfer, instead, is well modeled when the interval between consecutive observations is longer (for instance, $T = 24\,\text{h}$). Additionally, the batch mode can be considered as a limit case for T that tends to infinity.

Other continuous cultivation modes, like the chemostat, can be similarly simulated by setting a dilution rate $D > 0$.

5.4.1 Genetic stability at varying time interval

To understand how the time interval T between two consecutive OD checks affects the population dynamics, the following *in silico* experiments were performed. All the simulations consider a cultivation system with a cylindrical geometry of radius 1.8 cm, correspondig to the dimension of one vessel of the Multi-Cultivator photobioreactor (Photon Systems Instruments). The used parameters are a mutation rate per generation $m = 10^{-5}$, a production burden $\rho = 0.15$, a maintenance $l = 0.03\,\text{h}^{-1}$, a light intensity of $120\,\mu\text{mol photons/m}^2\text{/s}$.

For the dilution process, $OD_b = 0.6$ and $OD_c = 1.0$ were chosen as base and cut-off OD, respectively, whereas the time interval T was set at 30 min, 6 h, 24 h and 96 h. The process was started with a value of $w = 0$ and p such that the initial OD = 0.1. The conversion from biomass density, that is the actual unknown of the differential problem, to the OD value has been carried out with a conversion factor of $148\,\text{mg/L/OD}_{730}$,

Figure 5.6: Simulations of population dynamics at varying time interval. On the left side, trends of the OD contribution of the two sub-populations (producers and retro-mutants). On the right, trends of the producers percentage. From top to bottom, results obtained when OD checks are made every 30 min, 6 h, 24 h, and 96 h, respectively.

according to [197]. The remaining parameters are set as described above (Section 5.3.2). The results are reported in Figure 5.6.

The choice of the time interval affects the frequency of dilution. Indeed, it is possible to observe that when the time interval is short (i.e., $T = 30$ min or $T = 6$ h), the OD observations may not correspond to the occurance of a dilution, because the overcoming of the OD_c is the necessary condition to operate the dilution. This behavior can be clearly appreciated in the simulation results with $T = 6$ h (Figure 5.6), in which the higher growth rate of retro-mutants with respect to the one of producers makes the dilution frequency increase suddenly after about 35 days.

As can be understood looking at the right column of Figure 5.6, the longer is T the slower is the taking over of the population by the retro-mutants. This happens because of the non-linear dependence of the growth rate on the population size. When the population density is too high, the self-shading reduces the light availability in the inner regions of the photobioreactor with a consequent negative effect on cell growth.

Quantitatively, for the shorter T (30 min and 6 h) the producers reached the 50% of the total population after 30 days of cultivation. A bit more days are needed to reach the same percentage when the OD observations are performed once every 24 h, whereas the reaching of the 50% cannot be observed within the simulated 60 days when $T = 96$ h. The time interval, and therefore the frequency of dilution, influences the time-instant at which it is possible to appreciate the presence of retro-mutants inside the population.

5.4.2   Genetic stability at varying base OD

Similarly to the previous analysis, here it is presented how the arising of retro-mutants is affected by the value chosen for OD_b. The same geometrical and physical parameters of the previous study have been adopted for these simulations as well. The duration of the time interval between consecutive OD checks T has been set to 24 h. The base OD tested had values of 0.1, 0.3, 0.6 and 0.9. The results are reported in Figure 5.7.

It can be noted that the dilution frequency is lower when the base OD is very low (0.1). This happens because 24 h are not enough to overcome the cut-off OD of 1.0. Moreover, it is worth noting that when the base OD is high, the producers reach the 50% of the total population later compared to the case of low base OD. As already discussed in the previous analysis, also this fact is due to the non-linear dependence of the growth rate on the populazion size.

These results allow to asses the optimal working conditions of an evolution experiment for the evaluation of the genetic stability of engineered strains in the shortest time. Indeed, working at a sufficiently low base OD (e.g. 0.1 or 0.3) it is possible to adopt larger time intervals T (e.g., 24 h) (Figure 5.7) and get the same result, in terms of time-scale, obtained with higher base OD (e.g., 0.6) and shorter time intervals (e.g., 30 min) (Figure 5.6). This is of interest because repeated batch transfer is the most common technique for evolution experiments, since it is cheap and simple to implement for any laboratory, but it is carried-out manually and it is therefore constrained by the
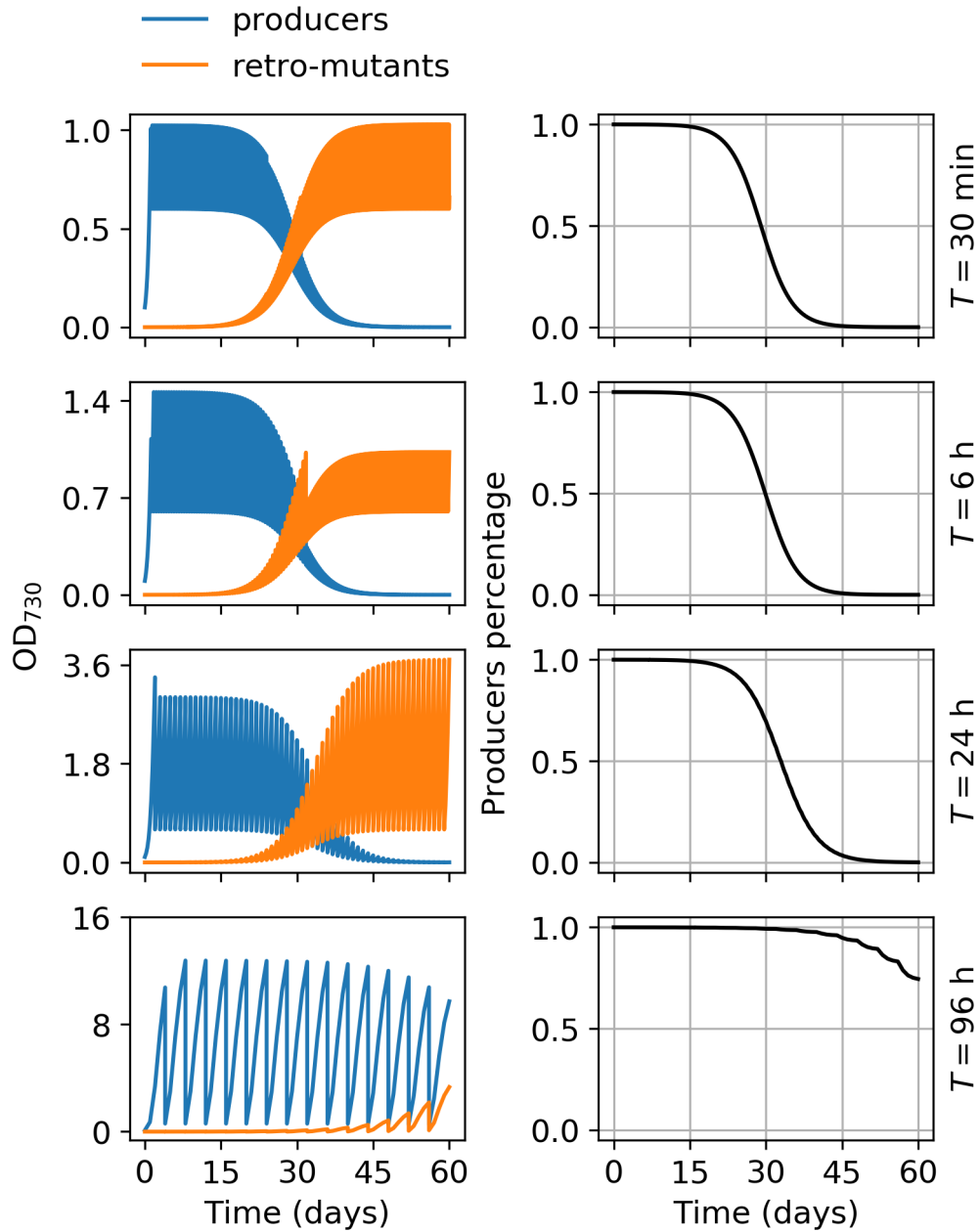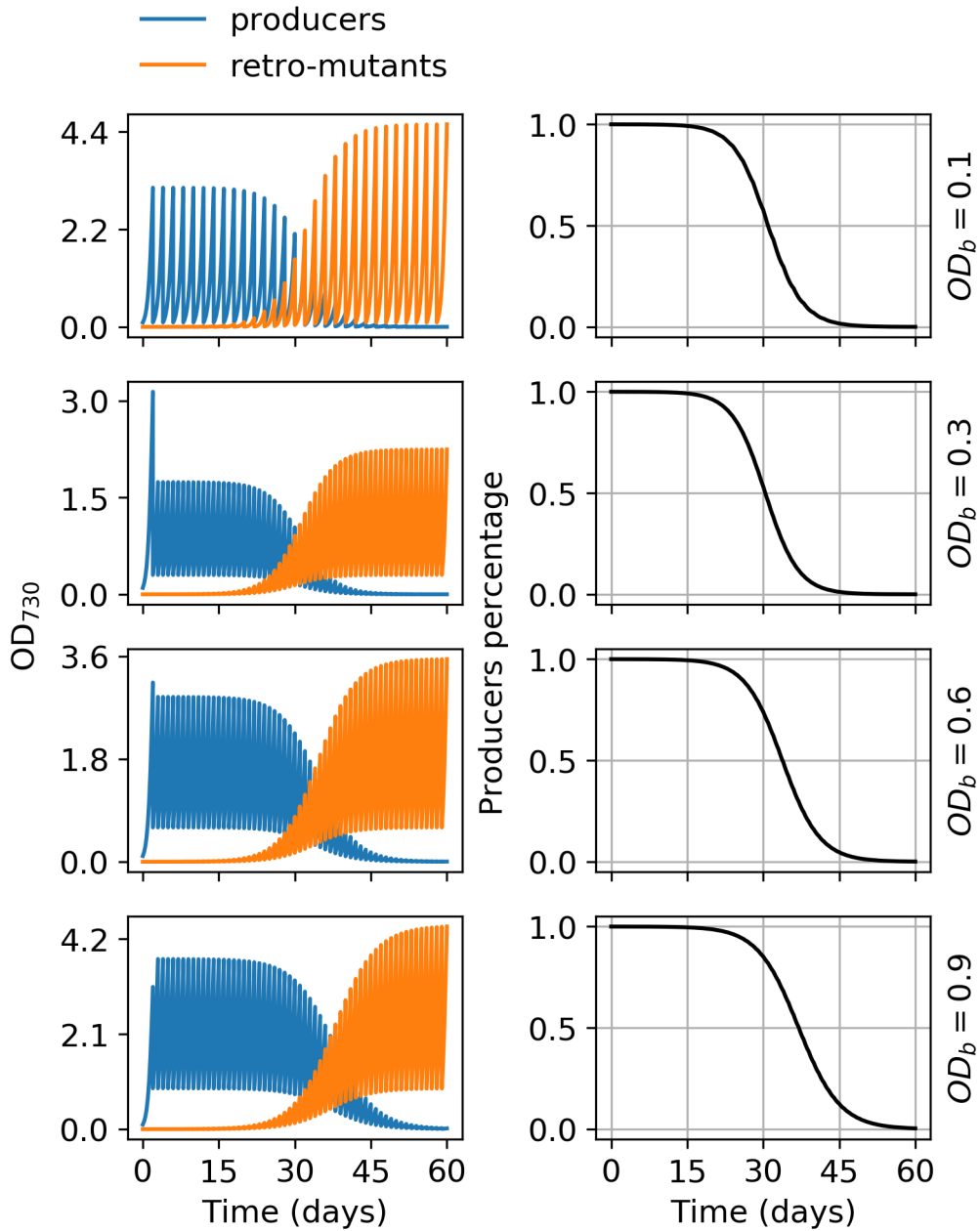
Figure 5.7: Simulations of population dynamics at varying OD base. On the left side, trends of the OD contribution of the two sub-populations (producers and retro-mutants). On the right, trends of the producers percentage. From top to bottom, results obtained when OD base is equal to 0.1, 0.3, 0.6, and 0.9, respectively.
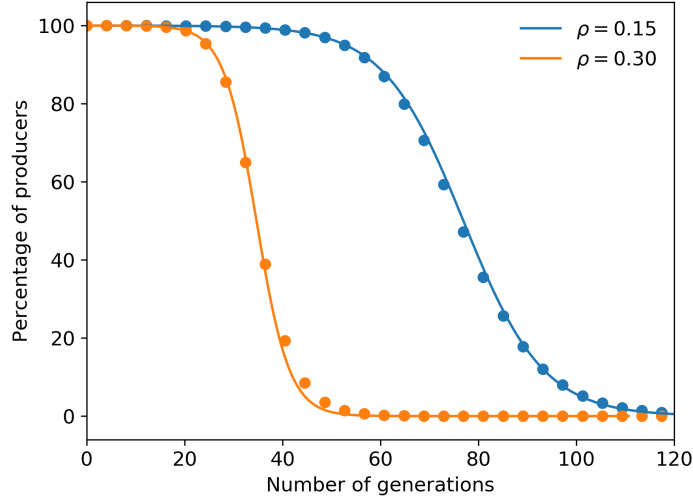
Figure 5.8: Trend of the percentage of photosynthetic producers with increasing number of generations of producers. The analytic solutions of the complete deterministic model (solid line) and the results of the stochastic model (circles) estimated with a production burden ρ of 15% and 30%, a mutation rate m of 10^{-5} per generation, and a population size N of 10^8. To be compared with Figure 5.2.

possibility to perform the sampling.

5.4.3   Comparison between time- and generation-scale

From the previous analyses, it emerges that longer time intervals between consecutive OD checks (T) (Figure 5.6) and higher base OD (OD_b) (Figure 5.7) produce delay in the appearance of retro-mutants. However, the delay in time does not necessarily correspond to a delay in terms of generations. To compare the results of the simulations in time- and generation-scale, the occurred generations in the *in silico* experiment have been counted using the approach described in Chapter 3.6.7. Figure 5.8 shows the trend of the percentage of producers in a generation-scale for the results of all the simulations reported in time-scale Figures 5.6 and 5.7. In addition, the production burden equal to 30% has been investigated.

Interestingly, given a production burden, all deterministic simulations (for various T and OD_b), reported in Figure 5.6 and 5.7, lead to identical results, that are perfectly overlapped in Figure 5.8. Moreover, the predicted trends are in accordance to the results obtained with the stochastic model described above.

By comparing Figures 5.2 and 5.8 it can be observed that, when m and ρ are known, the trend of the percentage of producers in a generation-scale is always described by the formula (5.10), also in the case of complex growth laws such as the photosynthetic

one.

5.5   Conclusions

Two literature deterministic models, one to describe photosynthetic growth [236] and one to describe the arising of mutations into a clonal population [237], were adapted and combined together to simulate the dynamics of retro-mutants in a photobioreactor.

The deterministic approach for mutations was first validated by comparing it with a stochastic one (i.e., Moran process). After that, the deterministic approach has been improved to account for the main aspects of the photosynthetic growth, resulting into a combined model. The latter has been used to simulate retro-mutants dynamics when a serial dilution technique is adopted. Results obtained with varying parameters (i.e., time intervals and base OD) allowed to identify the optimal set of conditions to practically design evolution experiments based on serial dilution mode in which it is possible to appreciate the arising of retro-mutants in the shortest experimental time. Additionally, the analytical solution of the deterministic model (5.10) has been demonstrated to fully describe the population dynamics of producers and retro-mutants even when complex phenomena and factors influencing growth are considered (e.g. photoinhibition, self-shading, geometry of the cultivation system). This means that when the population size is sufficiently large, the ratio between the sub-populations of producers and retro-mutants, in generation-scale, only depends on the production burden and on the mutation rate and not on the cultivation conditions adopted.

Chapter 6

Conclusions and future perspectives

In this work, cyanobacterial cell factories for the production of commodity chemicals, namely fumarate and malate, have been engineered. Besides the achievement of production, the focus has been on the pursuit of strain stability from the genetic point of view. In other words, the goal was to obtain strains that can hold their productivity for a number of generations compatible with industrial applications.

The appraoch adopted to this purpose was a growth-coupled strategy, in which the product synthesis is obligatorily linked to biomass formation. In the case of fumarate, by analyzing the GSMM of *Synechocystis* with different algorithms, a strict and stoichiometric coupling to the growth was achieved during continuous illumination by deleting just one gene. Furthermore, fumarate production was explored also in night-time, where the cyanobacterial metabolic activities are limited, but still present. By re-directing the carbon flux from the OPPP to the TCA cycle, it was possible to exploit the residual activities to push the synthesis of fumarate, even when the growth of *Synechocystis* is stopped.

The applicability of the growth-coupling approach here shown needed to be expanded beyond the list of candidates identified by the FRUITS algorithm. For this reason, a metabolic strategy relying on the usage of the strict growth-coupled metabolite fumarate, as a supply for the accumulation of the immediately downstream metabolite, malate, has been developed and validated. The malate productivity of the strain obtained was further improved by over-expressing the gene necessary for the conversion of fumarate into malate, that is the fumarase C.

Both the fumarate and malate producer strains obtained resulted to be genetically stable under prolonged continuous cultivation, since no mutants loosing the production trait (retro-mutants) appeared during the experiments, thus confirming that the metabolic engineering strategies adopted are succesfull.

To better understand the dynamic of the arising of retro-mutants inside a producing population, a mathematical model, tailored to photosynthetic microorganisms has been developed. Simulations performed using this model allowed to identify the optimal set of conditions to operate a lab-scale evolution experiment in the shortest time.

Nevertheless, there is still place for further optimization of the cyanabacterial cell factories here presented. For instance, the identification of the optimal composition of the medium and of the growing conditions could improve the productivity. Flux towards the TCA cycle can be enhanced by subjecting the cultures to nitrogen-starvation. In particular, in *Synechocystis* the levels of malate, fumarate and succinate increase under N-deprivation [267]. As demonstrated for fumarate, also malate production could benefit from the inhibition of the OPPP. Precisely, the deletion of the first enzyme of the OPP route, namely *zwf*, would re-direct the carbon flux towards the TCA cycle.

A deeper knowledge about the transporters system of *Synechocystis* would be extremely useful in order to improve the efflux capabilities of the target product(s). No C_4-dicarboxylate carriers have been characterized to date in this cyanobacterium, therefore no possible tranporters for fumarate and/or malate have been identified. The homology search presented in this work allowed us to find a putative candidate. However, the experimental results indicated that probably the locus identified is either part of a more complex transporter structure or is not directly involved in the transport of malate or fumarate.

The results concerning the fumarate and, above all, malate producers, indicate that the metabolic engineering strategy adopted could be further expanded. Indeed, these stably produced metabolites could be used as precursors for other synthetic pathways. For instance, malate can be a precursor for the synthesis of 2,4-dihydroxybutiric acid which may serve as an intermediate for the production of value added products (methionine, 1-3 propanediol, 1-4 butanediol etc.) [268]. The possibility to enlarge the pool of metabolites that can be accumulated, without perturbating their growth capabilities, makes cyanobacteria-based MCF a valid and sustainable alternative biotechnological platform for the production of commodity chemicals directly from CO_2 in the next future.

Appendix A

Amino acid sequence alignments

Table A.1: Amino acid sequence alignment of putative DctM (UniProtKB P74224) encoded by *sll1103* locus from *Synechocystis* and DctM subunit (UniProtKB A0ZHV0) from *Synechococcus* sp. WH8016.

Target/Query	Alignment
P74224	1 ---MVDYD---WLGPMMFVGALVFLGCGYPVAFSLGGVAILFAIIGAALG 44
	::.:| .|.|.||:..::.|..|:||||.|||:.::||::|...|
A0ZHV0	1 MGWVLSFDPSAVLAPGMFLALILALLSGFPVAFCLGGIGVIFALLGMLSG 50
P74224	45 SFDPIFLSAMPQRIFGIMANGTLLAIPFFIFLGSMLERSGIAEQLLETMG 94
	..:|.|::|:||||.|||.|.||||||.|:|:|||||.||||:|||:||
A0ZHV0	51 EIEPQFVTALPQRILGIMGNFTLLAIPAFVFMGSMLESSGIAERLLESMG 100
P74224	95 IILGHLRGGLALAVILVGTMLAATTGVVAATVVAMGLISLPIMLRYGYSK 144
	.:||.:||||||||:|||::|||||||||||..||:||||.||:.||.|
A0ZHV0	101 RLLGRVRGGLALAVVLVGSLLAATTGVVAATVTTMGMISLPAMLKAGYDK 150
P74224	145 ELASGVIVASGTLGQIIPPSVVLIVLADQLGVSVGDLFIGSLLPGLMMAG 194
	.||:|||||||||||||||:||:||.||||:|||||:|:|||||:||.
A0ZHV0	151 TLATGVIVASGTLGQIIPPSIVLVVLGDQLGISVGDLFMGALLPGLLMAA 200
P74224	195 SFALYVLIIAWLKPDLAPALP-AEVRNIGGQELRRRIVQVMLPPLVLILL 243
	.||:|||||:..:||:|||.|| ||: |.....::||.|||||.|||:
A0ZHV0	201 VFAIYVLIISAIKPELAPQLPQAEL----GATQPLQLVQSMLPPLSLILI 246
P74224	244 VLGSIFFGIASPTEAGAVGSIGAIALAHFNQRLNWKALWEVCDATLRITS 293
	||||||||||:|||||.:|::|||.||..|...:.|.|..||::|:|.|:
A0ZHV0	247 VLGSIFFGIATPTEAGVIGAVGAILLAALNGGFSRKQLSNVCESTMRTTA 296
P74224	294 MVMLILLGSTAFSLVFRGLEGDRFMFDLLANLPGGQIGFLAISMITIFIL 343
	|||.|||||||||||||:.||::.:.|:|.|||||::|||..||:.||:|
A0ZHV0	297 MVMAILLGSTAFSLVFRGVGGDQLIADVLLNLPGGRVGFLVFSMLIIFLL 346

Table A.1: (continue)

P74224	344 GFFIDFFEIAFIVLPLFKPVA-EALNLD-LIWYGVIVGANLQTSFLTPPF 391
	`|||||||||||||.:||..|.| :.|..| |||:||::||||||||||||`
A0ZHV0	347 GFFIDFFEIAFIAVPLLLPAARQLLGPDALIWFGVMIGANLQTSFLTPPF 396

P74224	392 GFALFYLRGVAPASLTTGQIYRGAVPFIGLQVLVLLLIIIFPALINWLPS 441
	`|||||||||||..:.|..|||||:||:||||.||.|||..|.|::|||.`
A0ZHV0	397 GFALFYLRGVAPQDVRTRDIYRGALPFVGLQVAVLALIIAVPGLVDWLPR 446

P74224	442 LSVQ------- 445
	`|:..`
A0ZHV0	447 LAAAMTPMPLT 457

Table A.2: Amino acid sequence alignment of putative DctM (UniProtKB P74224) encoded by *sll1103* locus from *Synechocystis* and DcuC transporter (UniProtKB J4IQ13) from *Nodularia spumigena*.

Target/Query	Alignment
P74224	1 MVDYDWLGPMMFVGALVFLGCGYPVAFSLGGVAILFAIIGAALGSFDP--48
	.|.:|.|
J4IQ13	1 --MLSTFAPLV 9
P74224	49 IFLSAMPQRIF-----------GIMANGTLL---AIP-FFIFLGSMLERS 83
	|.|.|| || |:.|.|..| .:| .|:.:...:..
J4IQ13	10 IILIAM---IFMFKRVDVRLSLGLSATGLFLIAGKLPQLFVTITQQMTNE 56
P74224	84 GIAEQLLETMGII-----------LGHLRGGLALAVILVGTMLAATTGVV 122
	....:...||.. |.| |.||.:..|..|.....|::
J4IQ13	57 KTVVPICTAMGFAYVLRLTECDRHLTH----LLLAPLRHGRWLLIPGGII 102
P74224	123 AATVVAMGLIS------------LPIMLRYGYSKELASGVIVASGTL-GQ 159
	||.:|.|.::| ||::|...:.:.|..:::...:: |:
J4IQ13	103 AAYIVNMAIVSQSSTAAIVGTVLLPLLLAVNITPVIAGSLLLLGSSMGGE 152
P74224	160 IIPPSVVLIV-LADQLGVSVGDLFIGSLLPGLMMAGSFALYVL-IIAWLK 207
	:..|..|.|| ||:..|..|..| :..:||..::|....|.|. |:|.:.
J4IQ13	153 LFNPGAVEIVKLAELTGQPVAKL-VAQVLPINLLASITTLIVFCILAVIL 201
P74224	208 PDLAPALPAEVRNI------GGQELRRRIVQVMLP--PLVLILLV----- 244
	...|..|..|:..: .|:.....:::.:| ||.|:.::
J4IQ13	202 SQKAVLLSPEITKVDSDVAQSGKPFHLNLIKALVPLLPLALLFIIPALVQ 251
P74224	245 ----------------LGSIFFGIASPTEAGAVGSIGAIALAHFNQRLN 277
	:.....|:..:|.|:| |.:|
J4IQ13	252 LPKEFSNNSVSIAAAMLIAVTAAGLTTPKESG-----GLVA--------- 287
P74224	278 WKALWEVCDATLRITSMVMLILLGSTAFSLVFRGLEGD---RFMFDLLAN 324
	|.:| .|.....:::.:|:: :|.|: .|::.: ..:.:.|||
J4IQ13	288 --AFFE--GAGFAYANIISIIIV-ATIFT---DGIKANGLIEVLRNALAN 329
P74224	325 LPGGQIGFLAISMITIFILGFFI-----DFFEIAFIVLPLFKPVAEALNL 369
	.| :|:. ||..||.|.: .....|..|:.:..|||..:||
J4IQ13	330 RP------VAVK-ITSLILPFTLAGVTGSGSAPAIAVMNVLVPVATTMNL 372
P74224	370 DLIWYGVIVGANLQTSFLTPPFGFALFYLRGVAPASLTTGQIYR----GA 415
	|.:.|.:.....|.....| ||...:.:.|.: ..
J4IQ13	373 DPVKIGALAAVAAQLGRTLSP----------VAAVVIMSATISKQPPLNL 412
P74224	416 VPFIGLQVLVLLLIIIFPALINWLPSLSVQ 445
	|..:.|.:|..|..:|...|.||:
J4IQ13	413 VKCVVLPLLAGLAAVIVATLCNWV------ 436

Table A.3: Amino acid sequence alignment of putative DctP (UniProt KB P73589) encoded by *sll1314* locus from *Synechocystis* and DctP subunit (UniProtKB K9SU31) from *Synechococcus* sp. PCC 7502.

Target/Query	Alignment
P73589	1 MKHSRRNFLALAGASSLLAIAAPKLLAEGIP------QEILNKILPLPGK 44
	||.||:|||.:||.:||.||...||.|:... :..|.|:|.|||:
K9SU31	1 MKFSRKNFLLMAGVTSLTAIGVEKLAAKDTKLSDTSLETELEKVLGLPGE 50
P73589	45 YGEYYSQAKIRAFHLHNQPDTSPLHKALEELWLEVFKQTEGELFVSPIPH 94
	||:.|.:|||:|||||||.:||||:.||.|||:||::|.||||:||:|.
K9SU31	51 YGKNYGKAKIKAFHLHNQPKSSPLHQNLEALWLDVFEKTNGELFISPLPQ 100
P73589	95 DASIPAGDPQAVQFITGGRFEIVSVAGPIIDKVAPDVIGVQNIPLLYQSA 144
	||::..||||||:.::.||||:||||.|||||:|.||||:||:..:|||:
K9SU31	101 DAALQGGDPQAVRLVSTGRFEVVSVAAPIIDKLASDVIGIQNLAFIYQSS 150
P73589	145 QDVFEIINQSLFAEALNGSVAQYNLTYLRNGTFNNGMRIVTSIASKPIYK 194
	::||||||||.:||||.|:.|||:|||.||..||||:||||.:||:|:||||.
K9SU31	151 KEVFEIINQPVFAEILDRSVAKYNLKYLPKGTFDNGMRNITSVAAKPIYN 200
P73589	195 LEDFQGLKIRIPPSNDMAMTMEALGAVPEKITMNQVFRALENGTVEAQEN 244
	|::|:.|.|||||||||....|:||||.|:..|||:|:..:|:..||||||
K9SU31	201 LDNFKDLIIRIPPSNDFQQAMQALGANPKFFTMNEVYDVLKNQIVEAQEN 250
P73589	245 PSSVALGFKLYEVTKYLNMTNHAWSGYNTFFNTSFWESLSPTVQAVIKEL 294
	|.|:|.||.||||||||||||||||||||||::||..||.:.:.||.||
K9SU31	251 PLSIAKGFALYEVTKYLNMTNHAWSGYNTFFNSNFWNKLSQSNRKVISEL 300
P73589	295 LPVYQAKQIRAQEEYNQQAYQQLIGKLGMVQTKPNLSQAPQKLIEVYRFI 344
	|||||||||:|||:||...:::|..|.||..:|:.|:|.||||.:|:.
K9SU31	301 LPVYQAKQIKAQEDYNSAIYKELTTKYGMTATQPDCSEAVQKLIPIYKSI 350
P73589	345 YSQLNSQAQSLIKNKLEEKTGIKFA 369
	|:||||||:||||:|||:|||:||:
K9SU31	351 YNQLNSQAKSLIKSKLEQKTGVKFS 375

Appendix B

List of Publications

Publication included in this thesis:

- Du, W., Jongbloets, J.A., Max Guillaume, M., van de Putte, B., Battaglino, B., Hellingwerf, K.J., Branco dos Santos, F. (2019). Exploiting day- and night-time metabolism of *Synechocystis* sp. PCC 6803 for fitness-coupled fumarate production around the clock. ACS Synthetic Biology. https://pubs.acs.org/doi/10.1021/acssynbio.9b00289.

  This article has been adapted and included in Section 4.2. PhD candidate contribution: writing and reviewing the paper.

Articles in preparation:

- Battaglino, B., Du, W., Jongbloets, J.A., Pagliano, C., Re, A., Saracco, G., Branco dos Santos, F. Stable malate production in cyanobacterium *Synechocystis* sp. PCC 6803.

  This article in preparation has been included in Section 4.3 and Section 4.4. PhD candidate contribution: strain engineering; Batch production experiments; Evolution experiment; Sequencing analysis of the expression cassettes; Measurement of intracellular metabolites; Data analysis; Writing the first draft of the manuscript.

- Battaglino, B., Arduino, A., Pagliano, C. Mathematical modeling study of the dynamics of a retro-mutant population of photosynthetic microorganisms.

  This article in preparation has been included in Chapter 5. PhD candidate contribution: design the study; *In silico* simulations; Writing the first draft of the manuscript.

Publication not included in this thesis:

- Abdel Azim, A., Cordara, A., Battaglino, B., Re, A. (2019). Book Chapter: Use of carbon dioxide in polymer synthesis, in 'Conversion of Carbon Dioxide into Hydrocarbons Vol. 2 Technology', Springer.

Bibliography

[1]   S. Venkata Mohan et al. "Waste biorefinery models towards sustainable circular bioeconomy: Critical review and future perspectives". In: *Bioresource Technology* 215 (2016), pp. 2–12. ISSN: 18732976. DOI: 10.1016/j.biortech.2016.03.130. URL: http://dx.doi.org/10.1016/j.biortech.2016.03.130.

[2]   Miguel Valdivia et al. "Biofuels 2020: Biorefineries based on lignocellulosic materials". In: *Microbial Biotechnology* 9.5 (2016), pp. 585–594. ISSN: 17517915. DOI: 10.1111/1751-7915.12387.

[3]   Sudhakar Takkellapati, Tao Li, and Michael A. Gonzalez. "An overview of biorefinery-derived platform chemicals from a cellulose and hemicellulose biorefinery". In: *Clean Technologies and Environmental Policy* 20.7 (2018), pp. 1615–1630. ISSN: 16189558. DOI: 10.1007/s10098-018-1568-5. URL: https://doi.org/10.1007/s10098-018-1568-5.

[4]   Annalisa Abdel Azim et al. *Use of carbon dioxide in polymer synthesis.* Springer International Publishing, 2020, pp. 1–43. DOI: 10.1007/978-3-030-28638-5.

[5]   Hyeon Gi Moon et al. "One hundred years of clostridial butanol fermentation". In: *FEMS microbiology letters* 363.3 (2016). ISSN: 15746968. DOI: 10.1093/femsle/fnw001.

[6]   Stanislav Obruca et al. "Production of poly(3-hydroxybutyrate-co-3-hydroxyvalerate) by Cupriavidus necator from waste rapeseed oil using propanol as a precursor of 3-hydroxyvalerate". In: *Biotechnology Letters* 32.12 (2010), pp. 1925–1932. ISSN: 01415492. DOI: 10.1007/s10529-010-0376-8.

[7]   Pearl Passanha et al. "The use of NaCl addition for the improvement of polyhydroxyalkanoate production by Cupriavidus necator". In: *Bioresource Technology* 163 (2014), pp. 287–294. ISSN: 18732976. DOI: 10.1016/j.biortech.2014.04.068. URL: http://dx.doi.org/10.1016/j.biortech.2014.04.068.

[8] Ying Wang, Yukihiro Tashiro, and Kenji Sonomoto. "Fermentative production of lactic acid from renewable materials: Recent achievements, prospects, and limits". In: *Journal of Bioscience and Bioengineering* 119.1 (2015), pp. 10–18. ISSN: 13474421. DOI: 10.1016/j.jbiosc.2014.06.003. URL: http://dx.doi.org/10.1016/j.jbiosc.2014.06.003.

[9] Yixing Zhang et al. "Enhanced D-lactic acid production from renewable resources using engineered Lactobacillus plantarum". In: *Applied Microbiology and Biotechnology* 100.1 (2016), pp. 279–288. ISSN: 14320614. DOI: 10.1007/s00253-015-7016-0.

[10] Mickel L.A. Jansen et al. "Saccharomyces cerevisiae strains for second-generation ethanol production: from academic exploration to industrial implementation". In: *FEMS yeast research* 17.5 (2017), pp. 1–20. ISSN: 15671364. DOI: 10.1093/femsyr/fox044.

[11] J. Choi and S. Y. Lee. "Factors affecting the economics of polyhydroxyalkanoate production by bacterial fermentation". In: *Applied Microbiology and Biotechnology* 51.1 (1999), pp. 13–21. ISSN: 01757598. DOI: 10.1007/s002530051357.

[12] Enrique Cubas-Cano et al. "Biotechnological advances in lactic acid production by lactic acid bacteria: lignocellulose as novel substrate". In: *Biofuels, Bioproducts and Biorefining* 12 (2018), pp. 290–303. DOI: 10.1002/bbb.1852.

[13] Kyeong Rok Choi et al. "Systems Metabolic Engineering Strategies: Integrating Systems and Synthetic Biology with Metabolic Engineering". In: *Trends in Biotechnology* 37.8 (2019), pp. 817–837. ISSN: 18793096. DOI: 10.1016/j.tibtech.2019.01.003. URL: https://doi.org/10.1016/j.tibtech.2019.01.003.

[14] Roman A. Voloshin et al. "Review: Biofuel production from plant and algal biomass". In: *International Journal of Hydrogen Energy* 41.39 (2016), pp. 17257–17273. ISSN: 0360-3199. DOI: 10.1016/j.ijhydene.2016.07.084. URL: https://doi.org/10.1016/j.ijhydene.2016.07.084.

[15] René H. Wijffels, Olaf Kruse, and Klaas J. Hellingwerf. "Potential of industrial biotechnology with cyanobacteria and eukaryotic microalgae". In: *Current Opinion in Biotechnology* 24.3 (2013), pp. 405–413. ISSN: 09581669. DOI: 10.1016/j.copbio.2013.04.004.

[16] Martin Koller, Alexander Muhr, and Gerhart Braunegg. "Microalgae as versatile cellular factories for valued products". In: *Algal Research* 6.PA (2014), pp. 52–63. ISSN: 22119264. DOI: 10.1016/j.algal.2014.09.002. URL: http://dx.doi.org/10.1016/j.algal.2014.09.002.

[17] Doris Gangl et al. "Biotechnological exploitation of microalgae". In: *Journal of Experimental Botany* 66.22 (2015), pp. 6975–6990. ISSN: 14602431. DOI: 10.1093/jxb/erv426.

[18]   Jesús Ruiz et al. "Towards industrial products from microalgae". In: *Energy and Environmental Science* 9.10 (2016), pp. 3036–3043. ISSN: 17545706. DOI: 10.1039/c6ee01493c.

[19]   Carl Safi et al. "Morphology, composition, production, processing and applications of Chlorella vulgaris: A review". In: *Renewable and Sustainable Energy Reviews* 35 (2014), pp. 265–278. ISSN: 13640321. DOI: 10.1016/j.rser.2014.04.007.

[20]   G. Panis and J. Rosales Carreon. "Commercial astaxanthin production derived by green alga Haematococcus pluvialis: A microalgae process model and a techno-economic assessment all through production line". In: *Algal Research* 18 (2016), pp. 175–190. ISSN: 22119264. DOI: 10.1016/j.algal.2016.06.007. URL: http://dx.doi.org/10.1016/j.algal.2016.06.007.

[21]   M. Carmen García-Malea et al. "Production of astaxanthin by Haematococcus Pluvialis: Taking the one-step system outdoors". In: *Biotechnology and Bioengineering* 102.2 (2009), pp. 651–657. ISSN: 00063592. DOI: 10.1002/bit.22076.

[22]   Masataka Kajikawa et al. "Accumulation of squalene in a microalga Chlamydomonas reinhardtii by genetic modification of squalene synthase and squalene epoxidase genes". In: *PLoS ONE* 10.3 (2015), pp. 1–21. ISSN: 19326203. DOI: 10.1371/journal.pone.0120446.

[23]   Julie A Z Zedler, Conrad W. Mullineaux, and Colin Robinson. "Efficient targeting of recombinant proteins to the thylakoid lumen in Chlamydomonas reinhardtii using a bacterial Tat signal peptide". In: *Algal Research* 19 (2016), pp. 57–62. ISSN: 22119264. DOI: 10.1016/j.algal.2016.07.007. URL: http://dx.doi.org/10.1016/j.algal.2016.07.007.

[24]   Doris Gangl et al. "Expression and membrane-targeting of an active plant cytochrome P450 in the chloroplast of the green alga Chlamydomonas reinhardtii". In: *Phytochemistry* 110 (2015), pp. 22–28. ISSN: 00319422. DOI: 10.1016/j.phytochem.2014.12.006. URL: http://dx.doi.org/10.1016/j.phytochem.2014.12.006.

[25]   Mary L. Hamilton et al. "Metabolic engineering of Phaeodactylum tricornutum for the enhanced accumulation of omega-3 long chain polyunsaturated fatty acids". In: *Metabolic Engineering* 22 (2014), pp. 3–9. ISSN: 10967176. DOI: 10.1016/j.ymben.2013.12.003. URL: http://dx.doi.org/10.1016/j.ymben.2013.12.003.

[26]   Fayza Daboussi et al. "Genome engineering empowers the diatom Phaeodactylum tricornutum for biotechnology". In: *Nature Communications* 5.May (2014), pp. 1–7. ISSN: 20411723. DOI: 10.1038/ncomms4831.

[27] David Jullesson et al. "Impact of synthetic biology and metabolic engineering on industrial production of fine chemicals". In: *Biotechnology Advances* 33.7 (2015), pp. 1395–1402. ISSN: 07349750. DOI: 10.1016/j.biotechadv.2015.02.011.

[28] Jeffrey D Orth, Ines Thiele, and Bernhard Ø Palsson. "What is flux balance analysis?" In: *Nature Biotechnology* 28 (Mar. 2010), p. 245. URL: https://doi.org/10.1038/nbt.1614%20http://10.0.4.14/nbt.1614%20https://www.nature.com/articles/nbt.1614%7B%5C#%7Dsupplementary-information.

[29] R. Mahadevan and C. H. Schilling. "The effects of alternate optimal solutions in constraint-based genome-scale metabolic models". In: *Metabolic Engineering* 5.4 (2003), pp. 264–276. ISSN: 10967176. DOI: 10.1016/j.ymben.2003.09.002.

[30] Stefan Schuster and Claus Hilgetag. "On Elementary Flux Modes in biochemical reaction systems at steady state". In: *Journal of Biological Systems* 2.2 (1994). DOI: 10.1142/S0218339094000131.

[31] Jamey D. Young et al. "An Elementary Metabolite Unit (EMU) Based Method of Isotopically Nonstationary Flux Analysis". In: *Biotechnology and Bioengineering* 99.3 (2008), pp. 686–699. DOI: 10.1002/bit.21632. URL: https://onlinelibrary.wiley.com/doi/abs/10.1002/bit.21632.

[32] Benner Steven A. and A. Michael Sismour. "Synthetic biology". In: *Nature Reviews Genetics* 6.7 (2005), pp. 533–543. ISSN: 1471-0064. DOI: 10.1038/nrg1637. URL: https://doi.org/10.1038/nrg1637.

[33] Ernesto Andrianantoandro et al. "Synthetic biology: New engineering rules for an emerging discipline". In: *Molecular Systems Biology* 2 (2006), pp. 1–14. ISSN: 17444292. DOI: 10.1038/msb4100073. URL: https://www.embopress.org/doi/full/10.1038/msb4100073.

[34] María Santos-Merino, Amit K. Singh, and Daniel C. Ducat. "New applications of synthetic biology tools for cyanobacterial metabolic engineering". In: *Frontiers in Bioengineering and Biotechnology* 7.FEB (2019), pp. 1–24. ISSN: 22964185. DOI: 10.3389/fbioe.2019.00033.

[35] Anne Mathilde Davy, Helene Faustrup Kildegaard, and Mikael Rørdam Andersen. "Cell Factory Engineering". In: *Cell Systems* 4.3 (2017), pp. 262–275. ISSN: 24054720. DOI: 10.1016/j.cels.2017.02.010. URL: http://dx.doi.org/10.1016/j.cels.2017.02.010.

[36] Akiko Tomitani et al. "The evolutionary diversification of cyanobacteria: Molecular-phylogenetic and paleontological perspectives". In: *Proceedings of the National Academy of Sciences of the United States of America* 103.14 (2006), pp. 5442–5447. ISSN: 00278424. DOI: 10.1073/pnas.0600999103. URL: https://www.pnas.org/content/103/14/5442.

[37] Thorsten Heidorn et al. *Synthetic Biology in Cyanobacteria.* Vol. 497. 2011, pp. 539–579. ISBN: 9780123850751. DOI: 10.1016/b978-0-12-385075-1.00024-x.

[38] Morgan M. Matson and Shota Atsumi. "Photomixotrophic chemical production in cyanobacteria". In: *Current Opinion in Biotechnology* 50 (2018), pp. 65–71. ISSN: 18790429. DOI: 10.1016/j.copbio.2017.11.008. URL: http://dx.doi.org/10.1016/j.copbio.2017.11.008.

[39] I. Berman-Frank et al. "Segregation of nitrogen fixation and oxygenic photosynthesis in the marine cyanobacterium Trichodesmium". In: *Science* 294.5546 (2001), pp. 1534–1537. ISSN: 00368075. DOI: 10.1126/science.1064082.

[40] A. Mitsui et al. "Strategy by which nitrogen-fixing unicellular cyanobacteria grow photoautotrophically". In: *Nature* 323.6090 (1986), pp. 720–722. ISSN: 00280836. DOI: 10.1038/323720a0.

[41] S. Andreas Angermayr, Aleix Gorchs Rovira, and Klaas J. Hellingwerf. "Metabolic engineering of cyanobacteria for the synthesis of commodity products". In: *Trends in Biotechnology* 33.6 (2015), pp. 352–361. ISSN: 18793096. DOI: 10.1016/j.tibtech.2015.03.009. URL: http://dx.doi.org/10.1016/j.tibtech.2015.03.009.

[42] Lun Yao et al. "Multiple Gene Repression in Cyanobacteria Using CRISPRi". In: *ACS Synthetic Biology* 5.3 (2016), pp. 207–212. ISSN: 21615063. DOI: 10.1021/acssynbio.5b00264.

[43] Philipp E. Savakis, S. Andreas Angermayr, and Klaas J. Hellingwerf. "Synthesis of 2,3-butanediol by Synechocystis sp. PCC6803 via heterologous expression of a catabolic pathway from lactic acid- and enterobacteria". In: *Metabolic Engineering* 20 (2013), pp. 121–130. ISSN: 10967184. DOI: 10.1016/j.ymben.2013.09.008. URL: http://dx.doi.org/10.1016/j.ymben.2013.09.008.

[44] Xufeng Liu et al. " Modular engineering for efficient photosynthetic biosynthesis of 1-butanol from CO 2 in cyanobacteria ". In: *Energy & Environmental Science* (2019). ISSN: 1754-5692. DOI: 10.1039/c9ee01214a.

[45] Justin Ungerer et al. "Sustained photosynthetic conversion of CO2 to ethylene in recombinant cyanobacterium Synechocystis 6803". In: *Energy and Environmental Science* 5.10 (2012), pp. 8998–9006. ISSN: 17545692. DOI: 10.1039/c2ee22555g.

[46] Vinod Puthan Veetil, S. Andreas Angermayr, and Klaas J. Hellingwerf. "Ethylene production with engineered Synechocystis sp. PCC 6803 strains". In: *Microbial Cell Factories* 16.1 (2017), pp. 1–11. ISSN: 14752859. DOI: 10.1186/s12934-017-0645-5.

[47] S. Andreas Angermayr and Klaas J. Hellingwerf. "On the use of metabolic control analysis in the optimization of cyanobacterial biosolar cell factories". In: *Journal of Physical Chemistry B* 117.38 (2013), pp. 11169–11175. ISSN: 15206106. DOI: 10.1021/jp4013152.

[48]   Xinyao Liu, Jie Sheng, and Roy Curtiss. "Fatty acid production in genetically modified cyanobacteria". In: *Proceedings of the National Academy of Sciences of the United States of America* 108.17 (2011), pp. 6899–6904. ISSN: 00278424. DOI: 10.1073/pnas.1103014108.

[49]   Kamonchanock Eungrasamee et al. "Improved lipid production via fatty acid biosynthesis and free fatty acid recycling in engineered Synechocystis sp. PCC 6803". In: *Biotechnology for Biofuels* 12.1 (2019), pp. 1–13. ISSN: 17546834. DOI: 10.1186/s13068-018-1349-8. URL: https://doi.org/10.1186/s13068-018-1349-8.

[50]   Aniek D. van der Woude et al. "Genetic engineering of Synechocystis PCC6803 for the photoautotrophic production of the sweetener erythritol". In: *Microbial Cell Factories* 15.1 (2016), pp. 1–12. ISSN: 14752859. DOI: 10.1186/s12934-016-0458-y.

[51]   Jay Shankar Singh et al. "Cyanobacteria: A precious bio-resource in agriculture, ecosystem, and environmental sustainability". In: *Frontiers in Microbiology* 7.APR (2016), pp. 1–19. ISSN: 1664302X. DOI: 10.3389/fmicb.2016.00529.

[52]   K. J. Hellingwerf and M. J. Teixeira de Mattos. "Alternative routes to biofuels: Light-driven biofuel formation from CO2 and water based on the 'photanol' approach". In: *Journal of Biotechnology* 142.1 (2009), pp. 87–90. ISSN: 01681656. DOI: 10.1016/j.jbiotec.2009.02.002.

[53]   Abuzer Çelekli et al. "A Multivariate Approach to Evaluate Biomass Production, Biochemical Composition and Stress Compounds of Spirulina platensis Cultivated in Wastewater". In: *Applied Biochemistry and Biotechnology* 180.4 (2016), pp. 728–739. ISSN: 15590291. DOI: 10.1007/s12010-016-2128-2. URL: http://dx.doi.org/10.1007/s12010-016-2128-2.

[54]   R. M.M. Abed, S. Dobretsov, and K. Sudesh. "Applications of cyanobacteria in biotechnology". In: *Journal of Applied Microbiology* 106.1 (2009), pp. 1–12. ISSN: 13652672. DOI: 10.1111/j.1365-2672.2008.03918.x.

[55]   G. Charles Dismukes et al. "Aquatic phototrophs: efficient alternatives to land-based crops for biofuels". In: *Current Opinion in Biotechnology* 19.3 (2008), pp. 235–240. ISSN: 09581669. DOI: 10.1016/j.copbio.2008.05.007.

[56]   Takatomo Fujisawa et al. "CyanoBase: A large-scale update on its 20th anniversary". In: *Nucleic Acids Research* 45.D1 (2017), pp. D551–D554. ISSN: 13624962. DOI: 10.1093/nar/gkw1131.

[57]   Bertram M. Berla et al. "Synthetic biology of cyanobacteria: Unique challenges and opportunities". In: *Frontiers in Microbiology* 4.AUG (2013), pp. 1–14. ISSN: 1664302X. DOI: 10.3389/fmicb.2013.00246.

[58]   Guodong Luan, Shanshan Zhang, and Xuefeng Lu. "ScienceDirect Engineering cyanobacteria chassis cells toward more efficient photosynthesis". In: *Current Opinion in Biotechnology* 62 (2020), pp. 1–6. ISSN: 0958-1669. DOI: `10.1016/j.copbio.2019.07.004`. URL: `https://doi.org/10.1016/j.copbio.2019.07.004`.

[59]   Jingjie Yu et al. "Synechococcus elongatus UTEX 2973, a fast growing cyanobacterial chassis for biosynthesis using light and CO_2". In: *Scientific reports* 5 (2015), p. 8132. ISSN: 20452322. DOI: `10.1038/srep08132`.

[60]   Justin Ungerer et al. "Comparative genomics reveals the molecular determinants of rapid growth of the cyanobacterium Synechococcus elongatus UTEX 2973". In: *Proceedings of the National Academy of Sciences of the United States of America* 115.50 (2018), E11761–E11770. ISSN: 10916490. DOI: `10.1073/pnas.1814912115`.

[61]   Artur Włodarczyk et al. "Unprecedented biomass and fatty acid production by the newly discovered cyanobacterium Synechococcus sp. PCC 11901". In: *bioRxiv* (2019). DOI: `10.1101/684944`.

[62]   Giuseppe Olivieri, Piero Salatino, and Antonio Marzocchella. "Advances in photobioreactors for intensive microalgal production: Configurations, operating strategies and applications". In: *Journal of Chemical Technology and Biotechnology* 89.2 (2014), pp. 178–195. ISSN: 10974660. DOI: `10.1002/jctb.4218`.

[63]   Diana Kirilovsky. "Photoprotection in cyanobacteria: The orange carotenoid protein (OCP)-related non-photochemical-quenching mechanism". In: *Photosynthesis Research* 93.1-3 (2007), pp. 7–16. ISSN: 01668595. DOI: `10.1007/s11120-007-9168-y`.

[64]   Norio Murata et al. "Photoinhibition of photosystem II under environmental stress". In: *Biochimica et Biophysica Acta - Bioenergetics* 1767.6 (2007), pp. 414–421. ISSN: 00052728. DOI: `10.1016/j.bbabio.2006.11.019`.

[65]   Esa Tyystjärvi. "Photoinhibition of Photosystem II and photodamage of the oxygen evolving manganese cluster". In: *Coordination Chemistry Reviews* 252.3-4 (2008), pp. 361–376. ISSN: 00108545. DOI: `10.1016/j.ccr.2007.08.021`.

[66]   Peter J. Nixon et al. "Recent advances in understanding the assembly and repair of photosystem II". In: *Annals of Botany* 106.1 (2010), pp. 1–16. ISSN: 03057364. DOI: `10.1093/aob/mcq059`.

[67]   Yagut Allahverdiyeva et al. "Flavodiiron proteins Flv1 and Flv3 enable cyanobacterial growth and photosynthesis under fluctuating light". In: *Proceedings of the National Academy of Sciences of the United States of America* 110.10 (2013), pp. 4111–4116. ISSN: 00278424. DOI: `10.1073/pnas.1221194110`.

[68] Luca Bersanini et al. "Flavodiiron protein Flv2/Flv4-related photoprotective mechanism dissipates excitation pressure of PSII in cooperation with phycobilisomes in cyanobacteria". In: *Plant Physiology* 164.2 (2014), pp. 805–818. ISSN: 00320889. DOI: 10.1104/pp.113.231969.

[69] Marina G. Rakhimberdieva et al. "Carotenoid-induced quenching of the phycobilisome fluorescence in photosystem II-deficient mutant of Synechocystis sp." In: *FEBS Letters* 574.1-3 (2004), pp. 85–88. ISSN: 00145793. DOI: 10.1016/j.febslet.2004.07.087.

[70] David J. Thomas et al. "Photoinhibition and light-induced cyclic electron transport in ndhB- and psaE- mutants of Synechocystis sp. PCC 6803". In: *Plant and Cell Physiology* 42.8 (2001), pp. 803–812. ISSN: 00320781. DOI: 10.1093/pcp/pce104.

[71] Murray R. Badger and G. Dean Price. "CO2 concentrating mechanisms in cyanobacteria: Molecular components, their diversity and evolution". In: *Journal of Experimental Botany* 54.383 (2003), pp. 609–622. ISSN: 00220957. DOI: 10.1093/jxb/erg076.

[72] Jeffrey C. Cameron et al. "Biogenesis of a bacterial organelle: The carboxysome assembly pathway". In: *Cell* 155.5 (2013), p. 1131. ISSN: 10974172. DOI: 10.1016/j.cell.2013.10.044. URL: http://dx.doi.org/10.1016/j.cell.2013.10.044.

[73] Shiho Tanaka et al. "Atomic-level models of the bacterial carboxysome shell". In: *Science* 319.5866 (2008), pp. 1083–1086. ISSN: 00368075. DOI: 10.1126/science.1151458.

[74] Inger Andersson and Anders Backlund. "Structure and function of Rubisco". In: *Plant Physiology and Biochemistry* 46.3 (2008), pp. 275–291. ISSN: 09819428. DOI: 10.1016/j.plaphy.2008.01.001.

[75] Tobias J. Erb and Jan Zarzycki. "A short history of RubisCO: the rise and fall (?) of Nature's predominant CO2 fixing enzyme". In: *Current Opinion in Biotechnology* 49 (2018), pp. 100–107. ISSN: 18790429. DOI: 10.1016/j.copbio.2017.07.017. URL: http://dx.doi.org/10.1016/j.copbio.2017.07.017.

[76] Hermann Bauwe, Martin Hagemann, and Alisdair R. Fernie. "Photorespiration: players, partners and origin". In: *Trends in Plant Science* 15.6 (2010), pp. 330–336. ISSN: 13601385. DOI: 10.1016/j.tplants.2010.03.006.

[77] Deng Liu and Himadri B. Pakrasi. "Exploring native genetic elements as plug-in tools for synthetic biology in the cyanobacterium Synechocystis sp. PCC 6803". In: *Microbial Cell Factories* 17.1 (2018), pp. 1–8. ISSN: 14752859. DOI: 10.1186/s12934-018-0897-8. URL: https://doi.org/10.1186/s12934-018-0897-8.

[78] Annesha Sengupta, Himadri B. Pakrasi, and Pramod P Wangikar. "Recent advances in synthetic biology". In: (2018), pp. 5457–5471.

[79] Ravendran Vasudevan et al. "Cyanogate: A modular cloning suite for engineering cyanobacteria based on the plant moclo syntax". In: *Plant Physiology* 180.1 (2019), pp. 39–55. ISSN: 15322548. DOI: 10.1104/pp.18.01401.

[80] Jan Eriksson et al. "Deletion mutagenesis of the 5' psbA2 region in Synechocystis 6803: Identification of a putative cis element involved in photoregulation". In: *Molecular Cell Biology Research Communications* 3.5 (2000), pp. 292–298. ISSN: 15224724. DOI: 10.1006/mcbr.2000.0227.

[81] Hsin Ho Huang et al. "Design and characterization of molecular tools for a synthetic biology approach towards developing cyanobacterial biotechnology". In: *Nucleic Acids Research* 38.8 (2010), pp. 2577–2593. ISSN: 03051048. DOI: 10.1093/nar/gkq164.

[82] Tao Zhu et al. "Enhancing photosynthetic production of ethylene in genetically engineered Synechocystis". In: 10 (2015), pp. 421–434. DOI: 10.1039/c4gc01730g.

[83] Elias Englund, Feiyan Liang, and Pia Lindberg. "Evaluation of promoters and ribosome binding sites for biotechnological applications in the unicellular cyanobacterium Synechocystis sp. PCC 6803". In: *Scientific Reports* 6.October (2016), pp. 1–12. ISSN: 20452322. DOI: 10.1038/srep36640. URL: http://dx.doi.org/10.1038/srep36640.

[84] Barbara Blasi et al. "Characterization of stress responses of heavy metal and metalloid inducible promoters in Synechocystis PCC6803". In: *Journal of Microbiology and Biotechnology* 22.2 (2012), pp. 166–169. ISSN: 10177825. DOI: 10.4014/jmb.1106.06050.

[85] Elias Englund et al. "Metabolic Engineering of Synechocystis sp. PCC 6803 for Production of the Plant Diterpenoid Manoyl Oxide". In: *ACS Synthetic Biology* 4.12 (2015), pp. 1270–1278. ISSN: 21615063. DOI: 10.1021/acssynbio.5b00070.

[86] Kati Thiel et al. "Translation efficiency of heterologous proteins is significantly affected by the genetic context of RBS sequences in engineered cyanobacterium Synechocystis sp. PCC 6803". In: *Microbial Cell Factories* 17.1 (2018), pp. 1–12. ISSN: 14752859. DOI: 10.1186/s12934-018-0882-2. URL: https://doi.org/10.1186/s12934-018-0882-2.

[87] Evgeny Nudler. "Flipping Riboswitches". In: *Cell* 126.1 (2006), pp. 19–22. ISSN: 00928674. DOI: 10.1016/j.cell.2006.06.024.

[88] Yoichi Nakahira et al. "Theophylline-dependent riboswitch as a novel genetic tool for strict regulation of protein expression in cyanobacterium synechococcus elongatus PCC 7942". In: *Plant and Cell Physiology* 54.10 (2013), pp. 1724–1735. ISSN: 00320781. DOI: 10.1093/pcp/pct115.

[89] Stephan Klähn et al. "A glutamine riboswitch is a key element for the regulation of glutamine synthetase in cyanobacteria". In: *Nucleic Acids Research* 46.19 (2018), pp. 10082–10094. ISSN: 13624962. DOI: 10.1093/nar/gky709.

[90] Donald A. Bryant Adam A. Perez, Dmitry A. Rodionov. "Identification and Regulation of Genes for Cobalamin Transport in". In: 198.19 (2016), pp. 2753–2761. ISSN: 10985530. DOI: 10.1128/JB.00476-16.Editor.

[91] Andrew H. Ng, Bertram M. Berla, and Himadri B. Pakrasi. "Fine-tuning of photoautotrophic protein production by combining promoters and neutral sites in the cyanobacterium Synechocystis sp. strain PCC 6803". In: *Applied and Environmental Microbiology* 81.19 (2015), pp. 6857–6863. ISSN: 10985336. DOI: 10.1128/AEM.01349-15.

[92] Patricia Armshaw et al. "Utilising the native plasmid, pCA2.4, from the cyanobacterium Synechocystis sp. strain PCC6803 as a cloning site for enhanced product production". In: *Biotechnology for Biofuels* 8.1 (2015), pp. 1–10. ISSN: 17546834. DOI: 10.1186/s13068-015-0385-x.

[93] Yi Ern Cheah, Stevan C Albers, and Christie A M Peebles. "A Novel Counter-Selection Method for Markerless Genetic Modification in Synechocystis sp . pcc 6803". In: (2012). DOI: 10.1002/btpr.1661.

[94] Stefania Viola, Thilo Rühle, and Dario Leister. "A single vector-based strategy for marker-less gene replacement in Synechocystis sp. PCC 6803". In: *Microbial Cell Factories* 13.1 (2014), pp. 1–12. ISSN: 14752859. DOI: 10.1186/1475-2859-13-4.

[95] Tadas Jakočiunas, Michael K. Jensen, and Jay D. Keasling. "CRISPR/Cas9 advances engineering of microbial cell factories". In: *Metabolic Engineering* 34 (2016), pp. 44–59. ISSN: 10967184. DOI: 10.1016/j.ymben.2015.12.003.

[96] Juliane Behler et al. "CRISPR-Based Technologies for Metabolic Engineering in Cyanobacteria". In: *Trends in Biotechnology* 36.10 (2018), pp. 996–1010. ISSN: 18793096. DOI: 10.1016/j.tibtech.2018.05.011. URL: http://dx.doi.org/10.1016/j.tibtech.2018.05.011.

[97] Austin L. Carroll et al. "Metabolic engineering tools in model cyanobacteria". In: *Metabolic Engineering* 50.March (2018), pp. 47–56. ISSN: 10967184. DOI: 10.1016/j.ymben.2018.03.014. URL: https://doi.org/10.1016/j.ymben.2018.03.014.

[98] Danuta Kaczmarzyk et al. "Diversion of the long-chain acyl-ACP pool in Synechocystis to fatty alcohols through CRISPRi repression of the essential phosphate acyltransferase PlsX". In: *Metabolic Engineering* 45.October 2017 (2018), pp. 59–66. ISSN: 10967184. DOI: 10.1016/j.ymben.2017.11.014. URL: https://doi.org/10.1016/j.ymben.2017.11.014.

[99] Chun Hung Huang et al. "CRISPR interference (CRISPRi) for gene regulation and succinate production in cyanobacterium S. elongatus PCC 7942". In: *Microbial Cell Factories* 15.1 (2016), pp. 1–11. ISSN: 14752859. DOI: 10.1186/s12934-016-0595-3.

[100] Gina C. Gordon et al. "CRISPR interference as a titratable, trans-acting regulatory tool for metabolic engineering in the cyanobacterium Synechococcus sp. strain PCC 7002". In: *Metabolic Engineering* 38 (2016), pp. 170–179. ISSN: 10967184. DOI: 10.1016/j.ymben.2016.07.007.

[101] Lei S. Qi et al. "Repurposing CRISPR as an RNA-γuided platform for sequence-specific control of gene expression". In: *Cell* 152.5 (2013), pp. 1173–1183. ISSN: 00928674. DOI: 10.1016/j.cell.2013.02.022. URL: http://dx.doi.org/10.1016/j.cell.2013.02.022.

[102] Justin Ungerer and Himadri B. Pakrasi. "Cpf1 Is A Versatile Tool for CRISPR Genome Editing Across Diverse Species of Cyanobacteria". In: *Scientific Reports* 6.October (2016), pp. 1–9. ISSN: 20452322. DOI: 10.1038/srep39681. URL: http://dx.doi.org/10.1038/srep39681.

[103] Robert E Blankenship et al. "Comparing Photosynthetic and the Potential for Improvement". In: *Science* 332.May (2011), pp. 805–810.

[104] Robert E. Blankenship. *Molecular Mechanisms of Photosynthesis.* Second edi. Wiley-Blackwell, 2014, p. 312. ISBN: 978-1-405-18976-7.

[105] N. Tandeau De Marsac. "Occurrence and nature of chromatic adaptation in cyanobacteria". In: *Journal of Bacteriology* 130.1 (1977), pp. 82–91. ISSN: 00219193.

[106] Dennis J. Nürnberg et al. "Photochemistry beyond the red limit in chlorophyll f–containing photosystems". In: *Science* 360.6394 (2018), pp. 1210–1213. ISSN: 10959203. DOI: 10.1126/science.aar8313.

[107] Zhong-chun Zhang et al. "Widespread occurrence and unexpected diversity of red-shifted chlorophyll producing cyanobacteria in humid subtropical forest ecosystems". In: 21 (2019), pp. 1497–1510. DOI: 10.1111/1462-2920.14582.

[108] Gaozhong Shen et al. "Characterization of chlorophyll f synthase heterologously produced in Synechococcus sp . PCC 7002". In: *Photosynthesis Research* 140.1 (2019), pp. 77–92. ISSN: 1573-5079. DOI: 10.1007/s11120-018-00610-9. URL: http://dx.doi.org/10.1007/s11120-018-00610-9.

[109] Nico J Claassens et al. "Potential of proton-pumping rhodopsins : engineering photosystems into microorganisms". In: *Trends in Biotechnology* 31.11 (2013), pp. 633–642. ISSN: 0167-7799. DOI: 10.1016/j.tibtech.2013.08.006. URL: http://dx.doi.org/10.1016/j.tibtech.2013.08.006.

[110] Que Chen et al. "Combining retinal-based and chlorophyll-based (oxygenic) photosynthesis : Proteorhodopsin expression increases growth rate and fitness of a ΔPSI strain of Synechocystis sp . PCC6803". In: *Metabolic Engineering* 52.November 2018 (2019), pp. 68–76. ISSN: 1096-7176. DOI: 10.1016/j.ymben.2018.11.002. URL: https://doi.org/10.1016/j.ymben.2018.11.002.

[111] Que Chen et al. "Functional expression of gloeobacter rhodopsin in PSI-less Synechocystis sp. PCC6803". In: *Frontiers in Bioengineering and Biotechnology* 7.MAR (2019), pp. 1–9. ISSN: 22964185. DOI: 10.3389/fbioe.2019.00067.

[112] Henning Kirst, Cinzia Formighieri, and Anastasios Melis. "Maximizing photosynthetic efficiency and culture productivity in cyanobacteria upon minimizing the phycobilisome light-harvesting antenna size". In: *Biochimica et Biophysica Acta - Bioenergetics* 1837.10 (2014), pp. 1653–1664. ISSN: 18792650. DOI: 10.1016/j.bbabio.2014.07.009. URL: http://dx.doi.org/10.1016/j.bbabio.2014.07.009.

[113] Jong-hee Kwon et al. "Reduced light-harvesting antenna : Consequences on cyanobacterial metabolism and photosynthetic productivity". In: *ALGAL* 2.3 (2013), pp. 188–195. ISSN: 2211-9264. DOI: 10.1016/j.algal.2013.04.008. URL: http://dx.doi.org/10.1016/j.algal.2013.04.008.

[114] Giorgio Perin et al. "The potential of quantitative models to improve microalgae photosynthetic efficiency". In: *Physiologia Plantarum* 166.1 (2019), pp. 380–391. ISSN: 13993054. DOI: 10.1111/ppl.12915.

[115] Shota Atsumi, Wendy Higashide, and James C Liao. "letters Direct photosynthetic recycling of carbon dioxide to isobutyraldehyde". In: *Nature Biotechnology* 27.12 (2009), pp. 1177–1180. ISSN: 1087-0156. DOI: 10.1038/nbt.1586. URL: http://dx.doi.org/10.1038/nbt.1586.

[116] Feiyan Liang and Peter Lindblad. "Synechocystis PCC 6803 overexpressing RuBisCO grow faster with increased photosynthesis". In: *Metabolic Engineering Communications* 4.October 2016 (2017), pp. 29–36. ISSN: 22140301. DOI: 10.1016/j.meteno.2017.02.002. URL: http://dx.doi.org/10.1016/j.meteno.2017.02.002.

[117] Aaron M. Appel et al. "Frontiers, opportunities, and challenges in biochemical and chemical catalysis of CO2 fixation". In: *Chemical Reviews* 113.8 (2013), pp. 6621–6658. ISSN: 00092665. DOI: 10.1021/cr300463y.

[118] Devin L. Trudeau et al. "Design and in vitro realization of carbon-conserving photorespiration". In: *Proceedings of the National Academy of Sciences of the United States of America* 115.49 (2018), E11455–E11464. ISSN: 10916490. DOI: 10.1073/pnas.1812605115.

[119] Arren Bar-Even et al. "Design and analysis of synthetic carbon fixation pathways". In: *Proceedings of the National Academy of Sciences of the United States of America* 107.19 (2010), pp. 8889–8894. ISSN: 00278424. DOI: 10.1073/pnas.0907176107.

[120] Iria Bernhardsgrütter et al. "Awakening the Sleeping Carboxylase Function of Enzymes: Engineering the Natural CO2-Binding Potential of Reductases". In: *Journal of the American Chemical Society* 141.25 (2019), pp. 9778–9782. ISSN: 15205126. DOI: 10.1021/jacs.9b03431.

[121] Hasan Demirci et al. "Coupled inter-subunit dynamics enable the fastest CO2-fixation by reductive carboxylases". In: *bioRxiv* (2019).

[122] Claudia Durall, Nita Rukminasari, and Peter Lindblad. "Enhanced growth at low light intensity in the cyanobacterium Synechocystis PCC 6803 by overexpressing phosphoenolpyruvate carboxylase". In: *Algal Research* 16 (2016), pp. 275–281. ISSN: 22119264. DOI: 10.1016/j.algal.2016.03.027. URL: http://dx.doi.org/10.1016/j.algal.2016.03.027.

[123] S Andreas Angermayr et al. "Energy biotechnology with cyanobacteria". In: *Current Opinion in Biotechnology* 20 (2009), pp. 257–263. DOI: 10.1016/j.copbio.2009.05.011.

[124] Daniel C. Ducat, Jeffrey C. Way, and Pamela A. Silver. "Engineering cyanobacteria to generate high-value products". In: *Trends in Biotechnology* 29.2 (2011), pp. 95–103. ISSN: 01677799. DOI: 10.1016/j.tibtech.2010.12.003. URL: http://dx.doi.org/10.1016/j.tibtech.2010.12.003.

[125] Caroline Baroukh et al. "A state of the art of metabolic networks of unicellular microalgae and cyanobacteria for biofuel production". In: *Metabolic Engineering* 30 (2015), pp. 49–60. ISSN: 10967184. DOI: 10.1016/j.ymben.2015.03.019. URL: http://dx.doi.org/10.1016/j.ymben.2015.03.019.

[126] Adam A. Pérez et al. "On the use of oxygenic photosynthesis for the sustainable production of commodity chemicals". In: *Physiologia Plantarum* 166.1 (2019), pp. 413–427. ISSN: 13993054. DOI: 10.1111/ppl.12946.

[127] Zhengxu Gao et al. "Photosynthetic production of ethanol from carbon dioxide in genetically engineered cyanobacteria". In: *Energy and Environmental Science* 5.12 (2012), pp. 9857–9865. ISSN: 17545692. DOI: 10.1039/c2ee22675h.

[128] S. Andreas Angermayr, Michal Paszota, and Klaas J. Hellingwerf. "Engineering a cyanobacterial cell factory for production of lactic acid". In: *Applied and Environmental Microbiology* 78.19 (2012), pp. 7098–7106. ISSN: 00992240. DOI: 10.1128/AEM.01587-12.

[129] B. Drosg et al. "Photo-autotrophic production of poly(hydroxyalkanoates) in cyanobacteria". In: *Chemical and Biochemical Engineering Quarterly* 29.2 (2015), pp. 145–156. ISSN: 03529568. DOI: 10.15255/CABEQ.2014.2254.

[130] Moritz Koch et al. "PHB is produced from Glycogen turn-over during nitrogen starvation in Synechocystis sp. PCC 6803". In: *International Journal of Molecular Sciences* 20.8 (2019). ISSN: 14220067. DOI: 10.3390/ijms20081942.

[131] John W.K. Oliver et al. "Cyanobacterial conversion of carbon dioxide to 2,3-butanediol". In: *Proceedings of the National Academy of Sciences of the United States of America* 110.4 (2013), pp. 1249–1254. ISSN: 00278424. DOI: 10.1073/pnas.1213024110.

[132] Ethan I. Lan and James C. Liao. "Metabolic engineering of cyanobacteria for 1-butanol production from carbon dioxide". In: *Metabolic Engineering* 13.4 (2011), pp. 353–363. ISSN: 10967176. DOI: 10.1016/j.ymben.2011.04.004. URL: http://dx.doi.org/10.1016/j.ymben.2011.04.004.

[133] Fernando Guerrero et al. "Ethylene Synthesis and Regulated Expression of Recombinant Protein in Synechocystis sp. PCC 6803". In: *PLoS ONE* 7.11 (2012). ISSN: 19326203. DOI: 10.1371/journal.pone.0050470.

[134] Yasutaka Hirokawa et al. "Metabolic engineering of Synechococcus elongatus PCC 7942 for improvement of 1,3-propanediol and glycerol production based on in silico simulation of metabolic flux distribution". In: *Microbial Cell Factories* 16.1 (2017), pp. 1–12. ISSN: 14752859. DOI: 10.1186/s12934-017-0824-4. URL: https://doi.org/10.1186/s12934-017-0824-4.

[135] Barbara Menin et al. "Non-endogenous ketocarotenoid accumulation in engineered Synechocystis sp. PCC 6803". In: *Physiologia Plantarum* 166.1 (2019), pp. 403–412. ISSN: 13993054. DOI: 10.1111/ppl.12900.

[136] Gao Chen et al. "Transgenic expression of delta-6 and delta-15 fatty acid desaturases enhances omega-3 polyunsaturated fatty acid accumulation in Synechocystis sp. PCC6803". In: *Biotechnology for Biofuels* 7.1 (2014), pp. 1–10. ISSN: 17546834. DOI: 10.1186/1754-6834-7-32.

[137] Travis C. Korosh et al. "Engineering photosynthetic production of L-lysine". In: *Metabolic Engineering* 44.October (2017), pp. 273–283. ISSN: 10967184. DOI: 10.1016/j.ymben.2017.10.010.

[138] Cory J. Knoot et al. "Cyanobacteria: Promising biocatalysts for sustainable chemical production". In: *Journal of Biological Chemistry* 293.14 (2018), pp. 5044–5052. ISSN: 1083351X. DOI: 10.1074/jbc.R117.815886.

[139] Pia Lindberg, Sungsoon Park, and Anastasios Melis. "Engineering a platform for photosynthetic isoprene production in cyanobacteria, using Synechocystis as the model organism". In: *Metabolic Engineering* 12.1 (2010), pp. 70–79. ISSN: 10967176. DOI: 10.1016/j.ymben.2009.10.001. URL: http://dx.doi.org/10.1016/j.ymben.2009.10.001.

[140] Fiona K. Bentley, Andreas Zurbriggen, and Anastasios Melis. "Heterologous expression of the mevalonic acid pathway in cyanobacteria enhances endogenous carbon partitioning to isoprene". In: *Molecular Plant* 7.1 (2014), pp. 71–86. ISSN: 17529867. DOI: 10.1093/mp/sst134. URL: http://dx.doi.org/10.1093/mp/sst134.

[141] Nadin Pade et al. "Insights into isoprene production using the cyanobacterium Synechocystis sp. PCC 6803". In: *Biotechnology for Biofuels* 9.1 (2016), pp. 1–16. ISSN: 17546834. DOI: 10.1186/s13068-016-0503-4.

[142] Wei Du et al. "Alignment of microbial fitness with engineered product formation: Obligatory coupling between acetate production and photoautotrophic growth". In: *Biotechnology for Biofuels* 11.1 (2018), pp. 1–13. ISSN: 17546834. DOI: 10.1186/s13068-018-1037-8. URL: https://doi.org/10.1186/s13068-018-1037-8.

[143] Bo Wang et al. "Engineering cyanobacteria for photosynthetic production of 3-hydroxybutyrate directly from CO2". In: *Metabolic Engineering* 16.1 (2013), pp. 68–77. ISSN: 10967176. DOI: 10.1016/j.ymben.2013.01.001. URL: http://dx.doi.org/10.1016/j.ymben.2013.01.001.

[144] Ni Wan et al. "Cyanobacterial carbon metabolism: Fluxome plasticity and oxygen dependence". In: *Biotechnology and Bioengineering* 114.7 (2017), pp. 1593–1602. ISSN: 10970290. DOI: 10.1002/bit.26287.

[145] Wei Xiong, Daniel Brune, and Wim F J Vermaas. "The γ-aminobutyric acid shunt contributes to closing the tricarboxylic acid cycle in Synechocystis sp. PCC 6803". In: *Molecular Microbiology* 93.4 (2014), pp. 786–796. ISSN: 13652958. DOI: 10.1111/mmi.12699.

[146] Shuyi Zhang and Donald A. Bryant. "The tricarboxylic acid cycle in cyanobacteria". In: *Science* 334.6062 (2011), pp. 1551–1553. ISSN: 10959203. DOI: 10.1126/science.1210858.

[147] Henning Knoop et al. "The metabolic network of Synechocystis sp. PCC 6803: Systemic properties of autotrophic growth". In: *Plant Physiology* 154.1 (2010), pp. 410–422. ISSN: 00320889. DOI: 10.1104/pp.110.157198.

[148] Dirk Steinhauser, Alisdair R. Fernie, and Wagner L. Araújo. "Unusual cyanobacterial TCA cycles: Not broken just different". In: *Trends in Plant Science* 17.9 (2012), pp. 503–509. ISSN: 13601385. DOI: 10.1016/j.tplants.2012.05.005.

111

[149] Masaharu Maruyama et al. "Time-resolved analysis of short term metabolic adaptation at dark transition in Synechocystis sp. PCC 6803". In: *Journal of Bioscience and Bioengineering* (2019). ISSN: 13474421. DOI: 10.1016/j.jbiosc.2019.03.016. URL: https://doi.org/10.1016/j.jbiosc.2019.03.016.

[150] Aniek D. Van der Woude et al. "Carbon sink removal: Increased photosynthetic production of lactic acid by Synechocystis sp. PCC6803 in a glycogen storage mutant". In: *Journal of Biotechnology* 184 (2014), pp. 100–102. ISSN: 18734863. DOI: 10.1016/j.jbiotec.2014.04.029. URL: http://dx.doi.org/10.1016/j.jbiotec.2014.04.029.

[151] Josefine Anfelt et al. "Genetic and nutrient modulation of acetyl-CoA levels in Synechocystis for n-butanol production". In: *Microbial Cell Factories* 14.1 (2015), pp. 1–12. ISSN: 14752859. DOI: 10.1186/s12934-015-0355-9.

[152] Steinn Gudmundsson and Juan Nogales. "Cyanobacteria as photosynthetic biocatalysts: A systems biology perspective". In: *Molecular BioSystems* 11.1 (2015), pp. 60–70. ISSN: 17422051. DOI: 10.1039/c4mb00335g.

[153] Henrike Niederholtmeyer et al. "Engineering cyanobacteria to synthesize and export hydrophilic products". In: *Applied and Environmental Microbiology* 76.11 (2010), pp. 3462–3466. ISSN: 00992240. DOI: 10.1128/AEM.00202-10.

[154] Gavin Kurgan et al. "Identification of major malate export systems in an engineered malate-producing Escherichia coli aided by substrate similarity search". In: *Applied Microbiology and Biotechnology* 103 (2019), pp. 9001–9011. DOI: 10.1007/s00253-019-10164-y.

[155] Stephen Van Dien. "From the first drop to the first truckload: Commercialization of microbial processes for renewable chemicals". In: *Current Opinion in Biotechnology* 24.6 (2013), pp. 1061–1068. ISSN: 09581669. DOI: 10.1016/j.copbio.2013.03.002. URL: http://dx.doi.org/10.1016/j.copbio.2013.03.002.

[156] Wei Du et al. "Challenges in the Application of Synthetic Biology Toward Synthesis of Commodity Products by Cyanobacteria via "Direct Conversion"". In: *Synthetic Biology of Cyanobacteria*. Ed. by Weiwen Zhang and Xinyu Song. Singapore: Springer Singapore, 2018, pp. 3–26. ISBN: 978-981-13-0854-3. DOI: 10.1007/978-981-13-0854-3_1. URL: https://doi.org/10.1007/978-981-13-0854-3%7B%5C_%7D1.

[157] Corinne Cassier-Chauvat, Théo Veaudor, and Franck Chauvat. "Comparative genomics of DNA recombination and repair in cyanobacteria: Biotechnological implications". In: *Frontiers in Microbiology* 7.NOV (2016), pp. 1–13. ISSN: 1664302X. DOI: 10.3389/fmicb.2016.01809.

[158] Tamami Kusakabe et al. "Engineering a synthetic pathway in cyanobacteria for isopropanol production directly from carbon dioxide and light". In: *Metabolic Engineering* 20 (2013), pp. 101–108. ISSN: 10967184. DOI: 10.1016/j.ymben.2013.09.007. URL: http://dx.doi.org/10.1016/j.ymben.2013.09.007.

[159] Jacob H. Jacobsen and Niels Ulrik Frigaard. "Engineering of photosynthetic mannitol biosynthesis from CO2 in a cyanobacterium". In: *Metabolic Engineering* 21 (2014), pp. 60–70. ISSN: 10967184. DOI: 10.1016/j.ymben.2013.11.004. URL: http://dx.doi.org/10.1016/j.ymben.2013.11.004.

[160] Veronica Carbonell et al. "Enhanced stable production of ethylene in photosynthetic cyanobacterium Synechococcus elongatus PCC 7942". In: *World Journal of Microbiology and Biotechnology* 35.5 (2019), pp. 1–9. ISSN: 15730972. DOI: 10.1007/s11274-019-2652-7. URL: https://doi.org/10.1007/s11274-019-2652-7.

[161] Kazutaka Takahama et al. "Construction and analysis of a recombinant cyanobacterium expressing a chromosomally inserted gene for an ethylene-forming enzyme at the psbAI locus". In: *Journal of Bioscience and Bioengineering* 95.3 (2003), pp. 302–305. ISSN: 13891723. DOI: 10.1263/jbb.95.302.

[162] Wei Du et al. "Nonhierarchical Flux Regulation Exposes the Fitness Burden Associated with Lactate Production in Synechocystis sp. PCC6803". In: *ACS Synthetic Biology* 6.3 (2017), pp. 395–401. ISSN: 21615063. DOI: 10.1021/acssynbio.6b00235.

[163] David Gresham and Maitreya J. Dunham. "The enduring utility of continuous culturing in experimental evolution". In: *Genomics* 104.6 (2014), pp. 399–405. ISSN: 10898646. DOI: 10.1016/j.ygeno.2014.09.015. URL: http://dx.doi.org/10.1016/j.ygeno.2014.09.015.

[164] Bram Van den Bergh et al. "Experimental Design, Population Dynamics, and Diversity in Microbial Experimental Evolution". In: *Microbiology and Molecular Biology Reviews* 82.3 (2018), pp. 1–54. ISSN: 1092-2172. DOI: 10.1128/mmbr.00008-18.

[165] Peter Rugbjerg et al. "Diverse genetic error modes constrain large-scale bio-based production". In: *Nature Communications* 9.1 (2018). ISSN: 20411723. DOI: 10.1038/s41467-018-03232-w. URL: http://dx.doi.org/10.1038/s41467-018-03232-w.

[166] Peter Rugbjerg and Morten O.A. Sommer. "Overcoming genetic heterogeneity in industrial fermentations". In: *Nature Biotechnology* (2019). ISSN: 15461696. DOI: 10.1038/s41587-019-0171-6. URL: http://dx.doi.org/10.1038/s41587-019-0171-6.

[167] Pierre Mermet-Bouvier and Franck Chauvat. "A conditional expression vector for the cyanobacteria Synechocystis sp. strains PCC6803 and PCC6714 or Synechococcus sp. strains PCC7942 and PCC6301". In: *Current Microbiology* 28.3 (1994), pp. 145–148. ISSN: 1432-0991. DOI: 10.1007/BF01571055.

[168] Stevan C. Albers and Christie A.M. Peebles. "Evaluating Light-Induced Promoters for the Control of Heterologous Gene Expression in Synechocystis sp. PCC 6803". In: *Biotechnology Progress* 33.1 (2017), pp. 45–53. ISSN: 15206033. DOI: 10.1002/btpr.2396.

[169] Daniel Camsund, Thorsten Heidorn, and Peter Lindblad. "Design and analysis of LacI-repressed promoters and DNA-looping in a cyanobacterium". In: *Journal of Biological Engineering* 8.1 (2014), pp. 1–23. ISSN: 17541611. DOI: 10.1186/1754-1611-8-4.

[170] Xinyao Liu and Roy Curtiss. "Nickel-inducible lysis system in Synechocystis sp. PCC 6803". In: *Proceedings of the National Academy of Sciences of the United States of America* 106.51 (2009), pp. 21550–21554. ISSN: 00278424. DOI: 10.1073/pnas.0911953106.

[171] Erin K. Zess, Matthew B. Begemann, and Brian F. Pfleger. "Construction of new synthetic biology tools for the control of gene expression in the cyanobacterium Synechococcus sp. strain PCC 7002". In: *Biotechnology and Bioengineering* 113.2 (2016), pp. 424–432. ISSN: 10970290. DOI: 10.1002/bit.25713.

[172] Ciarán L. Kelly et al. "A Rhamnose-Inducible System for Precise and Temporal Control of Gene Expression in Cyanobacteria". In: *ACS Synthetic Biology* 7.4 (2018), pp. 1056–1066. ISSN: 21615063. DOI: 10.1021/acssynbio.7b00435.

[173] Melissa Cano et al. "Glycogen Synthesis and Metabolite Overflow Contribute to Energy Balancing in Cyanobacteria". In: *Cell Reports* 23.3 (2018), pp. 667–672. ISSN: 22111247. DOI: 10.1016/j.celrep.2018.03.083. URL: https://doi.org/10.1016/j.celrep.2018.03.083.

[174] Juan Nogales et al. "Detailing the optimality of photosynthesis in cyanobacteria through systems biology analysis". In: *Proceedings of the National Academy of Sciences of the United States of America* 109.7 (2012), pp. 2678–2683. ISSN: 00278424. DOI: 10.1073/pnas.1117907109.

[175] Henning Knoop and Ralf Steuer. "A computational analysis of stoichiometric constraints and trade-offs in cyanobacterial biofuel production". In: *Frontiers in Bioengineering and Biotechnology* 3.APR (2015), pp. 1–15. ISSN: 22964185. DOI: 10.3389/fbioe.2015.00047.

[176] Kiyan Shabestary and Elton P. Hudson. "Computational metabolic engineering strategies for growth-coupled biofuel production by Synechocystis". In: *Metabolic Engineering Communications* 3 (2016), pp. 216–226. ISSN: 22140301. DOI: 10.1016/j.meteno.2016.07.003. URL: http://dx.doi.org/10.1016/j.meteno.2016.07.003.

[177] Philipp Erdrich et al. "Cyanobacterial biofuels: New insights and strain design strategies revealed by computational modeling". In: *Microbial Cell Factories* 13.1 (2014), pp. 1–15. ISSN: 14752859. DOI: 10.1186/s12934-014-0128-x.

[178] Paula Jouhten et al. "Metabolic anchor reactions for robust biorefining". In: *Metabolic Engineering* 40.August 2016 (2017), pp. 1–4. ISSN: 10967184. DOI: 10.1016/j.ymben.2017.02.010.

[179] Christopher R. Mehrer et al. "Growth-coupled bioconversion of levulinic acid to butanone". In: *Metabolic Engineering* 55.June (2019), pp. 92–101. ISSN: 10967184. DOI: 10.1016/j.ymben.2019.06.003.

[180] Anthony P. Burgard, Priti Pharkya, and Costas D. Maranas. "OptKnock: A Bilevel Programming Framework for Identifying Gene Knockout Strategies for Microbial Strain Optimization". In: *Biotechnology and Bioengineering* 84.6 (2003), pp. 647–657. ISSN: 00063592. DOI: 10.1002/bit.10803.

[181] François Le Borgne and Jérémy Pruvost. "Investigation and modeling of biomass decay rate in the dark and its potential influence on net productivity of solar photobioreactors for microalga Chlamydomonas reinhardtii and cyanobacterium Arthrospira platensis". In: *Bioresource Technology* 138 (2013), pp. 271–276. ISSN: 18732976. DOI: 10.1016/j.biortech.2013.03.056.

[182] D. Lips et al. "Many ways towards 'solar fuel': Quantitative analysis of the most promising strategies and the main challenges during scale-up". In: *Energy and Environmental Science* 11.1 (2018), pp. 10–22. ISSN: 17545706. DOI: 10.1039/c7ee02212c.

[183] Tomáš Zavřel et al. "A quantitative evaluation of ethylene production in the recombinant cyanobacterium Synechocystis sp. PCC 6803 harboring the ethylene-forming enzyme by membrane inlet mass spectrometry". In: *Bioresource Technology* 202 (2016), pp. 142–151. ISSN: 18732976. DOI: 10.1016/j.biortech.2015.11.062.

[184] Jeroen H. De Vree et al. "Comparison of four outdoor pilot-scale photobioreactors". In: *Biotechnology for Biofuels* 8.1 (2015), pp. 1–12. ISSN: 17546834. DOI: 10.1186/s13068-015-0400-2.

[185] W L Ogren. "Photorespiration: Pathways, Regulation, and Modification". In: *Annual Review of Plant Physiology* 35.1 (1984), pp. 415–442. DOI: 10.1146/annurev.pp.35.060184.002215.

[186] M. A.J. Parry et al. "Manipulation of Rubisco: The amount, activity, function and regulation". In: *Journal of Experimental Botany* 54.386 (2003), pp. 1321–1333. ISSN: 00220957. DOI: 10.1093/jxb/erg141.

[187] Maribel M. Loera-Quezada et al. "A novel genetic engineering platform for the effective management of biological contaminants for the production of microalgae". In: *Plant Biotechnology Journal* 14.10 (2016), pp. 2066–2076. ISSN: 14677652. DOI: 10.1111/pbi.12564.

[188] Asieh Aramvash et al. "An environmentally friendly and efficient method for extraction of PHB biopolymer with non-halogenated solvents". In: *Journal of Microbiology and Biotechnology* 25.11 (2015), pp. 1936–1943. ISSN: 17388872. DOI: 10.4014/jmb.1505.05053.

[189] Sonam Dubey et al. "1-Ethyl-3-methylimidazolium Diethylphosphate Based Extraction of Bioplastic "polyhydroxyalkanoates" from Bacteria: Green and Sustainable Approach". In: *ACS Sustainable Chemistry and Engineering* 6.1 (2018), pp. 766–773. ISSN: 21680485. DOI: 10.1021/acssuschemeng.7b03096.

[190] Brett G. Olivier, Johann M. Rohwer, and Jan Hendrik S. Hofmeyr. "Modelling cellular systems with PySCeS". In: *Bioinformatics* 21.4 (2005), pp. 560–561. ISSN: 13674803. DOI: 10.1093/bioinformatics/bti046.

[191] Timo R. Maarleveld et al. "A data integration and visualization resource for the metabolic network of Synechocystis sp. PCC 6803". In: *Plant Physiology* 164.3 (2014), pp. 1111–1121. ISSN: 00320889. DOI: 10.1104/pp.113.224394.

[192] Joost Boele, Brett G. Olivier, and Bas Teusink. "FAME, the Flux Analysis and Modeling Environment". In: *BMC Systems Biology* 6.8 (2012). URL: https://bmcsystbiol.biomedcentral.com/articles/10.1186/1752-0509-6-8.

[193] Haojie Jin et al. "Construction of a shuttle vector using an endogenous plasmid from the cyanobacterium synechocystis sp. PCC6803". In: *Frontiers in Microbiology* 9 (2018), pp. 1–13. ISSN: 1664302X. DOI: 10.3389/fmicb.2018.01662.

[194] Pascal Van Alphen et al. "Increasing the Photoautotrophic Growth Rate of Synechocystis sp . PCC 6803 by Identifying the Limitations of Its Cultivation". In: 1700764 (2018), pp. 1–8. DOI: 10.1002/biot.201700764.

[195] Yonglong Zhang et al. "MazF Cleaves Cellular mRNAs Specifically at ACA to Block Protein Synthesis in Escherichia coli". In: 12 (2003), pp. 913–923.

[196] Roberta Carpine et al. "Genetic engineering of Synechocystis sp. PCC6803 for poly-β-hydroxybutyrate overproduction". In: *Algal Research* 25.February (2017), pp. 117–127. ISSN: 22119264. DOI: 10.1016/j.algal.2017.05.013. URL: http://dx.doi.org/10.1016/j.algal.2017.05.013.

[197] Wei Du et al. "Photonfluxostat: A method for light-limited batch cultivation of cyanobacteria at different, yet constant, growth rates". In: *Algal Research* 20 (2016), pp. 118–125. ISSN: 22119264. DOI: 10.1016/j.algal.2016.10.004. URL: http://dx.doi.org/10.1016/j.algal.2016.10.004.

[198] Szybalski W. Bryson V. "Microbial selection". In: *Science* 80.116 (1952), pp. 45–51.

[199] Leonard Krall et al. "Assessment of sampling strategies for gas chromatography-mass spectrometry (GC-MS) based metabolomics of cyanobacteria". In: *Journal of Chromatography B: Analytical Technologies in the Biomedical and Life Sciences* 877.27 (2009), pp. 2952–2960. ISSN: 15700232. DOI: 10.1016/j.jchromb.2009.07.006.

[200] Marion Eisenhut et al. "Metabolome phenotyping of inorganic carbon limitation in cells of the wild type and photorespiratory mutants of the cyanobacterium Synechocystis sp. strain PCC 6803". In: *Plant Physiology* 148.4 (2008), pp. 2109–2120. ISSN: 00320889. DOI: 10.1104/pp.108.129403.

[201] Konstantin Okonechnikov et al. "Unipro UGENE: A unified bioinformatics toolkit". In: *Bioinformatics* 28.8 (2012), pp. 1166–1167. ISSN: 13674803. DOI: 10.1093/bioinformatics/bts091.

[202] Elisabeth Gasteiger et al. "ExPASy: The proteomics server for in-depth protein knowledge and analysis". In: *Nucleic Acids Research* 31.13 (2003), pp. 3784–3788. ISSN: 03051048. DOI: 10.1093/nar/gkg563.

[203] Steffen Klamt and Radhakrishnan Mahadevan. "On the feasibility of growth-coupled product synthesis in microbial strains". In: *Metabolic Engineering* 30 (2015), pp. 166–178. ISSN: 10967184. DOI: 10.1016/j.ymben.2015.05.006. URL: http://dx.doi.org/10.1016/j.ymben.2015.05.006.

[204] Adam M. Feist et al. "Model-driven evaluation of the production potential for growth-coupled products of Escherichia coli". In: *Metabolic Engineering* 12.3 (2010), pp. 173–186. ISSN: 10967176. DOI: 10.1016/j.ymben.2009.10.003. URL: http://dx.doi.org/10.1016/j.ymben.2009.10.003.

[205] Israel Goldberg and J Stefan Rokem. "Fumaric Acid Biosynthesis and Accumulation". In: *Bioprocessing of Renewable Resources to Commodity Bioproducts*. John Wiley & Sons, Ltd, 2014. Chap. 15, pp. 409–434. ISBN: 9781118845394. DOI: 10.1002/9781118845394.ch15. URL: https://onlinelibrary.wiley.com/doi/abs/10.1002/9781118845394.ch15.

[206] Xiulai Chen et al. "Mitochondrial engineering of the TCA cycle for fumarate production". In: *Metabolic Engineering* 31 (2015), pp. 62–73. ISSN: 10967184. DOI: 10.1016/j.ymben.2015.02.002. URL: http://dx.doi.org/10.1016/j.ymben.2015.02.002.

[207] Juan Nogales, Steinn Gudmundsson, and Ines Thiele. "Toward systems metabolic engineering in cyanobacteria: Opportunities and bottlenecks". In: *Bioengineered* 4.3 (2013). ISSN: 19491018. DOI: 10.4161/bioe.22792.

[208] Herwig Bachmann et al. "Experimental evolution and the adjustment of metabolic strategies in lactic acid bacteria". In: *FEMS microbiology reviews* 41.1 (2017), S201–S219. ISSN: 15746976. DOI: 10.1093/femsre/fux024.

[209] Henning Knoop et al. "Flux Balance Analysis of Cyanobacterial Metabolism: The Metabolic Network of Synechocystis sp. PCC 6803". In: *PLoS Computational Biology* 9.6 (2013). ISSN: 1553734X. DOI: 10.1371/journal.pcbi.1003081.

[210] Rajib Saha et al. "Diurnal Regulation of Cellular Processes in the Cyanobacterium". In: *mBio* 7.3 (2016), pp. 1–14. DOI: 10.1128/mBio.00464-16.Editor.

[211] Debolina Sarkar et al. "A diurnal flux balance model of Synechocystis sp. PCC 6803 metabolism". In: *PLoS Computational Biology* 15.1 (2019), pp. 1–29. ISSN: 15537358. DOI: 10.1371/journal.pcbi.1006692.

[212] Shrameeta Shinde et al. "Glycogen metabolism jump-starts photosynthesis through the oxidative pentose phosphate pathway (OPPP) in cyanobacteria". In: *bioRxiv* (2019), p. 657304. DOI: 10.1101/657304. URL: https://www.biorxiv.org/content/10.1101/657304v1.

[213] Katsunori Yoshikawa et al. "Integrated transcriptomic and metabolomic analysis of the central metabolism of Synechocystis sp. PCC 6803 under different trophic conditions". In: *Biotechnology Journal* 8.5 (2013), pp. 571–580. ISSN: 18606768. DOI: 10.1002/biot.201200235.

[214] E I Lan, S Y Ro, and J C Liao. "Oxygen-tolerant coenzyme A-acylating aldehyde dehydrogenase facilitates efficient photosynthetic n-butanol biosynthesis in cyanobacteria". In: *Energy and Environmental Science* 6.9 (2013), pp. 2672–2681. DOI: 10.1039/c3ee41405a. URL: https://www.scopus.com/inward/record.uri?eid=2-s2.0-84882392453%7B%5C%7Ddoi=10.1039%7B%5C%7D2Fc3ee41405a%7B%5C%7DpartnerID=40%7B%5C%7Dmd5=e0f8f4511d318cb883a9f82543d7f37f.

[215] Chandresh Thakker et al. "Metabolic engineering of carbon and redox flow in the production of small organic acids". In: *Journal of Industrial Microbiology and Biotechnology* 42.3 (2014), pp. 403–422. ISSN: 14765535. DOI: 10.1007/s10295-014-1560-y.

[216] Xiang Zou et al. "Biosynthesis of polymalic acid in fermentation: advances and prospects for industrial application". In: *Critical Reviews in Biotechnology* 39.3 (2019), pp. 408–421. ISSN: 15497801. DOI: 10.1080/07388551.2019.1571008. URL: https://doi.org/10.1080/07388551.2019.1571008.

[217] Peilian Wei et al. "Production of poly(malic acid) from sugarcane juice in fermentation by Aureobasidium pullulans: Kinetics and process economics". In: *Bioresource Technology* 224 (2017), pp. 581–589. ISSN: 18732976. DOI: 10.1016/j.biortech.2016.11.003. URL: http://dx.doi.org/10.1016/j.biortech.2016.11.003.

[218] Rintze M. Zelle et al. "Malic acid production by Saccharomyces cerevisiae: Engineering of pyruvate carboxylation, oxaloacetate reduction, and malate export". In: *Applied and Environmental Microbiology* 74.9 (2008), pp. 2766–2777. ISSN: 00992240. DOI: 10.1128/AEM.02591-07.

[219] Syed T. Ahmed, Nicole G.H. Leferink, and Nigel S. Scrutton. "Chemo-enzymatic routes towards the synthesis of bio-based monomers and polymers". In: *Molecular Catalysis* 467.February (2019), pp. 95–110. ISSN: 24688231. DOI: 10.1016/j.mcat.2019.01.036. URL: https://doi.org/10.1016/j.mcat.2019.01.036.

[220] Wei Du et al. "Exploiting Day- and Night-Time Metabolism of Synechocystis sp. PCC 6803 for Fitness-Coupled Fumarate Production around the Clock". In: *ACS Synthetic Biology* (2019), acssynbio.9b00289. ISSN: 2161-5063. DOI: 10.1021/acssynbio.9b00289. URL: https://pubs.acs.org/doi/10.1021/acssynbio.9b00289.

[221] Terry M. Bricker et al. "The malic enzyme is required for optimal photoautotrophic growth of Synechocystis sp. strain PCC 6803 under continuous light but not under a diurnal light regimen". In: *Journal of Bacteriology* 186.23 (2004), pp. 8144–8148. ISSN: 00219193. DOI: 10.1128/JB.186.23.8144-8148.2004.

[222] Tuomas Huokko et al. "Role of type 2 NAD(P)H dehydrogenase NdbC in redox regulation of carbon allocation in synechocystis". In: *Plant Physiology* 174.3 (2017), pp. 1863–1880. ISSN: 15322548. DOI: 10.1104/pp.17.00398.

[223] Jamey D. Young et al. "Mapping photoautotrophic metabolism with isotopically nonstationary 13C flux analysis". In: *Metabolic Engineering* 13.6 (2011), pp. 656–665. ISSN: 10967176. DOI: 10.1016/j.ymben.2011.08.002. URL: http://dx.doi.org/10.1016/j.ymben.2011.08.002.

[224] Lara J. Jazmin et al. "Isotopically nonstationary 13C flux analysis of cyanobacterial isobutyraldehyde production". In: *Metabolic Engineering* 42.October 2016 (2017), pp. 9–18. ISSN: 10967184. DOI: 10.1016/j.ymben.2017.05.001. URL: http://dx.doi.org/10.1016/j.ymben.2017.05.001.

[225] Robert A. Alberty. "Thermodynamic properties of weak acids involved in enzyme-catalyzed reactions". In: *Journal of Physical Chemistry B* 110.10 (2006), pp. 5012–5016. ISSN: 15206106. DOI: 10.1021/jp0545086.

119

[226] Barbara A. Lawrence et al. "31P NMR identification of metabolites and pH determination in the cyanobacterium Synechocystis sp. PCC 6308". In: *Current Microbiology* 34.5 (1997), pp. 280–283. ISSN: 03438651. DOI: 10.1007/s002849900182.

[227] Avi Flamholz et al. "EQuilibrator - The biochemical thermodynamics calculator". In: *Nucleic Acids Research* 40.D1 (2012), pp. 770–775. ISSN: 03051048. DOI: 10.1093/nar/gkr874.

[228] Ian T. Paulsen et al. "Microbial genome analyses: Comparative transport capabilities in eighteen prokaryotes". In: *Journal of Molecular Biology* 301.1 (2000), pp. 75–100. ISSN: 00222836. DOI: 10.1006/jmbi.2000.3961.

[229] I. G. Janausch et al. "C4-dicarboxylate carriers and sensors in bacteria". In: *Biochimica et Biophysica Acta - Bioenergetics* 1553.1-2 (2002), pp. 39–56. ISSN: 00052728. DOI: 10.1016/S0005-2728(01)00233-X.

[230] Ingo Janausch, Ok Kim, and Gottfried Unden. "DctA- and Dcu-independent transport of succinate in Escherichia coli: Contribution of diffusion and of alternative carriers". In: *Archives of Microbiology* 176.3 (2001), pp. 224–230. ISSN: 03028933. DOI: 10.1007/s002030100317.

[231] Jason A. Forward et al. "TRAP transporters: A new family of periplasmic solute transport systems encoded by the dctPQM genes of Rhodobacter capsulatus and by homologs in diverse gram-negative bacteria". In: *Journal of Bacteriology* 179.17 (1997), pp. 5482–5493. ISSN: 00219193. DOI: 10.1128/jb.179.17.5482-5493.1997.

[232] M. J. Quintero et al. "Identification of genes encoding amino acid permeases by inactivation of selected ORFs from the Synechocystis genomic sequence". In: *Genome Research* 11.12 (2001), pp. 2034–2040. ISSN: 10889051. DOI: 10.1101/gr.196301.

[233] Fábio Madeira et al. "The EMBL-EBI search and sequence analysis tools APIs in 2019". In: *Nucleic acids research* 47.W1 (2019), W636–W641. ISSN: 13624962. DOI: 10.1093/nar/gkz268.

[234] Sabine Fulda et al. "Proteomics of Synechocystis sp. strain PCC 6803 Identification of periplasmic proteins in cells grown at low and high salt concentrations". In: *European Journal of Biochemistry* 5907 (2000), pp. 5900–5907.

[235] Ting Zhang et al. "Regulating C4-dicarboxylate transporters for improving fumaric acid production". In: *RSC Advances* 7.5 (2017), pp. 2897–2904. ISSN: 20462069. DOI: 10.1039/c6ra24727j.

[236] Shuichi Aiba. "Growth Kinetics of Photosynthetic Microorganisms". In: *Advances in biochemical engineering*. Springer, Berlin, Heidelberg, 1982. ISBN: 978-3-540-11698-1. DOI: 10.1007/3540116982_3.

[237]   G. Neal Proctor. "Mathematics of Microbial Plasmid Instability and Subsequent Differential Growth of Plasmid-Free and Plasmid-Containing Cells, Relevant to the Analysis of Experimental Colony Number Data". In: *Plasmid* 32 (1994), pp. 101–130. DOI: 10.1006/plas.1994.1051.

[238]   Richard E. Lenski. "Experimental evolution and the dynamics of adaptation and genome evolution in microbial populations". In: *ISME Journal* 11.10 (2017), pp. 2181–2194. ISSN: 17517370. DOI: 10.1038/ismej.2017.69.

[239]   Anna Melbinger, Jonas Cremer, and Erwin Frey. "Evolutionary Game Theory in Growing Populations". In: *Physical Review Letters* 178101 (2010), pp. 1–4. DOI: 10.1103/PhysRevLett.105.178101.

[240]   S. E. Luria and Delbruck M. "Mutations of bacteria from virus sensitivity to virus resistance". In: *Genetics* 28.491 (1943).

[241]   B. R. Levin et al. "The Population Genetics of Antibiotic Resistance". In: *Clinical Infectious Diseases* 24.Supplement 1 (1997), S9–S16. DOI: 10.1093/clinids/24.supplement_1.s9.

[242]   Eduardo Ibargüen-Mondragón et al. "Mathematical modeling on bacterial resistance to multiple antibiotics caused by spontaneous mutations". In: *BioSystems* 117.1 (2014), pp. 60–67. ISSN: 03032647. DOI: 10.1016/j.biosystems.2014.01.005.

[243]   R. A. Fisher. "On the dominance ratio." In: *Proceedings of the Royal Society of Edinburgh* 42 (1922), pp. 321–341.

[244]   P. Moran. "Random processes in genetics." In: *Mathematical Proceedings of the Cambridge Philosophical Society* 54.1 (1958), pp. 60–71. DOI: 10.1017/S0305004\100033193.

[245]   P. Moran. "The statistical processes of evolutionary theory". In: (1962).

[246]   Martin A. Nowak. *Evolutionary dynamics - exploring the equations of life.* The Belknap Press of Harvard University Press, 2006, p. 363. ISBN: 978-0-674-02338-3.

[247]   Lília Perfeito et al. "Adaptive mutations in bacteria: High rate and small effects". In: *Science* 317.5839 (2007), pp. 813–815. ISSN: 00368075. DOI: 10.1126/science.1142284.

[248]   Quentin Béchet, Andy Shilton, and Benoit Guieysse. "Modeling the effects of light and temperature on algae growth: State of the art and critical assessment for productivity prediction during outdoor cultivation". In: *Biotechnology Advances* 31.8 (2013), pp. 1648–1663. ISSN: 07349750. DOI: 10.1016/j.biotechadv.2013.08.014.

[249] Eunyoung Lee, Mehregan Jalalizadeh, and Qiong Zhang. "Growth kinetic models for microalgae cultivation: A review". In: *Algal Research* 12 (2015), pp. 497–512. ISSN: 22119264. DOI: `10.1016/j.algal.2015.10.004`.

[250] Francis Mairet Olivier Bernard and Benoît Chachuat. "Modelling of Microalgae Culture Systems with Applications to Control and Optimization". In: *Advances in Biochemical Engineering/Biotechnology* (2015). DOI: `10.1007/10_2014_287`.

[251] Source Ecology and No Mar. "Light-Limited Growth and Competition for Light in Well-Mixed Aquatic Environments : An Elementary Model Author (s): Jef Huisman and Franz J . Weissing Stable URL : http://www.jstor.org/stable/1939554 REFERENCES Linked references are available on JSTOR f". In: 75.2 (2016), pp. 507–520.

[252] E. L. Tamiya et al. "Kinetics of growth of Chlorella, with special reference to its dependence on quantity of available light and on temperature". In: (1953), pp. 204–234.

[253] E. Molina Grima et al. "A Mathematical Model of Microalgal Growth in Light-Limited Chemostat Culture". In: *Journal of Chemical Technology & Biotechnology* 61 (1994), pp. 167–173. ISSN: 0268-2575. DOI: `10.1002/jctb.280610212`.

[254] J. H. Steele. "Environmental control of photosynthesis in the sea". In: *Limnology and Oceanography* 7.2 (1962), pp. 137–150.

[255] Olivier Bernard and Barbara Rémond. "Validation of a simple model accounting for light and temperature effect on microalgal growth". In: *Bioresource Technology* 123 (2012), pp. 520–527. ISSN: 09608524. DOI: `10.1016/j.biortech.2012.07.022`.

[256] Christopher A. Klausmeier, Elena Litchman, and Simon A. Levin. "Phytoplankton growth and stoichiometry under multiple nutrient limitation". In: *Limnology and Oceanography* 49.4 II (2004), pp. 1463–1470. ISSN: 00243590. DOI: `10.4319/lo.2004.49.4_part_2.1463`.

[257] Heikki Haario, Leonid Kalachev, and Marko Laine. "Reduced models of algae growth". In: *Bulletin of Mathematical Biology* 71.7 (2009), pp. 1626–1648. ISSN: 00928240. DOI: `10.1007/s11538-009-9417-7`.

[258] F. Rubio Camacho et al. "A mechanistic model of photosynthesis in microalgae". In: *Biotechnology and Bioengineering* 81.4 (2003), pp. 459–473. ISSN: 00063592. DOI: `10.1002/bit.10492`.

[259] A. Bernardi et al. "An identifiable state model to describe light intensity influence on microalgae growth". In: *Industrial and Engineering Chemistry Research* 53.16 (2014), pp. 6738–6749. ISSN: 15205045. DOI: `10.1021/ie500523z`.

[260] Carlos Martínez, Francis Mairet, and Olivier Bernard. "Theory of turbid microalgae cultures". In: *Journal of Theoretical Biology* 456 (2018), pp. 190–200. ISSN: 10958541. DOI: 10.1016/j.jtbi.2018.07.016.

[261] Hugh L. MacIntyre et al. "Photoacclimation of photosynthesis irradiance response curves and photosynthetic pigments in microalgae and cyanobacteria". In: *Journal of Phycology* 38.1 (2002), pp. 17–38. ISSN: 00223646. DOI: 10.1046/j.1529-8817.2002.00094.x.

[262] Charles P. Deblois, Axelle Marchand, and Philippe Juneau. "Comparison of Photoacclimation in Twelve Freshwater Photoautotrophs (Chlorophyte, Bacillaryophyte, Cryptophyte and Cyanophyte) Isolated from a Natural Community". In: *PLoS ONE* 8.3 (2013). ISSN: 19326203. DOI: 10.1371/journal.pone.0057139.

[263] Levi Straka. "Light-Dependent Growth Kinetics and Mathematical Modeling of Synechocystis sp. PCC 6803". PhD thesis. 2017, p. 164.

[264] Levi Straka and Bruce E. Rittmann. "Light attenuation changes with photoacclimation in a culture of Synechocystis sp. PCC 6803". In: *Algal Research* 21 (2017), pp. 223–226. ISSN: 22119264. DOI: 10.1016/j.algal.2016.11.024. URL: http://dx.doi.org/10.1016/j.algal.2016.11.024.

[265] Alessandro Cordara et al. "Analysis of the light intensity dependence of the growth of Synechocystis and of the light distribution in a photobioreactor energized by 635 nm light". In: *PeerJ* 2018.7 (2018), pp. 1–28. ISSN: 21678359. DOI: 10.7717/peerj.5256.

[266] Ryan L. Clark et al. "Light-optimized growth of cyanobacterial cultures: Growth phases and productivity of biomass and secreted molecules in light-limited batch growth". In: *Metabolic Engineering* 47.March (2018), pp. 230–242. ISSN: 10967184. DOI: 10.1016/j.ymben.2018.03.017.

[267] Takashi Osanai et al. "Capillary electrophoresis-mass spectrometry reveals the distribution of carbon metabolites during nitrogen starvation in Synechocystis sp. PCC 6803". In: *Environmental Microbiology* 16.2 (2014), pp. 512–524. ISSN: 14622912. DOI: 10.1111/1462-2920.12170.

[268] Thomas Walther et al. "Construction of a synthetic metabolic pathway for biosynthesis of the non-natural methionine precursor 2,4-dihydroxybutyric acid". In: *Nature Communications* 8.May (2017). ISSN: 20411723. DOI: 10.1038/ncomms158\28.

This Ph.D. thesis has been typeset by means of the TEX-system facilities. The typesetting engine was LuaLaTeX. The document class was `toptesi`, by Claudio Beccari, with option `tipotesi` `=scudo`. This class is available in every up-to-date and complete TEX-system installation.